Mechanics of Long-Term Behavior of High Temperature Polymer Composites

Contractors Report
AFOSR Grant No. F49620-95-1-0217
1997-98

Dr. Kenneth L. Reifsnider & Jack Lesko, P.I.s
Scott Case, Celine Mahieux, Brady Walther, and Blair Russell
Virginia Polytechnic Institute and State University
Materials Response Group
120 Patton Hall
Blacksburg, VA 24061-0219

REPORT DOCUMENTATION PAGE

AFRL-SR-BL-TR-98-

0835

1. AGENCY USE ONLY *(Leave blank)*	2. REPORT DATE	3. REPORT TYPE AND DATES COVERED
	1997-98	Final Technical Report 15 Mar 95 to 14 Aug 98

4. TITLE AND SUBTITLE
Mechanics of Long-Term Behavior of High Temperature Polymer Composites

5. FUNDING NUMBERS
F49620-95-1-0217
2302/BS

6. AUTHOR(S)
Dr. Kenneth L. Reifsnider
Dr. Jack Lesko

7. PERFORMING ORGANIZATION NAME(S) AND ADDRESS(ES)
Virginia Polytechnic Institute and State University
Materials Response Group
120 Patton Hall
Blacksburg, VA 24061-0219

8. PERFORMING ORGANIZATION REPORT NUMBER

9. SPONSORING/MONITORING AGENCY NAME(S) AND ADDRESS(ES)
AFOSR/NA
801 N. Randolph Street Room 732
Arlington, VA 22203-1977

10. SPONSORING/MONITORING AGENCY REPORT NUMBER
F49620-95-1-0217

11. SUPPLEMENTARY NOTES

12a. DISTRIBUTION AVAILABILITY STATEMENT
Approved for public release; distribution unlimited.

12b. DISTRIBUTION CODE

13. ABSTRACT *(Maximum 200 words)*

The general objective of the present program was to develop and assemble fundamental understandings and mechanistic mechanics and materials models needed to describe and anticipate the long-term mechanical behavior of polymer composites at high temperatures with variable time- and cycle - dependent mechanical loading. The primary points of departure of this program from previous work are the concentration on the effect of temperature on strength, as well as stiffness, and the concentration on using constituent behavior to predict the fiber-dominated strength and life of composite materials. Salient results of the effort include the development of micromechanical fiber-direction strength models for unidirectional composites that correctly predict temperature-dependent changes that are large compared to stiffness variations; the construction of a new equivalence concept between strain rate and temperature which correctly predicts instantaneous stiffness changes over seven orders of magnitude of strain rate; and postulation and initial validation of an entirely new concept for predicting instantaneous stiffness variations across primary and secondary transitions in polymers as a function of temperature, for use in robust design codes, especially for life prediction in virtual design spaces.

14. SUBJECT TERMS
fiber-dominated, polymer composites

15. NUMBER OF PAGES

16. PRICE CODE

17. SECURITY CLASSIFICATION OF REPORT	18. SECURITY CLASSIFICATION OF THIS PAGE	19. SECURITY CLASSIFICATION OF ABSTRACT	20. LIMITATION OF ABSTRACT
Unclassified	Unclassified	Unclassified	UL

Mechanics of Long-Term Behavior of High Temperature Polymer Composites

Contractors Report
AFOSR Grant No. F49620-95-1-0217
1997-98

Dr. Kenneth L. Reifsnider & Jack Lesko, P.I.s
Scott Case, Celine Mahieux, Brady Walther, and Blair Russell
Virginia Polytechnic Institute and State University
Materials Response Group
120 Patton Hall
Blacksburg, VA 24061-0219

Mechanics of Long-Term Behavior of High Temperature Polymer Composites

Objectives

The general objective of the present program is to develop and assemble fundamental understandings and mechanistic mechanics and materials models needed to describe and anticipate the long-term mechanical behavior of polymer composites at high temperatures with variable time- and cycle - dependent mechanical loading, in air.

Specific elements of this objective include efforts to:

- determine a basic understanding of the mechanics of temperature-driven property changes and long-term environmental degradation of polymer based composites,
- construct representations of the constitutive behavior of such materials, including coupling and degradation rates,
- use those representations in basic structural mechanics models to establish the remaining strength and life of material systems and structures, i.e., their durability, damage tolerance, reliability, and safety.

It is the general hope that this program will help to fill a basic scientific need to establish a coherent, systematic, and consistent mechanics framework for the description and prediction of the combined behavior of polymer composites under long-term severe conditions, including the coupled effects of creep, creep rupture, physical and chemical aging, residual / thermal stresses, and fatigue degradation (including degradation of the fiber / matrix interphase region). The scope of the program is illustrated in Fig. 1.

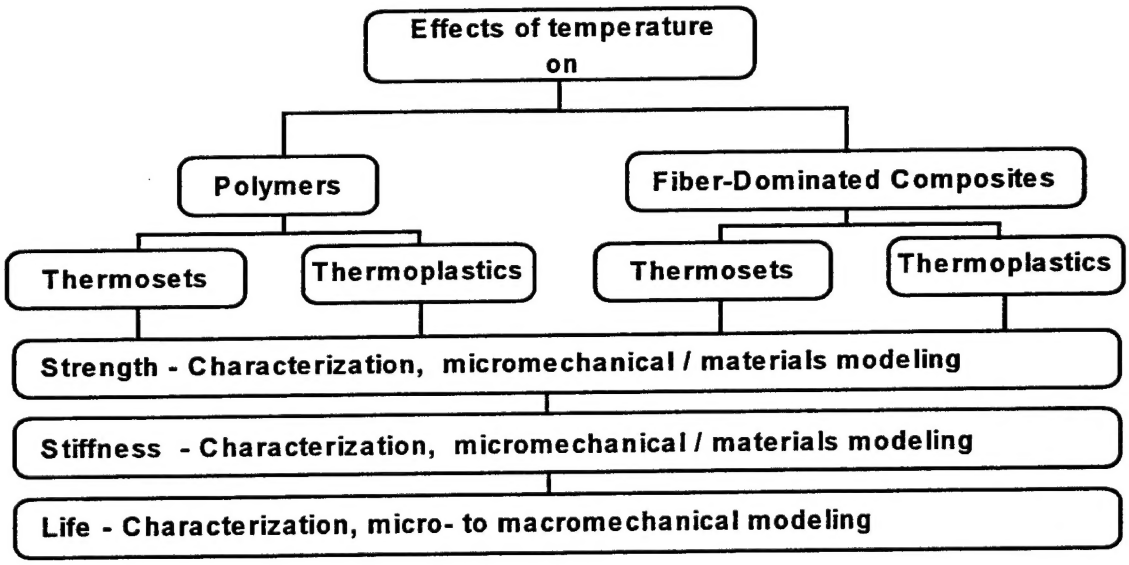

Figure 1 Scope of the present program.

The primary points of departure of this program from previous work are the concentration on the effect of temperature on strength, rather than stiffness, and the concentration on using constituent behavior (especially polymer matrix behavior) to predict the fiber-dominated strength and life of composite materials. The predictive nature of the effort should be emphasized. Empirical characterizations of the effect of temperature on stiffness and strength appear in the literature, albeit in fragmented form. But discussions of the atomic / molecular mechanisms that drive those changes are sparse, especially as a function of polymer material characteristics. Without the time and expense of making significant amounts of material and characterizing them, it is not generally possible to answer even simple questions, like "will the stiffness or strength *increase* or *decrease* over the range of expected service temperatures?" Both behaviors have been observed over ranges of temperature from, say, -40 degrees to temperatures above the Tg for common polymer composites. And the increasing use of thermosets introduces the variables associated with microstructure into these questions. Stiffness and strength of composites (even in fiber-controlled directions) depends on the crystallinity of the matrix material, for example, and that crystallinity is highly dependent upon the thermal history of the material. A basic understanding of these effects must be established to serve as the foundation of predictive methodologies for stiffness and strength of fiber-controlled polymer composites if the obvious benefits of these materials are to be exploited by high temperature devices such as the High Speed Civil Transport and numerous other applications in the planning stages. Indeed, our industrial partners in the turbine and power industries are quite anxious to find these answers. But they cannot afford to sustain the fundamental studies to develop the science of this subject, nor can they afford to sustain the cost of characterization of all possible combinations of constituents. Predictive models are essential to the advancement not only of the science and engineering of this subject, but also to the technology and economy associated with the applications of the subject.

Status of the Effort

This program is at the end of the third year of effort. A central feature of this program is the focus on the influence of matrix behavior on "fiber controlled" properties and performance (strength, stiffness, and life) which is generally more complex and often more important to applications than the matrix-controlled behavior that dominates the literature associated with high-temperature polymer behavior. In the early stages of the investigation, we found that the tensile strength of polymer composites in the fiber direction may be altered by 40 percent or more as a function of temperature, and that strength often has a maximum as a function of increasing temperature that is predicted by a micromechanical model that we have developed. We were able to further demonstrate this effect by altering the tensile strength of unidirectional material significantly by changing only the fiber coating, i.e., by changing less than one percent of the composite by volume. Subsequently, we have extended our understanding by beginning an extensive investigation of time-temperature-moisture effects on the bending strength, stiffness, and life of unidirectional PPS matrix composites. This provided a way to study and model controlled time-dependent "stress-rupture," and to investigate the coupling of time dependent and cycle dependent behavior as a function of temperature. The general vision for the work is to understand the materials science origins of these effects well enough to predict behavior for untested polymer-based composites.

Accomplishments / New Findings

Our general approach to the present program is to use precise experimental characterizations, and micromechanical and constitutive modeling to construct an integrated fundamental mechanics foundation for the description and prediction of the long-term behavior of "fiber-controlled" polymer composites under applied conditions that may include elevated temperature (in air and other environments) and cyclic or sustained mechanical loading. It is intended that this approach will create a mechanics methodology and capability that will not only enable predictive structural engineering (using PMCs under such conditions), but will also guide the designers of such material systems when durability and damage tolerance are important objectives.

Recent salient results include the following:

1. During the last year of effort, an entirely new concept has been conceived and developed to a first level, that can be used to predict, using basic physical properties, the variation of the instantaneous modulus of polymer-based materials (or behavior) as a function of temperature from low temperatures for which the polymer is well into the glassy state, continuously through the alpha and beta transition into the rubbery state.
2. Our micromechanical tensile strength model for unidirectional laminae has been successfully used to predict the dependence of uniaxial tensile strength (in the fiber direction) of carbon reinforced polymer composites as a function of temperature up to Tg of the materials, with no adjustable parameters, based on the constituent properties.
3. Kinetic damage mechanics concepts have been successfully used to correctly predict the combined and interactive effects of stress rupture (as a function of temperature) and fatigue for a fiber-dominated, PPS-based composite.
4. Based on our constitutive modeling and experimental results, and on an extensive search of the literature, we have postulated an entirely new equivalence concept between strain rate and temperature, and tested the idea over seven orders of magnitude of strain rate for an epoxy-based system.
5. We have recently extended a concept postulated by Landel to construct a stress-strain to failure envelope that is normalized for temperature and cross link density, added an analytical representation of the relationship, and developed data as a function of systematically varied cross link density for a vinyl ester system to validate the new ideas and methodologies.

A few highlights of these efforts will be outlined below; more details are provided in the Appendices noted at the beginning of those sections. Figure 1 illustrates the inter-relationship of some of these highlights.

Variation of Stiffness with Temperature Across Tg: (Appendix I)

A previous report discussed the end-loaded compression behavior of unidirectional AS4/PPS composites. This fundamental work was motivated by our continuing effort to understand how the matrix influences global behavior when the fibers "control" the properties. The study was based on the experimental study of the strength and life of unidirectional material under fiber-direction end-loaded bending of PPS-based unidirectional specimens, a test method that has many advantages for the

fundamental characterization of composites behavior. The experimental test program conducted to date (for NSF and the Wellstream Corporation) is quite extensive, and includes characterization at several elevated temperatures (with a concentration on 90 and 120 degrees C). It was discovered during the course of that work that although the quasi-static strength at 90 degrees C, for example, is slightly higher than the room-temperature value, the long-term behavior at that temperature displays stress rupture, even at strains that are of the order of 50 percent of the ultimate strain to failure under quasi-static loading. This is an excellent example of the behavior studied under the present program, and an obvious interest (and concern) to the applied community (although the authors know of no other reported behavior of this type for unidirectional material). The end-loaded bending method enables small specimens to be loaded under constant strain conditions, for long periods of time in a furnace or environmental chamber. This makes it possible to do systematic studies with a small amount of material, a critical feature of the present work to support our philosophy development.

The earlier effort motivated a second study, during the last year. That study addressed the question of how to construct models of strength that work over wide ranges of temperature. Indeed, since polymer composites are now being used in applications in which the temperature varies over values for which the polymer is glassy to values for which the polymer is well into the rubbery region, the object of our research was to find a model that correctly predicts the variation of stiffness of the polymer over those ranges, so that correct stress analysis (the first and most important element of a strength model) could be conducted. Since no such model (or even supporting philosophy) exists over that temperature range, we have postulated such a concept, and have done extensive experimental work to validate the approach. This advance is illustrated in Fig. 2.

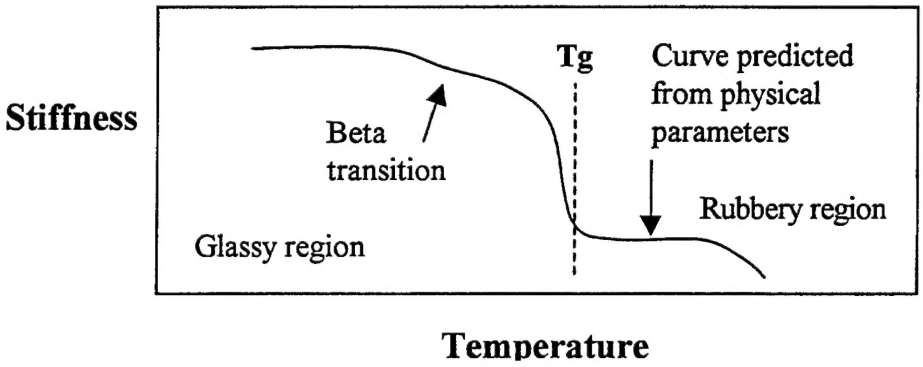

Figure 2 Illustration of predicted variation of instantaneous stiffness across the alpha and beta transition temperatures.

We have begun the study of how these predictions depend on various physical parameters, including microstructure such as crystallinity and cross-link density, and cooperativity of the molecules. The predictive capabilities of this modeling effort will be directly used in the micromechanics models of strength and strength degradation that are the basis of our life prediction code called MRLife. They will enable the designers of components to accurately estimate remaining strength and life in the presence of temperature changes that span the transition from glassy to rubbery behavior from a single set of characterization data, the first time that capability has ever been achieved.

Fiber-Controlled Tensile Strength: (Appendix II)
Our first fundamental effort in this area addressed the micro-mechanics of high temperature strength. Micromechanical strength models, including those developed by our Materials Response Group, represent global behavior in terms of the properties, geometry, and arrangement of the constituents (including the interphase regions); as such, they provide a key critical link between the time / temperature / stress / environment influences in terms of the degradation of the constituents and the global long-term behavior of the composites.

In a previous technical report we provided an example of the early results of this effort. In that report, we addressed the following simple question. If the micromechanical models that have been developed (by us and others) really are correct, then a "clean" way of validating them, in the present context, is to try to predict the effect of changing temperature on the quasi-static strength based on the measured behavior of the constituents. The first example we examined was the tensile strength of a unidirectional material. For this situation, in polymer composites, changes of as much as 40 percent in the tensile strength in the fiber direction can be affected by temperature. Moreover, these changes are not monotonic, and they are generally highly nonlinear. Our models follow this behavior, in general. These remarkable results are the subject of continuing study. One paper has been submitted for publication on this subject, so far.

We have also examined the effect of changing the interphase region between the fiber and the matrix. The quasi-static stiffness of the two systems was essentially identical. However, the quasi-static strength was about 27 percent different, and the two systems exhibited different fracture modes. This difference was effected by changing only the coating on the fibers, i.e., by altering less than 1 percent of the volume of the material.

These results have spurred a concentrated study with a broadened scope. We have now completed over 150 tests of unidirectional composites with various thermoset and thermoplastic matrix resins at various temperatures relative to the Tg of the matrix materials, to characterize the dependence of stiffness and quasi-static strength on temperature, as a function of the fiber coating (and attendant properties of the interphase region), and strain rate. Some of these results are discussed in Appendix II.

During the last year, we tested the fundamental validity of our micromechanical strength model for unidirectional composites, in the fiber direction, by characterizing the dependence of the stiffness and strength of a polymer matrix material, entering those properties into the model for strength of a composite, and comparing the predicted composite strength changes with observed results. An example of the results is shown in Fig. 3.

What is remarkable about the predictions in Fig. 3 is the fact that there are no adjustable parameters in the model, and only one set of data were used to make the predictions over the range of temperatures that exceeds the Tg of the material by 40 degrees Centigrade. A more complete description of this work appears in Appendix II.

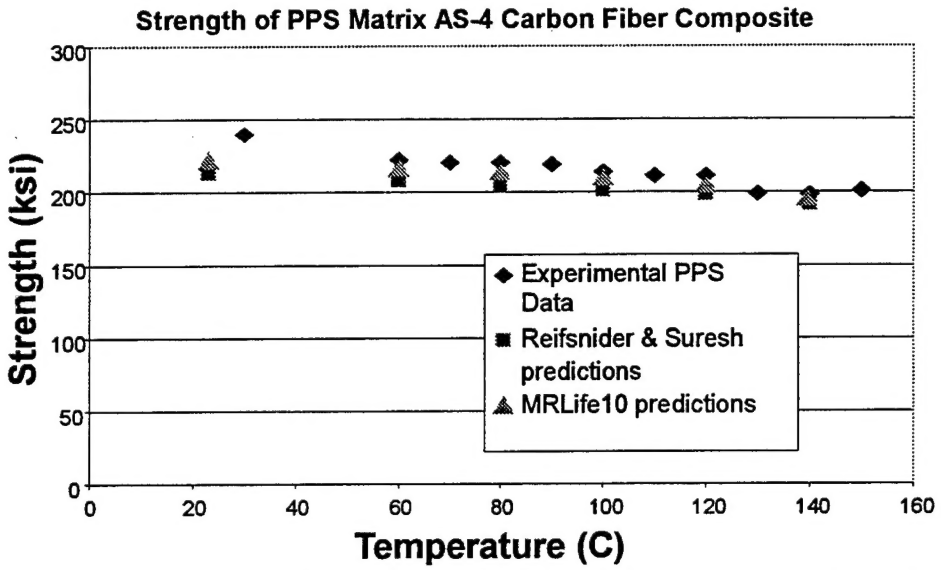

Figure 3 Predicted and observed variation of unidirectional composite tensile strength in the fiber direction as a function of test temperature.

Interactive Effects of Stress Rupture and Fatigue: (Appendix III)

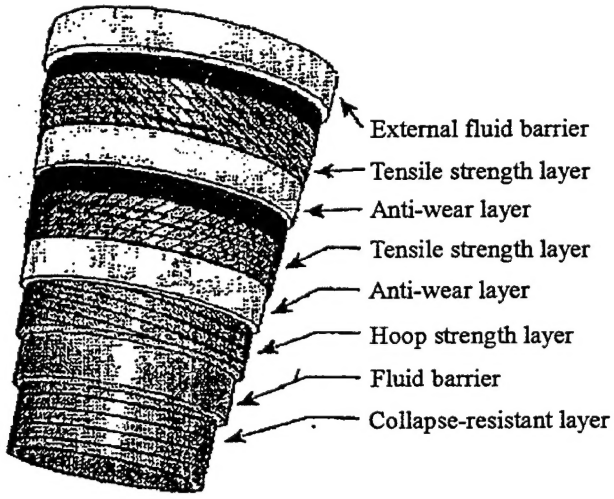

Figure 4 Schematic diagram of the construction of a high-pressure flexible pipe for off-shore industries, which was analyzed using results from the present program.

A third thrust of the past year was concerned with bringing the results of the present program to bear on applied problems. In particular, we attempted to predict the remaining strength and life of unidirectional carbon reinforced PPS composites under the combined conditions of fatigue and stress rupture at high temperatures. The motivation for doing this work was provided by the need for

designing a high-pressure flexible pipe for the off-shore industry; our industrial partner for this effort was the Wellstream corporation. The construction of the pipe is shown in Fig. 4.

To construct the global model for life prediction, room temperature fatigue data and at-temperature stress-rupture data (in tension) were combined using the critical element method and the micro-kinetic scheme we have described in earlier reports and papers (see list of publications). The results are shown in Fig. 5.

The figure shows that the combined behavior is quite different than any "linear" combination or superposition of the fatigue and stress-rupture behavior alone. The analysis method seems to capture that nonlinearity, and provides a mechanistic, predictive method of estimating the combined effects of cycle-dependent and time-dependent temperature effects.

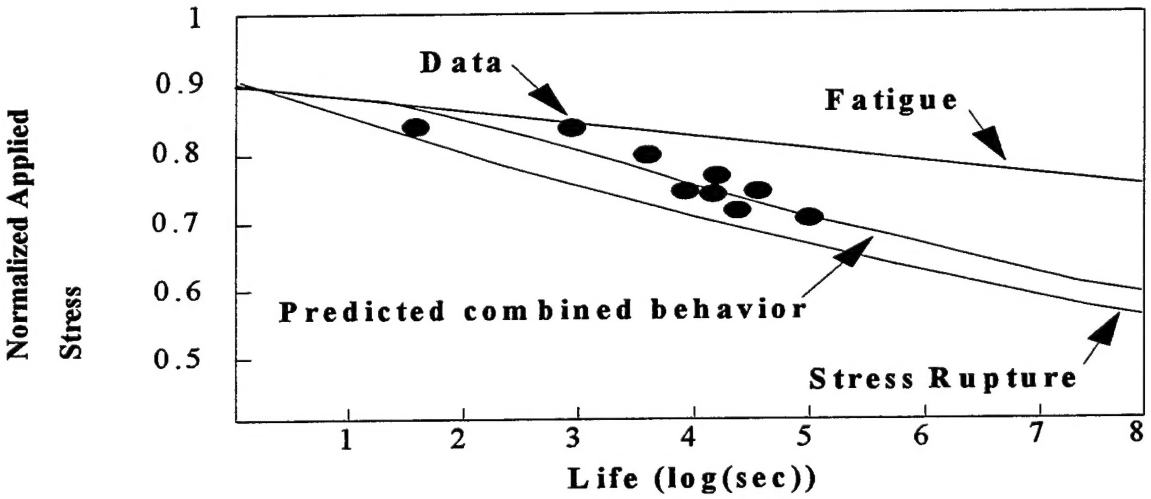

Figure 5 Predicted and observed combined stress-rupture / fatigue tensile behavior of unidirectional carbon/PPS coupons at 90 ^{0}C.

These results, and more particularly, the methodology is being used to design the first commercial product that Wellstream will deploy off the coast of Brazil in the Fall of 1998. The present program was directly responsible for the fundamental underpinning that made that analysis and deployment possible.

Strain Rate – Temperature Equivalence: (Appendix IV)
This focus on strain-rate is a new feature in the present program, and reflects a conceptual framework that we are constructing for the general subject. Like temperature, strain rate is usually discussed in terms of the effect of loading rate on stiffness in polymer-based systems; but little systematic information exists on the effect of strain rate on strength. However, if the fundamental basis for the effect of temperature on polymers is kinetic, for example, then one would expect temperature and strain rate to be "equivalent" (or inversely equivalent) parameters, i.e., an increase in temperature might be expected to produce the same effect on strength as a decrease in strain rate. We know, in fact, that this is true in some cases, and not true in others. The reasons for that are the object of this study. An

example of these results was presented in an earlier report, in the form of a preliminary study of the effect of strain rate on the strength of polymer-bonded metallic joints. In that study, three strain rates (over three orders of magnitude) and three temperatures (below the Tg) were used to compare the "tradeoff" between temperature and strain rate on lap-shear strength. The results were striking. They show large, systematic, but highly nonlinear effects. No simple "rule of thumb" could be used to characterize this situation; it awaits a comprehensive effort to provide a correct interpretation and generalized modeling (which would be greatly useful to the applied community).

In the present report, a much more comprehensive approach was taken. A summary of the results is given in Appendix IV. Data for the present effort were taken from the literature. Linear relationships for stiffness change for polymer matrix materials and glass reinforcing fibers as a function of either temperature or log of strain rate were extracted from experimental results from a wide range of authors. To achieve the objective of relating temperature and strain rate effects to strength (strain to failure and stress to failure, in this case), we introduced the postulate originally made (by Monkman and Grant) for the creep rupture of metals, i.e., that

$$t_b * \dot{\varepsilon} = C_1 \tag{1}$$

where t_b is the time to break, and C_1 is a material constant. Remarkably, as shown in Appendix IV, a variety of polymer matrix and glass fiber data fit this relationship, over more than seven orders of magnitude of strain rate. In order to establish a specific temperature-strain rate equivalence, and test the concepts with actual calculations, an Arrhenius relationship between time and temperature was used for epoxy matrix materials, resulting in the relationship

$$T = \left[\frac{2.30 * G * \log\left(\frac{t_s}{C_1 * (\dot{\varepsilon})^{-m}} \right)}{\Delta H} + \frac{1}{T_0} \right]^{-1} \tag{2}$$

where G is the quasi-static shear modulus, and ΔH is the activation energy for the material in question. Then combining equation (1), a linear relationship between stiffness and log of strain rate, such as

$$E = A * \log(\dot{\varepsilon}) + B \tag{3}$$

and the identity that $t_b * \dot{\varepsilon} = \varepsilon_b$, it was possible to start from quasi-static data for stiffness at room temperature, and predict the stiffness at any other strain rate by estimating how much you would have to change the temperature at the current rate to produce the same stiffness as one should measure at the new strain rate. Then those predictions were compared to actual measurements of the stiffness at various strain rates to validate the concepts. An example of those comparisons is shown in the figure, below. This concept has been tried for literally dozens of data sets, with comparable results.

The utility of this new approach is evident. Like temperature, strain rate is often quite different over the history of use of any engineering component. If we are to have robust design models that do not require unreasonable amounts of characterization data (especially if we are to try to construct virtual design spaces), then we must be able to predict (or at least anticipate with reasonable accuracy) the

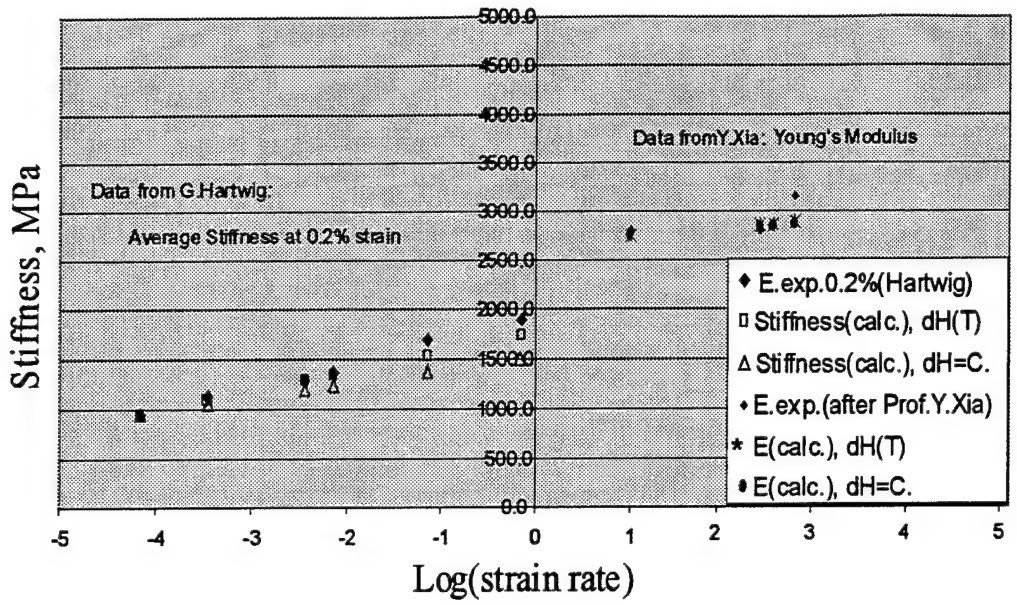

Figure 6 Comparison of predicted stiffness at several strain rates with observed values. Predictions were based on equivalent temperatures using temperature-strain rate equivalence concepts.

dependence not only of stiffness but strength and strain to failure on strain rate. If the stiffness of the material is know as a function of temperature, we have shown that the stiffness, strength, and strain to failure of the material as a function of strain rate can be estimated, at least for the materials we have examined. For example, if we have room temperature quasi-static strength and strain to failure, we can estimate the stiffness, strength, and strain to failure under impact conditions, a prediction of obvious value to the community concerned with estimating safety and damage tolerance under crash conditions or as a result of munitions. We believe that this is a new window of opportunity to construct robust design models.

Influence of Polymer Network Structure on Mechanical Response: (Appendix V)
As we noted in the discussion of Appendix I, the stiffness of polymers changes greatly with temperature, across the Tg of the material. We are developing models that will allow us to estimate those changes from basic data, such as the cross link density of the polymer, the glassy stiffness, and some information about the location of the Tg itself. However, the modeling parameters are functions of the internal structure of the polymer, especially the molecular weight and the cross link density. In order to better understand that dependence, we have undertaken a study of the nature of the behavior for two common polymers. In addition, we used that study to investigate the possibility of constructing a failure envelope that relates break stress to break strain for a given polymer, in the form of a master curve that applies to a wide range of temperatures and strain rates.

Vinyl ester and epoxy network polymers were studied for these tasks. Vinyl ester resins were studied for the influence of the network structure on their viscoelastic, physical and mechanical properties. The crosslink density of the resins was altered by changing the molecular weight of the vinyl ester oligomer and by varying the styrene used during the crosslinking reaction. The glass transition temperatures of the polymers and the breadth of the glass transition regions were

found to increase systematically with the increase of crosslink density without additional influence of the composition. Cooperativity studies were also performed in the glass formation temperature region of the networks. The cooperativity of the systems seemed to be influenced by both the crosslink density and the styrene content. A linear correlation was found between the fracture toughness of the networks and the cooperative domain size at the glass transition temperature normalized by the crosslink density. The crosslink density of the epoxy resins was varied with three different molecular weights of the crosslinking agent poly(oxypropylene)diamine. The tensile stress-strain behavior of the polymers due to the change in the crosslink density was studied. Ultimate tensile properties of the systems were also obtained to re-examine the existence of a proposed master failure envelope. Only this last feature will be summarized here.

The tensile failure properties of the Epon/Jeffamine copolymer epoxy resins were studied. The data fit very well on the flow of the failure envelope plotted with the data examined by Landel, etc. More interestingly, the epoxy resins extend the failure envelope down to a more highly crosslinked region (Fig. 7). The previous literature data were able to fit the failure envelop from above 40% strain at break ($\log 100\varepsilon_b >= 1.6$). The lower region of the strain-to-break is extended by the epoxy resins. Another striking feature of the results is that the scattering of the data due to experimental errors also falls on the flow of the master failure envelope.

The stress-strain behavior can be described by an analog of the Martin, Roth, and Stiehler equation,[1]

$$\sigma = E\left(\frac{\varepsilon}{\lambda^2}\right)^{A\left(\lambda-\frac{1}{\lambda}\right)} \tag{4}$$

where E is the equilibrium tensile modulus, λ is the extension ratio equal to $\varepsilon + 1$, and A is a constant. A relationship in the analog of the MRS equation,

$$\left(\frac{\sigma_b}{\nu_e}\frac{273}{T}\right) = E\left(\frac{\varepsilon_b}{\lambda_b{}^2}\right)^{A\left(\lambda_b-\frac{1}{\lambda_b}\right)} \tag{5}$$

where the left-hand side of the expression is the base of the y-axis used in the failure envelope, ε_b is the strain-to-break, λ_b is the extension ratio at break ($\lambda_b = \varepsilon_b + 1$), and A is a constant taken to be 0.43. This expression, replacing the stress and strain variables with the normalized failure stress and strain, turns out to fit the failure envelope markedly well (Fig. 8). More work is needed to investigate this correlation.

Nevertheless, the results shown above present numerous opportunities. It would appear that, for a given polymer, a relationship between the stress to failure and the strain to failure can be established that is normalized for molecular weight, cross link density, and Tg. Moreover, that master relationship is not a function of temperature and strain rate, in the sense that failure points for a given material move to different locations on the master curve for changes in those variables but still fall on the same curve. The engineering utility of such a failure envelope is enormous. It is another key piece of the puzzle of predicting strength and remaining strength of polymer based systems as explicit functions of temperature, and strain rate in this case.

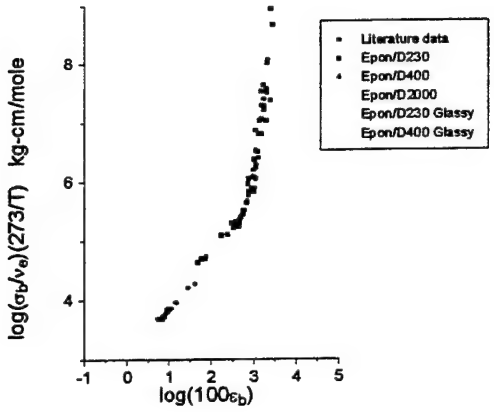

Figure 7 – The ultimate tensile properties of the epoxy resins in the context of the literature data obtained for the EPDM and butadiene.

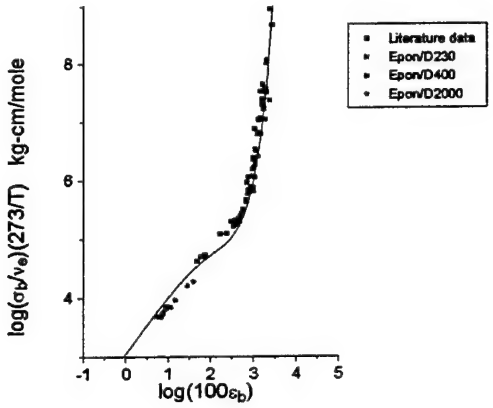

Figure 8 – Literature data and the Epon 828/Jeffamine network systems fitted on the expression in an analog of the MRS equation

Special Features of the Investigation:

The present program has several special features. Under NSF funding, high temperature composites are being made and tested; some of those specimens are available to the present effort. We have the advantage of knowing exactly what is in those specimens and how they were fabricated. This allows us to systematically vary various constituents and the interphase region between the fibers and matrix, known to have a very great influence on long-term behavior. Other specimens for this study are being provided by the Wellstream Corporation in connection with an ATP program we have with them to provide life prediction design codes for composite off-shore components. This effort is quite extensive, and provides a remarkable opportunity for interaction with this program. Finally, we are working closely with General Electric, United Technologies, and Pratt and Whitney to develop life prediction philosophy and methodologies that can be used in their design codes for high temperature polymer composites. These efforts provide immediate application and validation of the fundamental results and understandings being generated under the present effort. Finally, we have presented our work at Wright Patterson AFB and discussed the details with personnel there, especially Arvind Nagar and Nicholas Pagano on a continuing basis. Beyond their fundamental interest in our work, we are also negotiating with Pratt and Whitney (West Palm Beach) to work with them on an Air Force sponsored program to establish design methods for high temperature polymer composites.

A second special feature has to do with the concentration on fiber controlled behavior. The bulk of the literature that addresses the subject at hand has to do with matrix dominated properties and performance, especially viscoelasticity. However, most applications of PMCs are specifically designed to avoid such behavior by arranging fiber architectures that are fiber controlled. We have chosen to concentrate on fiber controlled behavior for that reason. As it happens, the effects of the matrix and

fiber-matrix interphase region on long-term behavior of fiber controlled PMC systems is often large and significant, although their effect on quasi-static properties is often minor for fiber controlled conditions. What is more surprising is that, while environment-affected matrix behavior is widely discussed and much of the basic mechanics of that behavior has been identified, fiber controlled behavior appears to be more complex (and more important), but comparatively little is known about this subject.

Applications and Complementary Efforts:
The present program is also a fundamental core activity around which a larger program of complimentary activities has been built. One element of that effort is a program to develop "Life Prediction Methods for High Temperature Polymer Composites for the HSCT Program," funded by NASA. That program involves characterization of candidate materials for the HSCT, such as K3B-based systems, and the use of those data to support the application of our MRLife simulation code to the prediction of remaining strength and life for such materials at elevated temperatures, in air. That work is being done on notched coupons. That effort serves the present program by providing materials and data, and experience in the characterization and examination of high temperature polymer systems. Some of the work in that program concerned with fundamental issues related to the temperature-dependent behavior of polymer composites overlap with the present program.

Another complementary activity has to do with our MRLife simulation code. That code (series) is updated each August, and has been developed over about 12 years. The code is not sold; it is made available to the community through a users group, called the Predictive Methodology Group, for which users purchase membership in turn for support in learning and running the code. In the last three years or so, the acceptance of the code in the applications community has grown quite rapidly, and the users group has expanded to more than a dozen companies, including Allied Signal, General Electric, Pratt and Whitney, United Technologies, Rolls Royce, Westinghouse, Babcock and Wilcox, Martin Marietta, Johnson & Johnson, Goodyear, Owens Corning, and Boise Cascade. The primary attraction of the code is its' ability to predict remaining strength in the presence of the combined effects of cycle and time dependent degradation processes. *Remarkably, the MRLife code is now being used by every major jet engine manufacturer in the U.S.; it can be said that MRLife has a chance to become an industry standard!*

Personnel Supported

Funding from this program is being used to support a Ph.D. student (Celine Mahieux), and to provide partial support for a post-doctoral research faculty (Scott Case) who directs the simulation work, and some support for hourly help from undergraduate students as needed for library searches, etc. Occasional support is also used for Mac McCord, a laboratory instrument maker to assist in the experimental activities of the program.

Publications

The following publications have appeared or have been submitted:

S.W. Case, R.B. Plunkett, and K.L. Reifsnider, "Simulation Methods for Life and Remaining Strength Prediction of High-Temperature Polymeric Composites Subjected to Cyclic Loads," High Temperature and Environmental Effects on Polymeric Composites, ASTM STP 1302, T.S. Gates and A.H. Zureick, Eds., Am. Society for Testing and Materials, 1997, pp. 35-49

K.L. Reifsnider and S.W. Case, "Mechanics of Temperature-Driven Long-Term Environmental Degradation of Polymer-Based Composite Systems," submitted to ASME Symp. on Durability and Damage Tolerance, I. ME Congress and Exposition, San Francisco, 1995.

K. Reifsnider, S. Case and N. Iyengar, "Recent Advances in Composite Damage Mechanics," Proc. Conf. On Spacecraft Structures, Materials and Mechanical Testing, Grand Hotel Huis ter Duin, Noordwijk, the Netherlands, 27-29 March 1996, ESA SP-386, June 1996 (Plenary Lecture), pp. 483-490

S. Case and K. Reifsnider, "Micromechanical Analysis of Fiber Fracture in Unidirectional Composite Materials," Int. J. Solids Structures, Vol. 33, No. 26, 1996, pp. 3795-3812

K. Reifsnider, S. Case, and Y.L. Xu, "A Micro-Kinetic Approach to Durability Analysis: The Critical Element Method," Prog. In Durability Analysis of Composite Systems, Cardon, Fukuda & Reifsnider (eds.), 1996, Balkema, Rotterdam, p. 3

K. Reifsnider, N. Iyengar, S. Case, and Y.L. Xu, "Damage Tolerance and Durability of Fibrous Material Systems: A Micro-Kinetic Approach," in Durability Analysis of Structural Composite Systems, A. Cardon (ed.), 1996, Balkema, Rotterdam, p. 123

K. L. Reifsnider, "Durability and Damage Tolerance: Testing, Simulation, and Other Virtual Realities," ASTM STP 1242, S.J. Hooper (ed.), American Society for Testing and Materials, 1997, pp. 45-59

Case, S., Caliskan, A. Iyengar, N. And Reifsnider, K.L., "Performance Simulation of High-Temperature Polymeric Composite Materials Using MRLife," Proc. ASME Aerospace Div., ASME, 1996, pp. 375-380

K.L. Reifsnider, S.W. Case and M. Elahi, "Predictive Methodologies for Elevated Temperature High-Cycle Fatigue of Structural Composite Materials," in Structural Materials Symposium Proceedings in Honor of Professor Paul C. Paris, W.O. Soboyejo and T.S. Srivatsan, Eds., the Minerals, Metals, and Materials Society, 1997, p. 461

Caliskan, A.G., Case, S.W., and Reifsnider, K.L., "A Micromechanics Approach to Predict Strength and Stiffness of Polymer Matrix Composites," Proc. Joint ASME/ASCE/SES Summer Meeting, Northwestern University, June/July 1997

Mahieux, C.A., Russell, B.E. and Reifsnider, K.L., 1998, "Stress Rupture of Unidirectional High Performance Thermoplastic Composites in End-Loaded Bending at Elevated Temperatures. Part I: Experimental Characterization of the Failure Mode, J. Composite Materials, Vol. 32, No. 14, pp. 1311-1321

Case, S.W. Iyengar, N. and Reifsnider, K.L., "Life Prediction Toll for Ceramic Matrix Composites at Elevated Temperatures," ASTM Seventh Symp. On Composites: Fatigue and Fracture, May 7-8, 1997; in press

Interactions / Transitions

Our plans for transition of the fundamental work being done on this program have been described earlier, and will include the incorporation of this work into our MRLife code to provide to the applications community. Presently, our interactions with others on the subject of high temperature polymer composites include:

1. NASA Langley, Tom Gates, HSCT program; characterization and life modeling of K3B based composites
2. United Technologies, Hartford, Tony Dennis; durability and life prediction of high temperature composites (members of the users group for MRLife)
3. Pratt and Whitney, West Palm Beach, Ron Cairo; using MRLife; also teaming with that group to propose research.
4. General Electric, Cincinnati, Tom Dunyak; using MRLife; teaming with that group to propose research.
6. Air Force Wright Aeronautical Labs; gave seminar to the structural integrity group, at invitation of Arvind Nagar; also discussing interaction with Larry Zawada; extensive discussions with Nicholas Pagano. During the last three years, Prof. Reifsnider has acted as dissertation advisor and co-chairman of the Dissertation Committee for David Mollenhauer, a Ph.D. student on leave from Wright Patterson AFB. Dr. Mollenhauer completed his doctoral program in August of 1997.
7. Johnson and Johnson; they will be using our MRLife code for polymer composites that are designed to be absorbed systematically by the human body.
8. Wellstream Corporation, Panama City; Mark Kalman: This off-shore company uses polymer composites in their high-pressure flexible pipe. That pipe is being designed with the help of MRLife, with data and models directly taken from the present program. The pipe is scheduled for commercial deployment off the coast of Brazil in mid November of 1998.

9. Goodyear Corporation will use MRLife to predict the life of truck tires to isolate the effect of time-dependent chemical and thermodynamic effects and mechanical degradation as a function of elastomer compounding and mechanical design.

Discoveries / Inventions

There have been no inventions in the program, to date.

Honors / Awards

Dr. Reifsnider is a Fellow of ASTM and the American Society for Composites, and holds the Distinguished Research Award from the latter. He has given over 100 invited lectures in 21 countries. In the last five years, he has given: keynote lectures at the International Conference on the Durability of Composite Systems (Belgium, 1995), the Japan Society of Mechanical Engineers Conference on Composites (Tokyo, 1995), Int. Conf. on Interfaces (Cambridge, 1993), Int. Conf. Materiaux Advances (Paris, 1997); and plenary lectures at DURACOSYS (Belgium, 1993), Fatigue 96 (Berlin, 1996), Int. Conf. Composites Engn. (New Orleans, 1996), European Space Agency (Holland, 1996). Dr. Reifsnider is North American Editor of the International Journal of Fatigue, and the Journal of Applied Composites. This year Dr. Reifsnider gave the R.B. Pond Materials Science Lecture at the Johns Hopkins University, and the Distinguished Polymers Lecture for the Polymer Division of the American Chemical Society at NIST. In the Fall of 1998, Dr. Reifsnider served as Chairman, pro tem, of the National Materials Advisory Board of the National Research Council.

Celine Mahieux, Ph.D. candidate working under sponsorship of this program, has also received several awards this year, including the 1996/97 Paul E. Torgersen Distinguished Research Award for excellence in graduate research (a university wide competition), and honorable mention for the presentation titled "Microbuckling in Unidirectional Fiber Reinforced Polymer Composites" at the 75th annual meeting of the Virginia Academy of Science, 1997.

1 T. L. Smith, *Journal of Polymer Science*, Part A, Vol. 1, 3597, 1963

Appendix I

Effect of Temperature on the Stiffness of Polymer-Based Systems

C.A. Mahieux and K.L. Reifsnider

Effect of temperature on the stiffness of polymer-based systems

C.A. Mahieux and K.L. Reifsnider

1. Introduction

1.1 Interest

Unidirectional composites are often considered to be "fiber controlled" materials. If the temperature has no or little effect on the properties of the fibers (e.g. strength, stiffness), it is often assumed that the properties of the composite will remain constant in the fiber direction, even for large temperature changes.

However if we consider typical numerical values for carbon fiber polymer matrix composites (E_{fiber}=180 MPa, V_{fiber}=20%, E_{matrix}=4.10^3 MPa below Tg and E_{matrix}=1 MPa above Tg) and calculate the stiffness of a unidirectional composite according to a simple rule of mixtures, we get an axial stiffness E_{11} of the overall composite of 30 MPa below Tg and 27 MPa above Tg. In the axial direction the stiffness change is of 11% for the overall composite (this change would be 20% for a polymer composite reinforced with 50% of E-glass fibers). This trend is accentuated for low volume fractions of fibers. In the transverse direction, the change in the stiffness of the same composite in its glassy and rubbery state would be of one order of magnitude.

These very basic computations demonstrate the fact that the variation of the stiffness of the composite with temperature can not be ignored, even in the axial direction of "fiber-dominated" composites.

Macromechanics models and durability tools require a knowledge of the composite quasi-static properties. Most of the tests to evaluate these properties require laboratory work and destructive testing. Ideally, we could eliminate those if we knew the evolution of the properties of the composites' constituents under service conditions.

Composite materials are more and more extensively used over wide ranges of service conditions. Therefore it becomes necessary to have an accurate description of the variations of the material properties under various and extreme conditions. In our case, we will focus on temperature. To enable the use of polymer matrix composites within a transition region, we need to be able to analytically describe the changes of the polymers'

properties with temperature. In this paper, we will restrict our discussion to changes in the stiffness of the material.

The goal of this study is to establish an explicit engineering relationship between stiffness and temperature of a polymer that can be easily integrated into micromechanics models. This relationship can be applied to any polymer (thermosets, thermoplastics, amorphous, linear, semi-crystalline, cross-linked, low molecular weight, high molecular weight materials…) for the entire range of temperatures: from the glassy state to the flow region. This model will enable us to quantitatively describe the stiffness changes across the transition region (without making or testing the material) and to evaluate the overall composite performance through the entire temperature range.

1.2 Background

In the literature, a very small number of studies deal with explicitly relating the changes in the modulus of the polymer to variations of temperature. In the rubbery region however, the temperature dependence is fairly well established[1]. In this region, the modulus can be computed using equation (1):

$$E = \frac{\rho RT}{M_c} \qquad (1)$$

where M_c is the molecular weight between cross-links. However this dependence can only be applied above the glass transition of the material.

In the glassy state, different theories enable us to compute the modulus variations when they are small. For example, Van Krevelen[2] suggests the following relationship:

$$G = G(T_{ref}) \cdot \ln\left[\left(\frac{T_{ref}}{T_m} - \frac{T}{T_g}\right) + e^1\right] \qquad (2)$$

where G is the shear modulus, and the subscripts m and g refer to melting and glass transition. However, this equation only applies to the glassy state and does not relate to the microstructure of the polymer.

Computational theories also enable an accurate description of the variation of the crystalline phase of the polymer modulus with temperature. These theories are complex and are usually restricted to one polymer and a fairly limited temperature range[3].

One can note that most of the literature focuses on the effect of time upon the stiffness of the polymer (KWW[4], Rouse[5], the traditional viscoelastic models[6] (spring and dashpots) and the time-temperature equivalence (WLF[7])). However, none of these equations explicitly relate modulus and temperature. Other shortcomings of these equations are as follow:

- The KWW equation does not consider the details of the polymer microstructure and require the use of relaxation times. The concept of relaxation time is not well established and is still being discussed[8].
- The Rouse model does not work over large temperature ranges[6].
- The viscoelastic models are only applicable to the viscoelastic region (above Tg) and are phenomenological. Furthermore, we also need to consider cases where the mechanical response of the material is instantaneous and does not allow enough time for a viscoelastic response. Impact and fast strain rate experiments illustrate this need.
- The WLF equation is semi-empirical and is only a time-temperature equivalence tool. A relationship between modulus and temperature can not be obtained through the WLF equation (unless an accurate modulus versus time scheme is established). As transition temperatures are easier to measure and interpret than relaxation times, we will therefore concentrate on expressing the stiffness of the material as an explicit function of temperature. Further work could focus on the rate or time-dependency of the modulus using time-temperature superposition schemes. However, this case will not be included in the present paper.

We would like to adopt a more general approach than the existing theories listed above, and be able to describe the polymer behavior over the entire temperature spectrum, including the transitions, and relate the mechanical response of the polymer to its microstructure. From a thermodynamical standpoint, one can relate the Gibbs energy G to the temperature T, the pressure P and the compressibility K[9] by:

$$\left[\frac{\partial^2 G}{\partial P^2}\right]_T = -K \cdot V \qquad (3)$$

If we knew the form of the Gibbs free energy in the transition regions, we could directly integrate equation (3) to obtain an explicit relationship between modulus and temperature. To the authors' knowledge, such a description of Gibbs energy for a polymer on the entire temperature range (glassy to flow) has not yet been established. For this reason, the present study introduces the concept of statistics of bond survival as a possible scheme to predict the temperature dependence of the modulus of any polymer.

The nature and magnitude of relaxation mechanisms in polymers vary as a function of various parameters. We can divide the parameters influencing the modulus of a polymer into two categories: the parameters intrinsic to the state of the polymer, such as nature of the polymer (cross-linked, semi-crystalline, amorphous), the percent of crystallinity, the density, the molecular weight, the transition temperatures and the chemical structure. The second category includes the extrinsic parameters (experimental conditions): strain and deformation state, strain rate and frequency, moisture, and time and temperature. Variation of the extrinsic parameters can induce a variation of the intrinsic parameters. For example a variation of straining temperature can induce a change in the percent of crystallinity of the material, can modify the glass temperature of the polymer and alter the molecular conformation of the molecules. The different parameters previously stated are not independent and are often related. We will focus on the influence of temperature on the state of the polymer and try to integrate microstructure into the analysis. As molecular weight and crystallinity seem to be the most widely studied in the literature among all of these parameters, we will mainly focus on these two parameters. However our study can be extended to the case of crosslinked polymers.

Section 2 of this paper summarizes the molecular behavior of a typical polymer with temperature. The discussion focuses on the evolution of the states of the inter/intra-molecular bonds when temperature changes. The statistics of the process is discussed and a scheme is established to enable the direct calculation of the elastic modulus of the polymer as a function of temperature. In section 3, analytical results are compared to experimental data excerpted from different sources in the literature. Results for various

polymers exhibiting secondary relaxations, and copolymers are shown. Our own experiments on various polymers are presented in section 4 and compared to the analytical predictions in section 5. Finally, the implications and the limits of this model are discussed (section 6) and recommendations for future work are suggested in section 7.

2. Theoretical modeling

The well-known modulus versus temperature curve for a typical polymer exhibiting a secondary relaxation is illustrated by Figure 1.

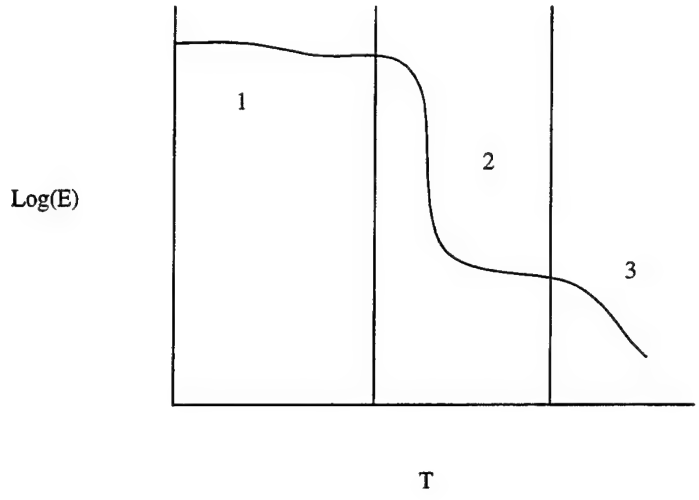

Figure 1. Modulus versus temperature for a typical polymer.

We will not detail the molecular motions that have been carefully reviewed in other studies. We will rather focus on the behavior of the inter- and intra-molecular bonds, as discussed by Ashby[10]. The two types of bonds, the strong covalent intramolecular covalent bonds and the weak bonds between two different molecules, are shown schematically in Figure 2.

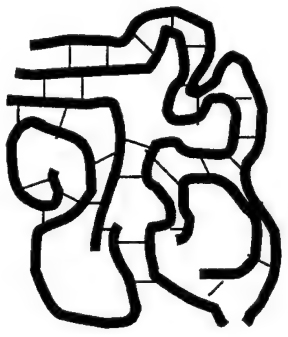

Figure 2. Schematic of bonds in polymer materials.

Region 1, commonly referred as the glassy region is characterized by a quasi-elastic behavior of the polymer. The modulus is constant over a long range of temperatures and most of the bonds stretch without breaking. However, for some polymers, the thermal energy is high enough to allow rotation of side groups. For this situation one (or several) secondary relaxations can be observed, characterized by a significant drop in the modulus. In this case, the secondary bonds need to break to allow the side groups to rearrange. However the activation energy required for this very local movement is low, and these relaxations can occur at low temperatures (lower than the glass temperature).

The alpha transition, also referred as the glass transition, results in a dramatic drop in Young's modulus (region 2) followed by a plateau (rubbery region). In region 2, the molecules start sliding against each other[10]. However the movement of the molecules is still restricted by the presence of entanglement, cross-links, crystallites, fillers... The movements of a molecule can be thought as trapped in a tube (concept of reptation introduced by De Genne[11]), where the molecule can move in a snake-like fashion (Figure 3). In order to be able to reptate, the molecule needs to break secondary bonds (referred as "bond melting" by Ashby[10]) as in the case of the secondary relaxation, but over a large part of each molecule. However in this region, some elastic parts still survive and the molecular chain will keep some memory of its original position. As temperature is further increased, all of the secondary bonds are broken and the molecules can move freely (unless crosslinks are present); the modulus of the polymer starts dropping again (viscous flow, region 3).

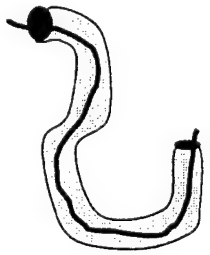

Figure 3. Reptation.

Spring and dashpot models lead us to discuss relaxation times as a representation of local behavior. The relationship between modulus and temperature is often written as:

$$E(t) = \sum_{i=1}^{N} E_i \exp\left(-t/\tau_i\right) \qquad (4)$$

Where τ_i are the relaxation times. One can define the distribution function H as:

$$H(\tau) = \tau E(\tau) \qquad (5)$$

Equation (4) can then be written as:

$$E(t) = \int_{-\infty}^{+\infty} H(\tau) \exp\left(-t/\tau\right) d(\ln \tau) \qquad (6)$$

In the viscoelastic region, reptation is sometimes[10] modeled by an equation of the type:

$$E \propto \exp\left(-\frac{Q}{RT}\right) \qquad (7)$$

Where Q is the activation energy of the process. However, When one bond breaks, there is a non-negligible influence on the other bonds. If we consider the process of bonds rupture, a Weibull distribution[12] would seem to be more appropriate than the Boltzman distribution of equation (7). Let us first consider the beta transition. The mechanical response is driven by the motion of small chain segments (only a few monomers long). Considering the number and strength of the bonds involved in this relaxation process we can associate a Weibull coefficient m_1 to the beta relaxation. In this case (6) becomes for the beta transition:

$$H_1(\tau) = \exp\left(-\left(\frac{t}{\tau_1}\right)^{m_1}\right) \qquad (8)$$

or exchanging time for temperature[6] for instantaneous response and introducing a conversion constant:

$$H_1(T) = H_0^1 \exp\left(-\left(\frac{T}{\beta_1}\right)^{m_1}\right) \qquad (9)$$

Where β_1 is the characteristic temperature (i.e. beta transition temperature) and H_0^1 a reference value for the beta transition (i.e. magnitude of the relaxation). For the following transitions (alpha, flow), the number of segments involved in the relaxation

increases. For each relaxation, new Weibull coefficients related to the number of bond failures required for a given relaxation to occur and to the strength of the intermolecular bonds can be associated with the relaxation.

Finally, as we have different mechanisms occurring, we can sum the different components:

$$E = \sum_{i=1}^{N} H_i \exp\left(-\left(\frac{T_i}{T_{ref_i}}\right)^{m_i}\right) \qquad (3)$$

In our case, we will consider one to three transitions (1<N<3). The H_i coefficients (magnitude of the transition step) can be obtained by different means. We can subtract the value of the material's stiffness before and after the transition, leading to equation (4) (case of a material that does not undergo any transition prior to flowing), equation (5) (material with two transitions, e.g., glass and flow) and equation (6) (material undergoing three transitions, e.g., beta, glass and flow):

$$E = E_1 \exp\left(-\left(\frac{T}{T_3}\right)^{m_3}\right) \qquad (4)$$

$$E = (E_1 - E_3)\exp\left(-\left(\frac{T}{T_2}\right)^{m_2}\right) + E_3\left(-\left(\frac{T}{T_3}\right)^{m_3}\right) \qquad (5)$$

$$E = (E_1 - E_2)\exp\left(-\left(\frac{T}{T_1}\right)^{m_1}\right) + (E_2 - E_3)\exp\left(-\left(\frac{T}{T_2}\right)^{m_2}\right) + E_3\left(-\left(\frac{T}{T_3}\right)^{m_3}\right) \qquad (6)$$

The T_i correspond to the temperatures at each transition (as given by the maximum of the peaks on the tangent delta versus temperature of a DMA curve, or by the inflection point of a DSC plot) in Kelvin. The remaining difficulty is for the flow region. In this first approach, we will not try to detail the behavior of the material in the flow region. We will only show the applicability of this approach to the flow region by using flow temperatures given in the literature.

The E_i represent the intantaneous stiffness of the material at the beginning of each plateau or region. E_1 is the instantaneous modulus at very low temperature of the

polymer, E_2 is the instantaneous modulus right after the beta transition, E_3 is the instantaneous stiffness at the beginning of the rubbery plateau. A reliable experiment leading to consistent values for stiffness measurements is the ultrasound method. The obtained modulus corresponds to a tensile experiment performed at very high strain rate or cyclic frequency. The drops in modulus in the different regions (H_i) represent the "importance" of the relaxation processes. These values depend on the chemistry of the polymer (stiffness of the backbone), molecular weight, crystallinity and degree of crosslinking. An increased crystallinity will produce only a slight increase in the glassy state stiffness but can produce a large rise in the value of the modulus of the rubbery plateau. Therefore, the magnitude of the glass transition step will decrease as the crystallinity is increased. The transition temperatures will also be increased as the crystallites impede the rearrangement of the molecules under the applied stress. Increased molecular weight and cross-linking will stiffen the material to a lesser extent.

The last parameters (m_i) are Weibull moduli, corresponding to the statistics of the bond breakage. To allow rotations of side groups for the secondary relaxations, the strength of the bonds that need to be broken depends on the relative position of the side group to the other molecular chain. Therefore there will be a wide distribution of bond strengths and we would expect m to be small. Reptation involves translation of the main chains. If the material is very homogenous (narrow distribution of bond strengths) as in the case of amorphous materials, we would expect m to be very large. However, this parameter is going to depend on the degree of impediment of the molecular motion (cross-linking, molecular weight and crystallinity...). If the movement of the molecular chains is severely restricted at precise locations (by crosslinking, etc), we would expect m to be really low (approaching a Boltzman distribution). For crosslinked materials the slope of the drop in the viscous flow region will decrease with increasing degree of crosslinking. For heavily crosslinked materials, the flow region can even disappear.

One might question the form of these equations, thinking that these equations would fit any curve, given that we fix the height of the plateau and the temperatures. However, we must first remember that these equations have a physical basis: in order for the relaxations to occur, the secondary bonds need to break. In polymers, there is a distribution of these molecular bond strengths. The number of segments involved also

varies from one relaxation to the other (always increases as the temperature increases). Finally when one of the secondary bond breaks, other bonds are influenced (in the manner that broken fibers interact with unbroken fibers in a fiber bundle). Secondly, the reference temperatures and moduli can be independently measured or calculated. The reference temperatures correspond to the inflection point of the transitions and not the temperature (T_i) corresponding to the plateau's height (E_i). Therefore we are not forcing the value of the modulus at any temperature. The reader might also notice the similarity of the mathematical form of equation (3) with the KWW equation[4]. These two equations are stretched exponentials. However the differences can be noted as follow:

- equation (3) is based on physical considerations (bond failure)
- equation (3) refers to measurable, well defined physical quantities (transition temperatures and instantaneous stiffnesses)
- equation (3) is applicable on the entire temperature range (up to flow of the polymer).

To validate this new approach, the curves generated by equation (6) are compared to the experimental data found in the literature in section 3.

3. Feasibility

To validate the feasibility of our approach we used some data on some random polymers available in the literature. We will not get into the detail of the fitting in this section. The parameters will be discussed in great detail in section 4.

3.1 Literature data

For details on how the experimental results were obtained, we will refer to the different authors.

Equation (6) was first used with PMMA. The experimental data from Ashby[10] were taken on the amorphous linear polymer.

The second set of experimental data used was the variations of the loss shear modulus of PVDC from Schmieder and Wolf[13].

The storage modulus (measured at 1 Hz) of a high molar mass Thiophene-based poly(arylene ether ketone) from Brennan et. al.[14]: poly(1,4-BFB, BisA), M_n=20 000 $g.mol^{-1}$ was also compared to our model.

The model was also compared to the experimental data for the loss modulus of a polyethylene oxide-salt complex $(PEO)_{0.82}(Fe(SCN)_3)_{0.18}$ measured at 3 Hz (M_w=600 000) from Bartellota et. al.[15].

Two poly(ether ether ketone)-polymethylsiloxane block copolymers were also studied using data from Risch et. al.[16]. PEEK-PSX copolymers were obtained from PEEK block with a number average of 4900 (5K) and PSX block number-average molecular weights of 3200 (3K) and 4900 (5K). In this case we used equation (6) to model the presence of two glass transitions.

The results are shown in Figure 4, 5, 6, 7, 8 and 9. Surprisingly the m_1, m_2, and m_3 coefficients were consistently equal to 5, 20, 20 for all materials except for the Thiophene-based poly(arylene ether ketone), where m_3 = 1 due to the high degree of cross-linking.

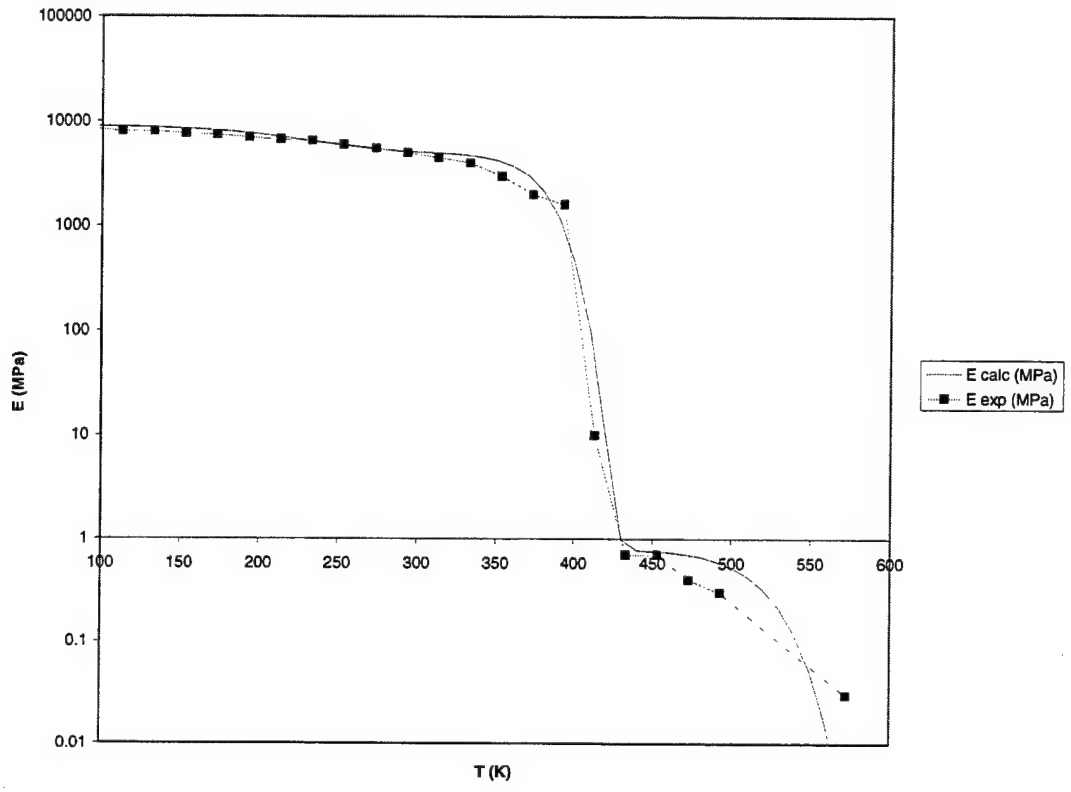

Figure 4. PMMA.

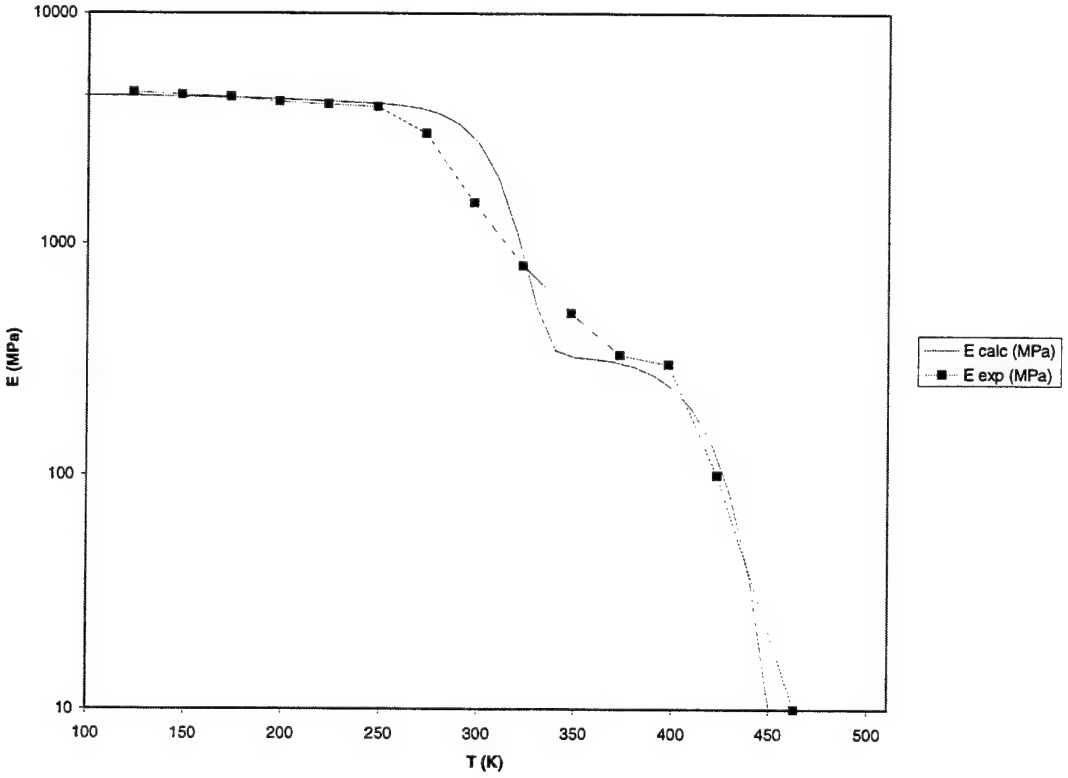

Figure 5. PVDC.

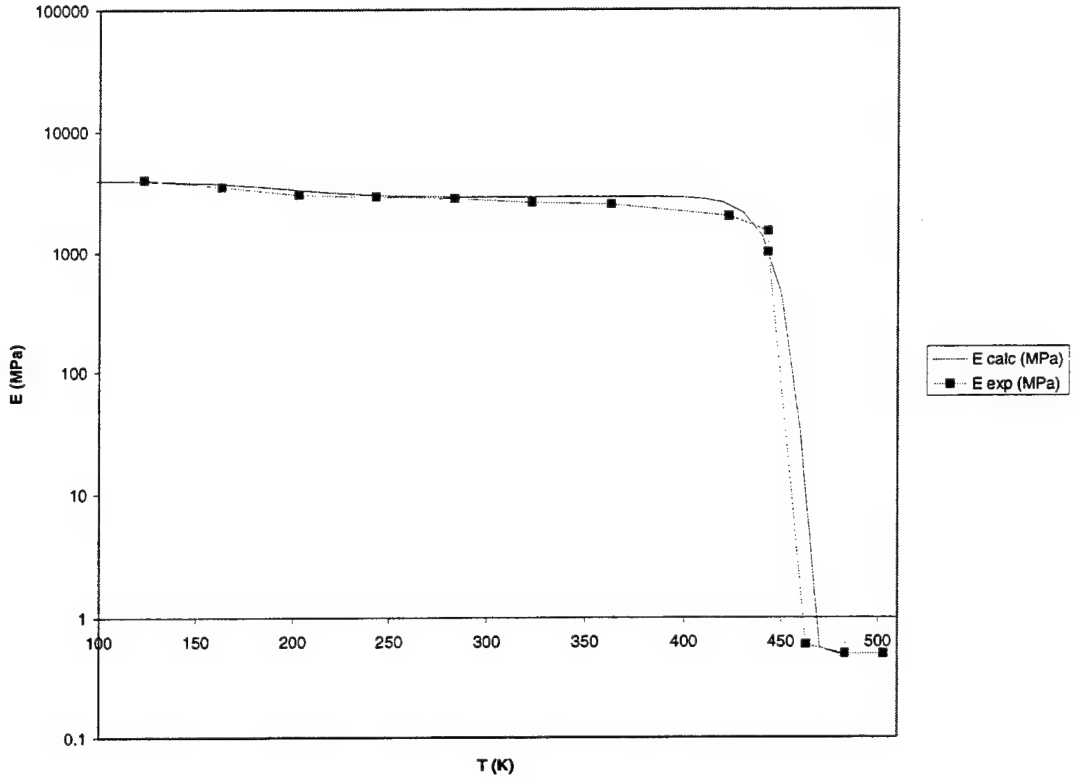

Figure 6. Poly(1,4-BFB, Bis A).

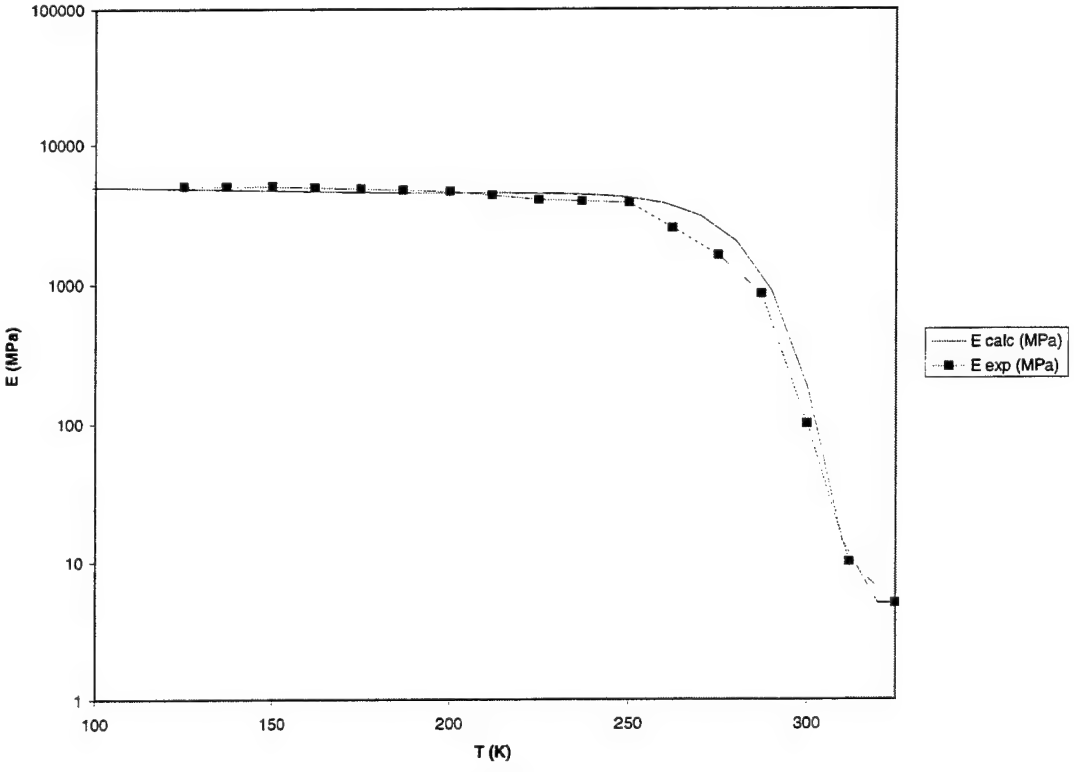

Figure 7. $(PEO)_{0.82}(Fe(SCN)_3)_{0.18}$.

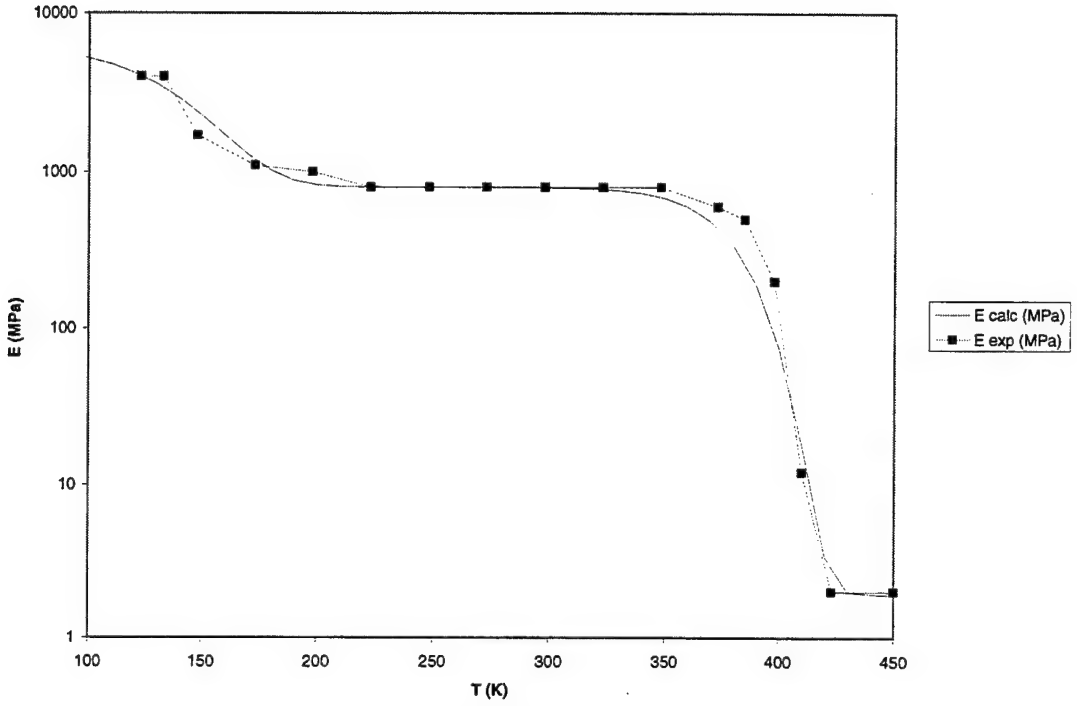

Figure 8. PEEK(5K)PSX(3K).

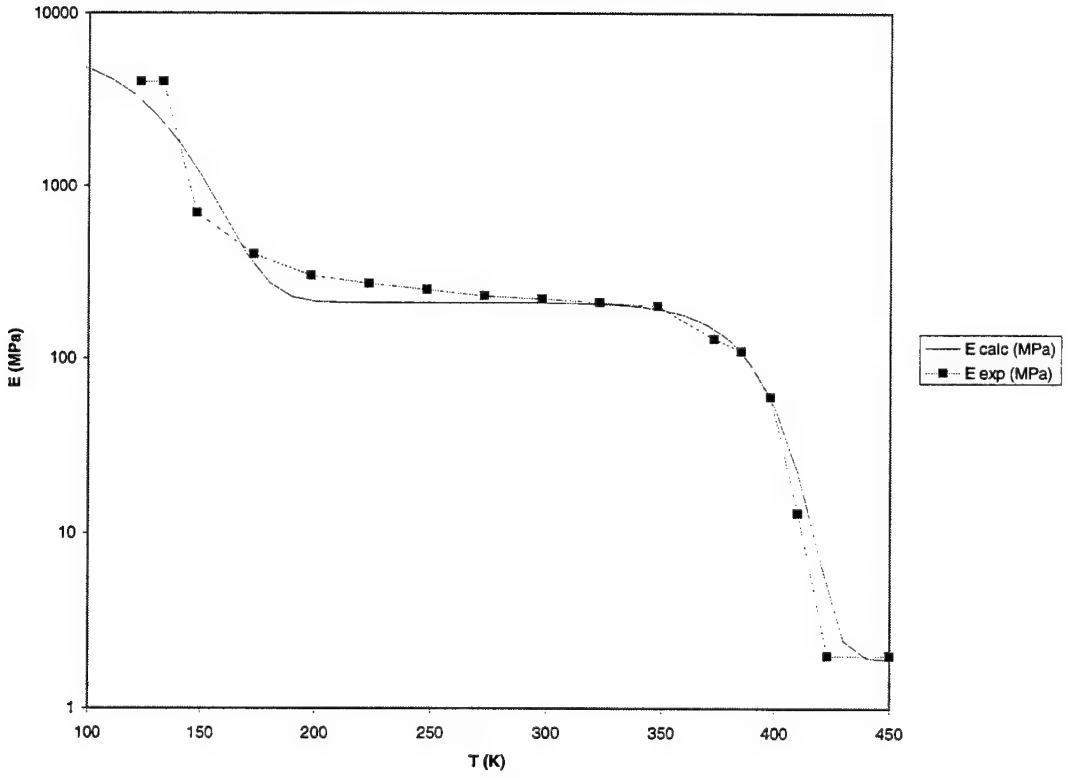

Figure 9. PEEKt(5K)PSX(5K).

3.2 Discussion

The model fits the data successfully even for extreme temperatures. Equation (6) seems to describe the behavior of polymers with temperature. However, in order to use equations (4), (5) and (6) in a systematic manner, we need to be able to compute all the parameters or to obtain them from independent experiments.

The biggest challenge is to understand the significance of the m_1, m_2, and m_3 parameters in equations (4), (5), and (6). The m_1 and m_2 coefficients were consistently equal to 20 for all the two-transition polymers described in part 3.1. Intuitively, it seems that the m_2 and m_3 coefficients must be related to the degree of impediment of the molecular motion in the different regions, i.e., crystallinity, crosslinking, molecular weight... We can observe the fact that the m_2 coefficient drives the slope of the glass transition. The m_2 coefficient, almost constant for our previous cases, might be related to the breadth of the molecular weight distribution or to the percent of crystallinity. However it is difficult to get details on the chemical properties of the materials used in the experiments excerpted from the literature.

Further experiments were required to determine if these coefficients remain constant for polymers with very different properties (i.e., molecular weight and crystallinity). Careful systematic experiments were performed and are presented in section 4.

4. Experimental work

The purpose of the experimental study was to establish if the model could be applied to various commercial polymers, thermoset and thermoplastic with very different properties (molecular weight and crystallinity).

4.1 Materials selection

The different polymers were arbitrarily chosen. Three thermoplastics: Poly(methyl methacrylate) (PMMA), Poly(ether ether ketone) (PEEK) and Poly(phenylene sulfide) (PPS), one thermoset: Poly(butadiene), and one composite: AS4/PPS were selected.

4.1.1 PMMA

PMMA is a linear amorphous thermoplastic.

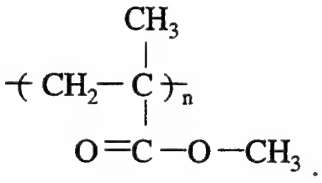

This polymer is characterized by its transparency. The glass transition for the polymer is 105°C (221F), the heat deflection temperature is between 74 (167F) and 100°C (212F)[17]. This polymer exhibits the presence of secondary relaxations. The beta transition occurs around 0°C[10]. The density of the polymer is 1.188 g/cm^3 [18]. Commercial PMMA (plexiglas) typically has high molecular weights with broad distributions. High molecular weight material can be obtained by pouring low-molecular-weight polymer and monomer into a mold. During polymerization autoacceleration occurs (the molecular weight increases dramatically owing to a suppression of the termination step)[18]. The molecular weight may be over 10^6 g/mole. Two different grades of plexiglas were obtained from Rohm and Haas. Little information could be obtained from the company concerning the molecular details of the material.

- plexiglas MC: Low molecular weight PMMA Mw around 150 000 g/mole. Traces of ethyl acrylate (EA) can be found in the polymer.

- plexiglas G: very high molecular weight PMMA (around 10^6 g/mole).

The samples were supplied as 10.15x10.15 mm (4"x 4") plates with a thickness of 3 mm.

4.1.2 PEEK

PEEK is a linear aromatic polymer.

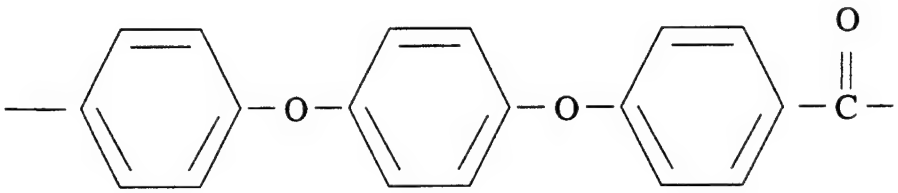

From the literature[19], the glass transition is 143°C (289F) and the melting point is 334°C (633 F). PEEK also has a beta relaxation around –30°C for the crystallized material[20]. The temperature of maximum crystallization from melt is 256°C (493F) and 185°C (365F) from solid. The specific gravity of the amorphous phase is 1.265 and 1.320 for the fully crystalline state.

Different grades of PEEK were supplied by Victrex.

- 150 G: with a melt viscosity (MV) of 0.150 kN.s.m^{-2}.

- 450 G: with a melt viscosity (MV) of 0.450 kN.s.m^{-2}.

The molecular weight (as given by light scattering) can be calculated from these values[21]:

$$\log_{10}(MV) = -15.06 + 3.21\log_{10}(Mw)$$

- 150G: Mw = 27 222 g/mole.

- 450G: Mw = 38 331 g/mole.

The material was supplied as pellets.

4.1.3 PPS

PPS is a linear polymer.

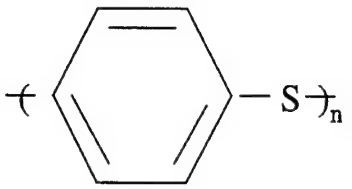

The melting as found in the literature[19] is of 285°C. The crystallization temperature is around 230°C from melt and 130°C from solid. The glass temperature is around 85°C. Two grades of PPS were supplied by Phillips Petroleum Company: PR09 and PR10X2. According to Phillips[22], the typical molecular weight for the grade PR09 is 65 000-70 000 g/mole. PR10X2 has a lower molecular weight, around 55 000 to 65 000 g/mole. These numbers were determined by exclusion chromatography. The supplier claimed that scatter of the results is typical and stated that these numbers can vary by as much as 10%. The PPS from Phillips was in a powder form.

Another grade of PPS (0320 PO) was supplied by Fortron Celanese. The molecular weight for this material could not be determined. The PPS Celanese was received as pellets.

Note 1: For the last two thermoplastics, one must keep in mind that the molecular weights are approximate, considering the difficulties in measuring the molecular weight of these two materials (due to the poor solubility).

Not 2: Also the different temperatures are just indications and vary depending on the molecular weight and crystallinity of the polymers.

4.1.4 Rubber

Polybutadiene is a thermoset (elastomer) with the following molecular structure:

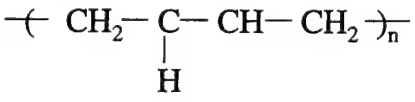

Polybutadiene was supplied by Goodyear in three different grades: 50 000 g/mol, 100 000 g/mol and 240 000 g/mol. The first molecular weight was too low and the material would flow even at room temperature.

4.1.5 Composite

AS4/PPS material was provided by Baycomp. The volume fraction of fibers was 50% in volume. The material was supplied as a 0.5" x 0.04" rolled tape.

4.2 Materials processing and samples preparation

Unlike PMMA and polybutadiene that did not need any further modification before testing, PPS and PEEK needed to be put into a plate form in order to be tested.

4.2.1 PEEK processing

The first attempt to process the PEEK was done by compression molding of the pellets of PEEK 150 following the instructions from Victrex[23]. The mold was charged with 102% of the theoretical weight of the polymer required to forming the component (0.5 lbs). The 152 x 152 mm (6"x 6") mold was then placed in a hot press at 400°C (752F) for 20 minutes. Then the heat and pressure loads were disabled and the mold was left on the lower plate of the press until room temperature was reached. At this point we realized that most of the material had escaped from the mold, leaving only an extremely thin film of material on the bottom of the mold.

The second attempt to process the PEEK was made by injection molding. Robert Young (Department of Chemical Engineering, Virginia Tech) injected the polymer according to the procedure described in the literature[24]: the polymer was injected using an Arburg Allrounder Model 221-55-250 in a 75 x 80 x 1.6 mm mold. The injection pressure was held constant at 5 MPA, the holding pressure at 10 MPa and the flow at 10 cm^3/s. The temperature was varied from the "solids conveying zone to the nozzle": Zone 1: 380°C, Zone 2: 400°C, Zone 3: 400°C, and Zone 4: 400°C. The temperature of the mold was 200°C.

4.2.2 PPS processing

The PPS Celanese was received as pellets. The PPS from Phillips was received as powder straight from the reactor. The material was pelletized in an extruder at around 290°C. The PPS powders were injection molded following the same procedure than in the PEEK case. The temperatures of the different zones were Zone 1: 250°C, Zone 2: 290°C, Zone 3: 280°C, and Zone 4: 270°C. The mold was at 140°C.

4.2.3 Samples making

For each material the samples were made by sawing the plates using a band saw in dry conditions. The final samples had a size of 25.4 x 6.35 mm (1" x ¼") for the DMA samples ("long samples"). Some extra smaller samples were also cut off the plates for DSC testing ("short samples"). The thickness of the final samples was approximately 3 mm for the PMMA and 1.5 mm for PEEK and PPS.

4.3 Crystallinity modifications

Each semi crystalline material: PEEK 150, PEEK 450, PPS PR9, PPS PR10, PPS Celanese, AS4/PPS composite, was tested as received. Then various heat treatments were applied to the samples in order to modify the crystallinity of the various polymers.

4.3.1 Reaching the maximum crystallinity of the material

4.3.1.1 PEEK

In order for the material to reach the highest crystallinity level possible, the specimens were annealed at elevated temperatures for relatively long times (PEEK and PPS are fast crystallizers). The PEEK samples (2 long samples, 1 short sample) of each grade were placed on an Aluminum plate in the oven (fisher scientific isotemp vacuum oven model 282A) at 180°C (crystallization temperature) for one hour.

4.3.1.2 PPS

Similarly, the PPS samples were placed in the oven at 130°C for 1 to 3 hours (for Celanese material).

4.3.1.3 Composite

The composite was placed at 130°C for several hours in the oven.

4.3.2 Getting amorphous material

The process of getting amorphous polymers is more complex because of the fact that PEEK and PPS are very fast crystallizers. Several tries have been necessary to achieve satisfactory results. One must also note that very high temperatures are involved and the use of a tube furnace (Labline model 4305, inner diameter: 78 mm) was necessary. The temperature was recorded by a thermocouple twisted on a screw attached to the aluminum plate. The temperature in the oven varies by 10F when compared to the set point of the furnace.

4.3.2.1 PPS

The first attempts were made on the PPS Celanese material. The first sample was placed on a 10mm thick plate coated with some release agent (TFE release agent for preheated molds, Miller Stephenson, MS-136 N(CO2)) then put in the furnace at 330°C for a couple of minutes then quenched in ice water. This sample was found to have a crystallinity similar to the fully crystalline material. We guess that the specimen did not have time to reach the melting temperature. The specimen even crystallized some more.

A second specimen was put in the oven for 1 hour 30 minutes at a temperature of 330°C then quenched in ice water. The sample maintained its overall shape. However the corners of the sample became a little bit rounder and some small bubbles (less than 0.5mm diameter) appeared on the side that was in contact with the aluminum plate. The obtained specimen was dark brown and transparent.

As the feasibility of the process was established, the specimens were treated in a more systematic way. For each type of PPS, 2 long specimens and 1 short specimen were placed on the 75 x 38 x 10 mm aluminum plate (the preheated mold was previously sprayed with release agent) at temperatures around 330°C for more that 1 hour then quenched in ice water (Figures 10 and 11).

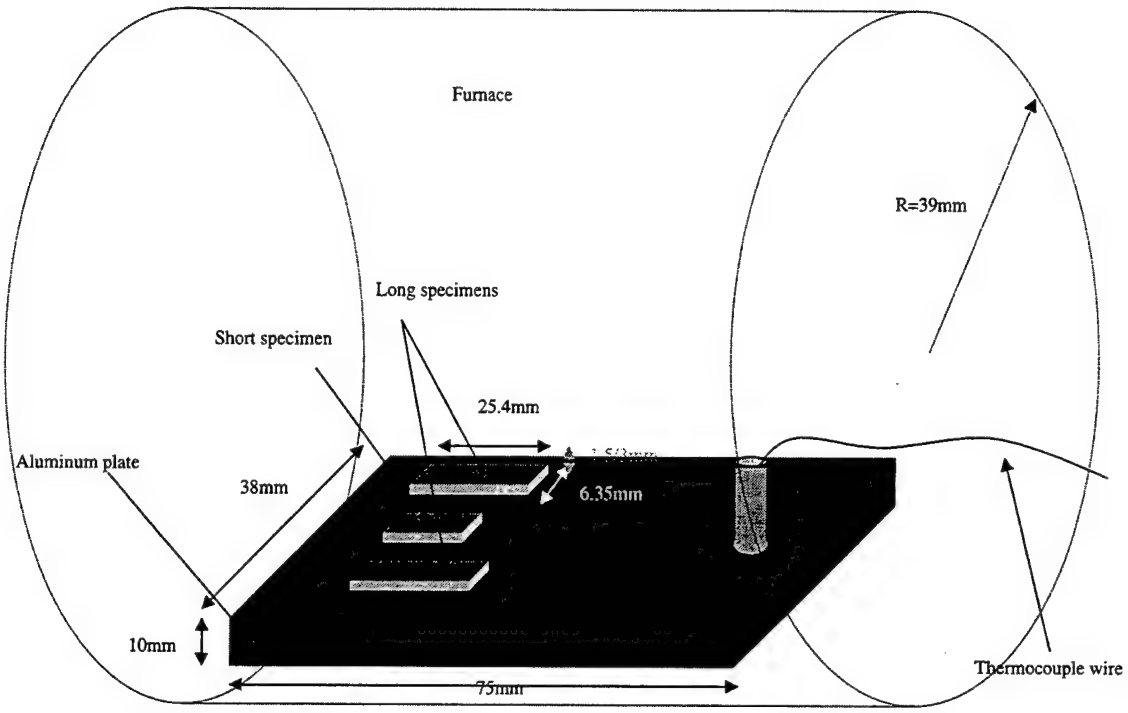

Figure 10. Specimens in the tube furnace.

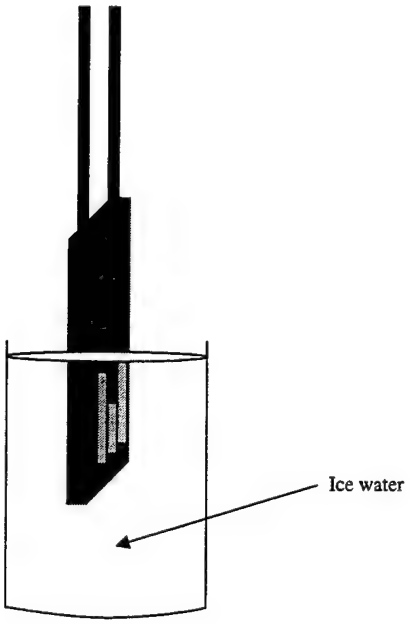

Figure 11. Quenching of the samples.

The exact procedure for each sample and observations can be summarized as follows:

-PPS Celanese: the samples were left in the oven at 330°C for 1 hour 30 minutes then quenched in ice water. The resulting samples had a regular shape, small bubbles on one side (contact with Aluminum plate) and are very transparent.

-PPS PR09: the samples were left for 1 hour at 330°C then quenched ice water. The resulting specimens maintained most of their original shape but exhibited a lot of bubbles on one side (up to 2mm diameter). The samples were transparent.

-PPS PR10: the samples were placed in the oven for 2 hours at 330°C. Then quenched in ice water. As the specimens were still opaque, they were put back in the furnace at a slightly higher temperature (340°C) for one hour. The specimens were quenched again in ice water. The specimens retained their shape, no bubbles appeared on the surface of the samples, the color turned very dark brown but remained opaque.

4.3.2.2 PEEK

Using the same methods, the crystallinity of the PEEK samples were modified:

-PEEK 150: the 3 samples were placed on the aluminum plate and in the tube furnace at 365°C for 1 hour 30 minutes, then quenched in ice water. Due to the low molecular weight, the samples flowed. They were reshaped to their original shape by using the alternating saw. The obtained samples are a little bit smaller and wider than the original samples. The samples were mainly transparent. However, one can note the presence of darker spots (clouds).

-PEEK 450: the changes for the higher molecular weight PEEK were more difficult to perform, due to the facts that the material retains its chemical and mechanical integrity at higher temperatures. The first samples were placed in the furnace at 365°C for one our then taken out of the furnace. At these points it was clear that the specimens did not melt entirely. The specimens were put two extra hours in the oven. The furnace went up to 455°C and the specimens were burnt. 3 more samples were placed in the oven at an intermediate temperature: 365°C for two hours. The resulting samples retained their shapes, did not exhibit the presence of bubbles and were fully transparent.

4.3.3 Getting intermediate crystallinity

4.3.3.1 PEEK

Intermediate crystallinity values were obtained for PEEK by putting the amorphous specimens in the oven at 180°C for one to two minutes then taking them out of the oven, and letting them cool at room temperature. PEEK is a very fast crystallizer. If the specimen was in the oven for more than 2 minutes, the sample became fully crystallized. But one minute was just enough for the specimen to get to temperature, and the percent of crystallinity was very low.

4.3.3.2 PPS

Intermediate crystallinity samples were obtained similarly: the specimen was put in the oven at 130°C for 2 minutes then taken out and let cool down at room temperature.

4.3.3.3 Composite

The composite was taken as received and placed in the oven at 130°C for two minutes.

4.4 Material characterization

Two methods were used to measure the crystallinity of the different samples.

4.4.1 Density measurements

Density measurements were performed on the different polymers as received and on the fully crystallized samples. Density measurements are only valid if the material is gas free. To check if our samples met this requirement, the material as received and fully crystallized was X-rayed. It can be observed in Figure 12 that the material seems to be adequate for this testing.

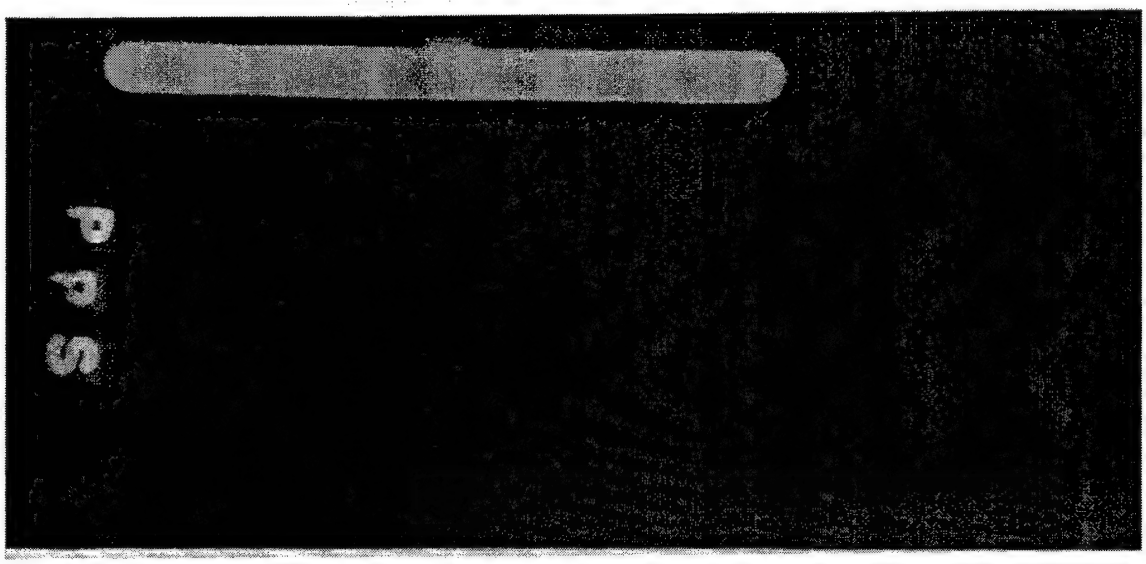

Figure 12. X-rays of PPS Celanese.
Plate as received and two specimens after1 hour at 130°C.

The specimens were first weighed in air then in distilled water, making sure that no air bubbles were trapped around the specimen. The temperature of the water was recorded at the beginning and at the end of the series of measurements. The procedure set up using a Mettler Toledo kit for AT/AG and PG/PG-S/PR balances is shown in Figure 13.

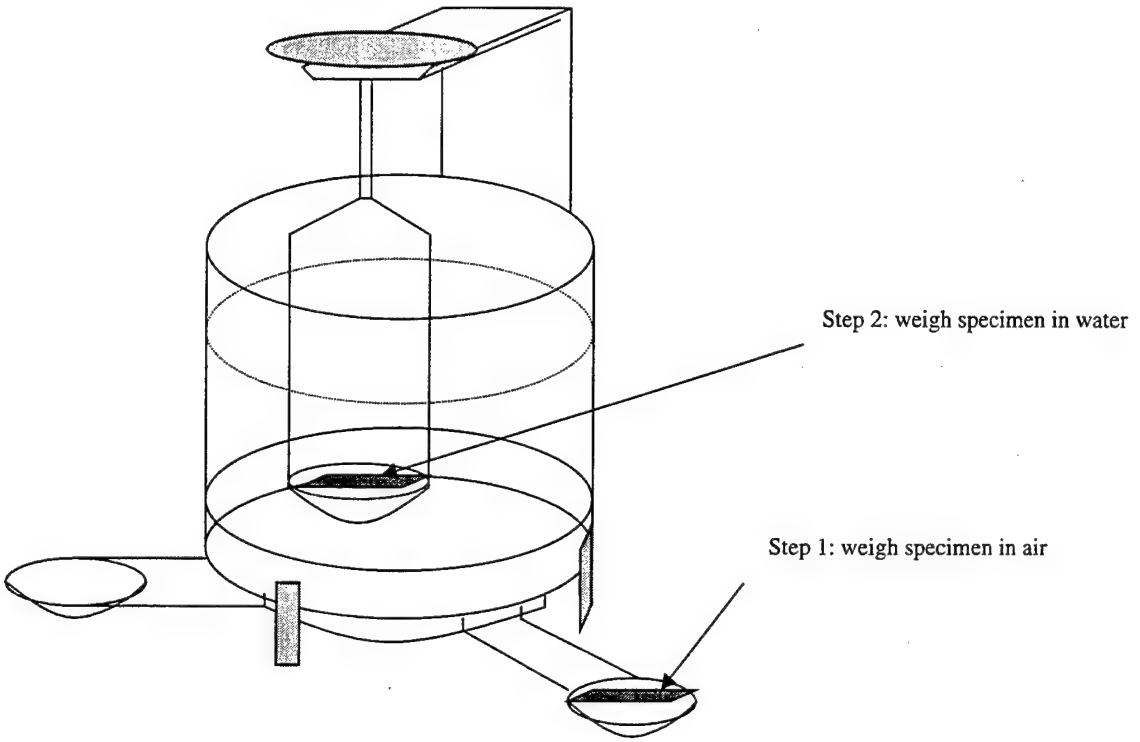

Figure 13. Density measurements set up.

Three measurements were performed per sample. The measurements in air were very reproducible. The measurements in water show an error smaller than 1%.

The density is determined by Archimede's principle:

$$\rho = \frac{A}{A-B} \times \rho_o \qquad (7)$$

Where ρ is the density of the sample, A is the mass of the sample in air, B in the distilled water, and ρ_o is the density of the distilled water. This last quantity varied with temperature[25].

Table 1 summarizes the different measurements at a temperature varying between 26.5°C and 27°C.

The error indicated in Table 1 is the absolute error ($Max_{i=1,3}(abs(d_i - d_{av}))$). To check the results, the density of the PMMA G sample was also measured. The density of this amorphous polymer was found equal to 1.181. In the literature[18] the reported density is 1.188 (relative error $\frac{d_{theory} - d_{experimental}}{d_{theory}} \times 100$ of 0.6%).

Specimen	In air (g) (average)	In water (g) (average)	Calculated density (g/cc)
PPMA G as received	0.360	0.0570	1.184 ± 0.003
PPS Celanese as received	0.264	0.0673	1.338 ± 0.005
PPS Celanese annealed	0.263	0.0679	1.344 ± 0.003
PPS PR09 as received	0.308	0.0792	1.341 ± 0.003
PPS PR09 annealed	0.299	0.0782	1.348 ± 0.005
PPS PR10 as received	0.414	0.103	1.328 ± 0.001
PPS PR10 annealed	0.419	0.108	1.343 ± 0.004
PEEK 150 as received	0.292	0.0676	1.296 ± 0.006
PEEK 150 annealed	0.277	0.0638	1.296 ± 0.003
PEEK 450 as received	0.301	0.0675	1.284 ± 0.003
PEEK 450 annealed	0.279	0.0631	1.289 ± 0.006

Table 1. Density Measurements.

The crystallinity content can be calculated according to the following rule of mixtures:

$$d_{sample} = (1-x)\, d_{amorphous} + x\, d_{100\,\%\ crystalline} \qquad (8)$$

where d refers to the density and x is the percent of crystallinity present in the polymer samples. For our material systems, the following values from the literature were used:

- PPS: $d_{amorphous}$[26] = 1.32
- PPS: $d_{crystalline}$[26] = 1.43
- PEEK: $d_{amorphous}$[27] = 1.263
- PEEK: $d_{crystalline}$[27] = 1.4

The corresponding crystallinity contents were calculated and are summarized in the graph of Figure 14. The specimens as received seem to have a crystallinity very close to the annealed samples except for the PPS PR10 samples. This result is logical considering the

fact that the temperatures of the injection molding process were chosen in order to maximize the crystallinity of the polymers.

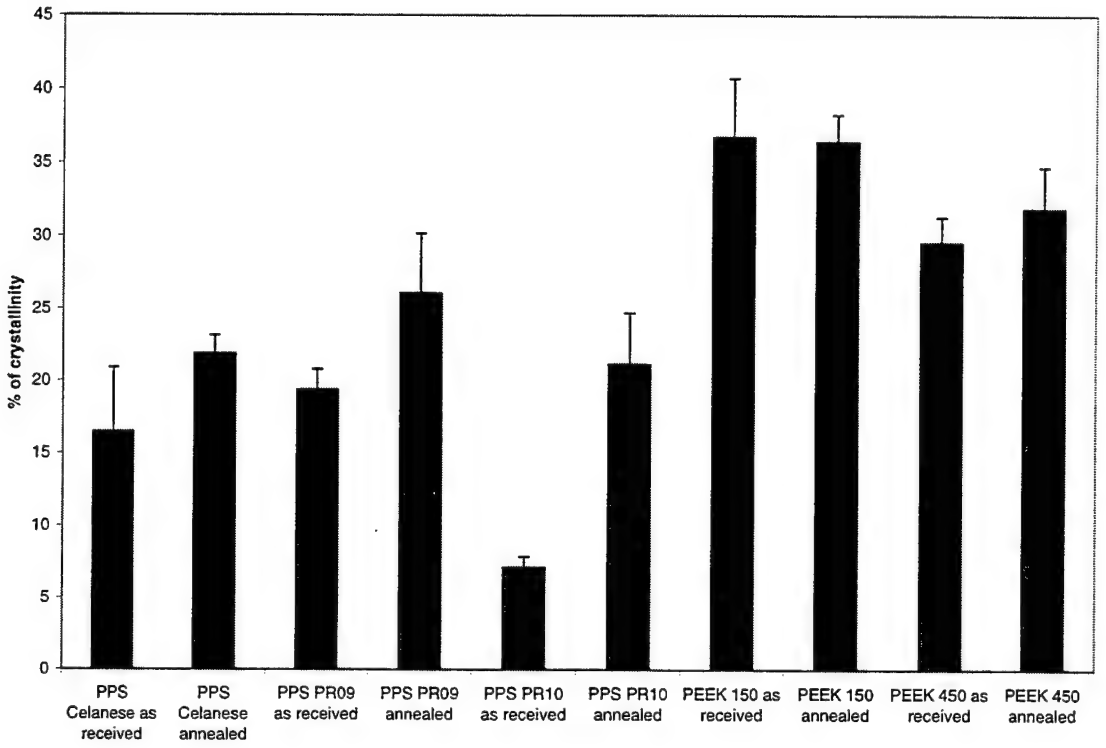

Figure 14. Crystallinity contents.

The advantage of the crystallinity determination via density measurements is that it is a non-destructive test. Also the determination is done on the exact same sample that will be mechanically tested. However, this method could not be used for the amorphous samples due to the presence of air bubbles in the material. Furthermore, some of these results seemed strange intuitively (i.e. PPS PR10) and the crystallinity contents are low for fully crystallized polymers. A source of error can be that we assume a two-phase polymer when using equation (8). Also we rely on the values of the amorphous and crystalline phase densities found in the literature. These might be different for our materials. All the samples have not been scanned and we suspect the presence of air bubbles in some of the samples.

4.4.2 DSC

In order to evaluate the crystallinity of all the samples, including the amorphous and intermediate crystallinity samples, and to validate the density measurements, Dynamic Scanning Calorimetry (DSC) experiments were performed. Unfortunately, this type of testing is a destructive evaluation: the measurements were performed on the short specimens that were heated and quenched at the same time than the long specimens for DMA.

The DSC used for these experiments was a Dupont DSC model 910. Measuring crystallinity via DSC is a delicate process and a careful calibration of the equipment was necessary and can be described as follows.

4.4.2.1 Calibration procedure

The DSC was first balanced with two empty pans, and a straight baseline was obtained. Three DSC were run on Indium sample. The melting enthalpy and melting point of this metal is well know ($\Delta H = 28$ J/g, Tm = 156°C)[28]. The experimental melting temperature and enthalpy were recorded for 3 different testing rates: 10°C/min, 20°C/min and 30°C/min. The melting temperature increased with heating rate in a linear manner (Figure 15). The enthalpy measurements remained almost constant and equal to25.7 at 20°C/min, showing an error of 2.3 J/g when compared to the theoretical value for Indium.

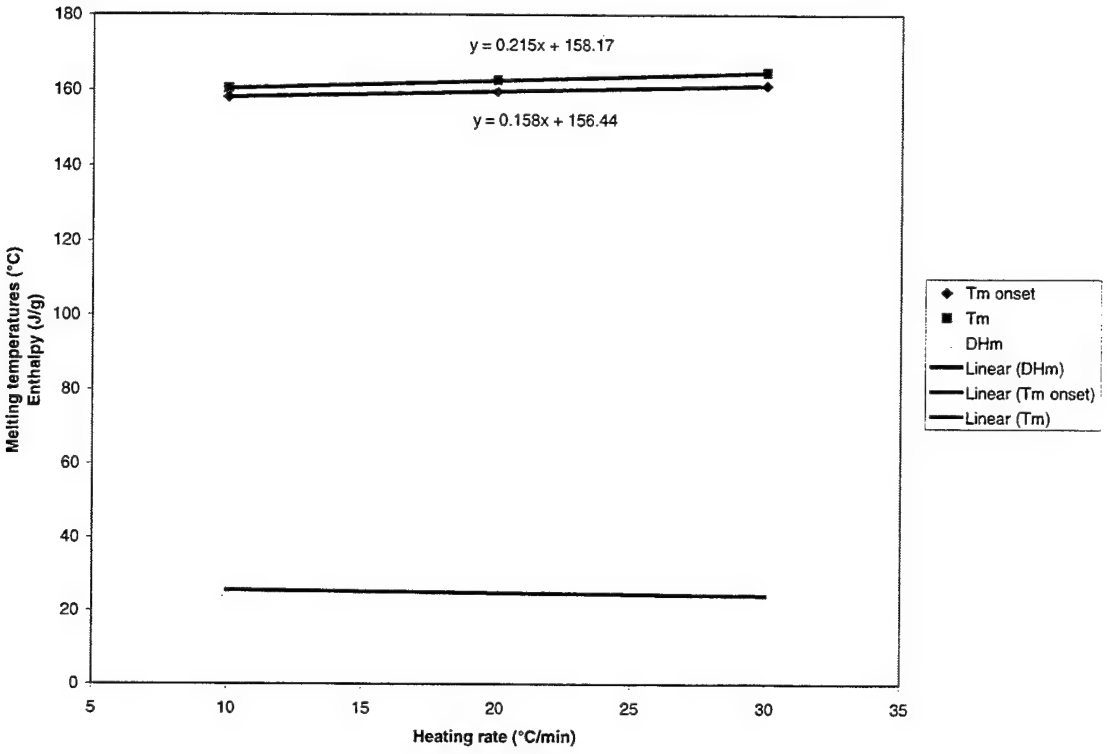

Figure 15. Calibration curves.

Several of our specimens exhibited two peaks: one endotherm during crystallization and one exotherm during melting. The enthalpy of a transition is dependent on temperature. To get the crystallinity of the material, we need to know the enthalpy variations with temperature.

From thermodynamics[29] we know that:

$$\Delta H_f(T) = \Delta H_f(T_{ref}) + \int_{T_{ref}}^{T} \Delta C_p dT \qquad (9)$$

The valued of $\Delta H_f(T_{ref})$ can be found in the literature for PEEK (160 $J.g^{-1}$ at 663 K)[30] and for PPS (111.6 $J.g^{-1}$ at 553 K)[31]. The variation of C_p with temperature was obtained by molecular group additivity[2].

For PPS we find:

$$\Delta H(T) = -175.86 + 0.8188T - 0.00054T^2 \qquad (10)$$

For PEEK we find:

$$\Delta H(T) = -243.15 + 0.9336T - 0.000491T^2 \qquad (11)$$

The crystallinity can be calculated thanks to equation (12).

$$X\% = \frac{\Delta H(T_f) - \Delta H(T_c)}{\Delta H_{100\% crystalline}} \cdot 100 \qquad (12)$$

The DSC measurements for crystallinity purposes are not very accurate for the following reasons:

-the DSC was giving an initial error on the Indium sample during calibration

-the measure of the enthalpy depends on our choice of the starting and ending point of the peak, necessary to measure the area underneath the peak

-we only tested a small piece of a sample that was not the one that will be tested in the DMA. If the samples are heterogeneous, the results will not be exact.

Another source of error is the theoretical value for the melting enthalpy. Disagreement on the theoretical values for PEEK and PPS are common in the literature. However, the DSC measurement will give an approximation of the amount of crystallinity in the material. It is recommended to consider the calculated values as indicators of the relative differences from one sample to another (rather than considering the absolute values).

4.4.2.2 DSC Results

DSC of all the specimens was performed at 20°C/min (standard heating rate to minimize molecular rearrangement). The DSC results are summarized in the table 2.

Material	Tc (K)	Tm (K)	ΔHc measured (J/g)	ΔHm measured (J/g)	Crystallinity via DSC	Crystallinity via density
PPS Celanese amorphous	413	561	22	39	2	
PPS Celanese intermediate	432	561	5	42	30	
PPS Celanese as received		536		38	36	17
PPS PR09 amorphous	413	561	22	38	2	
PPS PR09 intermediate	410	558	15	49	21	
PPS PR09 as received		557		59	52	20
PPS PR10 amorphous	427	547	5	19	10	
PPS PR10 intermediate	441	546	89	28	15	
PPS PR10 as received	403	560	5	62	47	7
PPS PR10 Annealed		561		43	38	
PPS composite as received	409	556	6	13	2	
PPS composite annealed		556		31	28	
PEEK 150 amorphous	453	620	22	38	-2	

PEEK 150 intermediate	458	624	10	27	5	
PEEK 150 as received		624		36	24	37
PEEK 450 amorphous	456	617	21	35	-2	
PEEK 450 intermediate	450	620	13	33	5	
PEEK 450 as received		619		36	24	29

Table 2. Crystallinity measurements.

As can be observed, the crystallinity results are very different when obtained by density measurements and DSC. Several reasons for this discrepency have already been suggested. We will consider the DSC measurement in our analysis because we need values for all our samples. The crystallinity contents seem a little high for PPS as received (typical crystallinity of 30%)[31]. But are still acceptable. The transparent samples also lead to crystallinities close to zero (the negative values are close to zero, and will be considered as null).

As previously indicated, intermediate crystallinity contents were hard to obtain, for PEEK that crystallizes very fast (3 minutes at 180°C result in a fully crystallized material and 1 minute leads to very low crystallinity contents). For the two PEEK samples, the crystallinities for the intermediate samples are very low. We will realize later that DMA of these specimens will lead to results too close to the amorphous samples. For this reason, another scheme was used to obtain results on intermediate crystallinity values. The intermediate sample that will be used later was obtained by running a DMA up to melting at 2°C/min then cooling down the specimen in air. The same sample was then placed again in the DMA. Due to this process, no crystallinity was measured for these samples.

4.5 Summary of the samples and properties

The samples and their properties of interest are summarized in Table 3.

Material	Molecular weight (g/mol)	Crystallinity (%)
PMMA MC	150 000	0
PMMA G	10^6	0
Rubber 100 K	10^5	0
Rubber 240 K	$2.4\ 10^5$	0
PPS Celanese amorphous	?	2
PPS Celanese intermediate	?	30
PPS Celanese as received	?	36
PPS PR09 amorphous	65 000-70 000	2
PPS PR09 intermediate	65 000-70 000	21
PPS PR09 as received	65 000-70 000	52
PPS PR10 amorphous	55 000-65 000	10
PPS PR10 intermediate	55 000-65 000	15
PPS PR10 as received	55 000-65 000	47
PPS PR10 annealed	55 000-65 000	38
PPS composite as received	?	2
PPS composite annealed	?	28
PEEK 150 amorphous	27 000	0
PEEK 150 intermediate	27 000	?
PEEK 150 as received	27 000	24
PEEK 450 amorphous	38 000	0
PEEK 450 intermediate	38 000	?
PEEK 450 as received	38 000	24

Table 3. Summary of the samples.

We will keep in mind that the crystallinity and molecular weight measurements are extremely difficult for PEEK and PPS. The above values will be considered as indications for trends and not absolute values.

4.6 DMA

Dynamic Mechanical Analysis was performed by Polymer Solutions (Blacksburg, VA) on the different samples. Each sample was tested from –100°C up to flow of the material at different frequencies: 50 Hz, 20 Hz, 10 Hz, 5 Hz and 1 Hz. Tangent delta and storage modulus were recorded in bending as a function of temperature. The samples were tested at a heating rate of 2°C/min. We will not deal in the present paper with rate effects. The results at 20 Hz were arbitrarily chosen and are shown in section 5.

5. DMA results and model validation

5.1 Varying the crystallinities

For the two thermoplastics (PEEK and PPS) and the composite it is possible to study the influence of crystallinity on the parameters used in equation (4), (5) and (6).

5.1.1 PPS

5.1.1.1 PPS Celanese

The experimental results and theoretical fit are shown in figure 16 for the amorphous material, the intermediate crystallinity and the sample as received. As the specimen "as received" was not fully crystallized, a sample was left in the oven at 130°C for several hours. The crystallinity content increased 6%, but the effect of the DMA is not significant. It seems that above a given crystallinity content the results of the DMA remain almost constant. Similar experiments on the other materials showed the same trend. The results of the DMA for the different sample of PPS show the trend expected from the literature: the magnitude of the drops during the transition increases with a decreasing amount of crystallinity in the material. All the curves meet after the melting point of PPS Celanese (540K). The melting and flow regions are not distinct. The material starts flowing immediately after the melting temperature. The amorphous sample exhibits the presence of a rise of the modulus right after the glass transition, due to the fact that the material reaches the crystallization temperature. The rate of the testing is slow (2°C/min) and therefore, the material is allowed to recrystallize. We only tried to fit our model to the section of the curve located before the crystallization temperature.

No secondary transition could be observed. Therefore equation (5) was used to model the behavior. The necessary parameters are the heights of the glassy and rubbery plateaus and the transition temperatures (glass transition and melting-flow as indicated by the DSC or tan delta). We also need the two Weibull moduli associated with the different transitions. All these parameters are summarized in table 4. The glass transition temperature increases slightly with increasing crystallinity. The glass temperature varies between 97°C (amorphous) and 112°C (crystallized). The flow temperature is hard to

define from our experimental results and the temperature chosen was the beginning of the final drop.

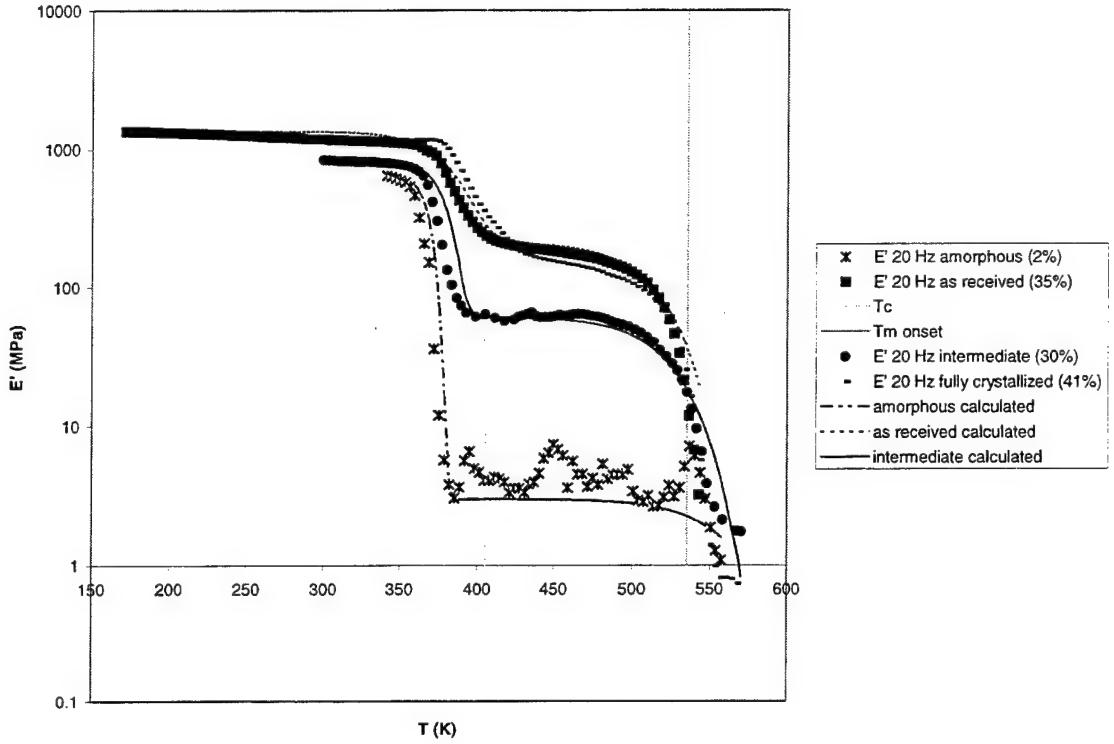

Figure 16. Experimental and theoretical results for various crystallinities of PPS Celanese.

Material	T_2	T_3	E_2 (MPa)	E_3 (MPa)	m_2	m_3
PPS Celanese amorphous	370	520	646	3	20	20
PPS Celanese intermediate	380	530	832	61	40	20
PPS Celanese as received	385	570	1348	212	20	20

Table 4. Parameters for PPS Celanese.

5.1.1.2 PPS PR09

The results for the PPS PR09 samples are summarized in table 5 and Figure 17. The intermediate crystallinity content is low and we can observe recrystallization for the amorphous sample as well as for the intermediate sample.

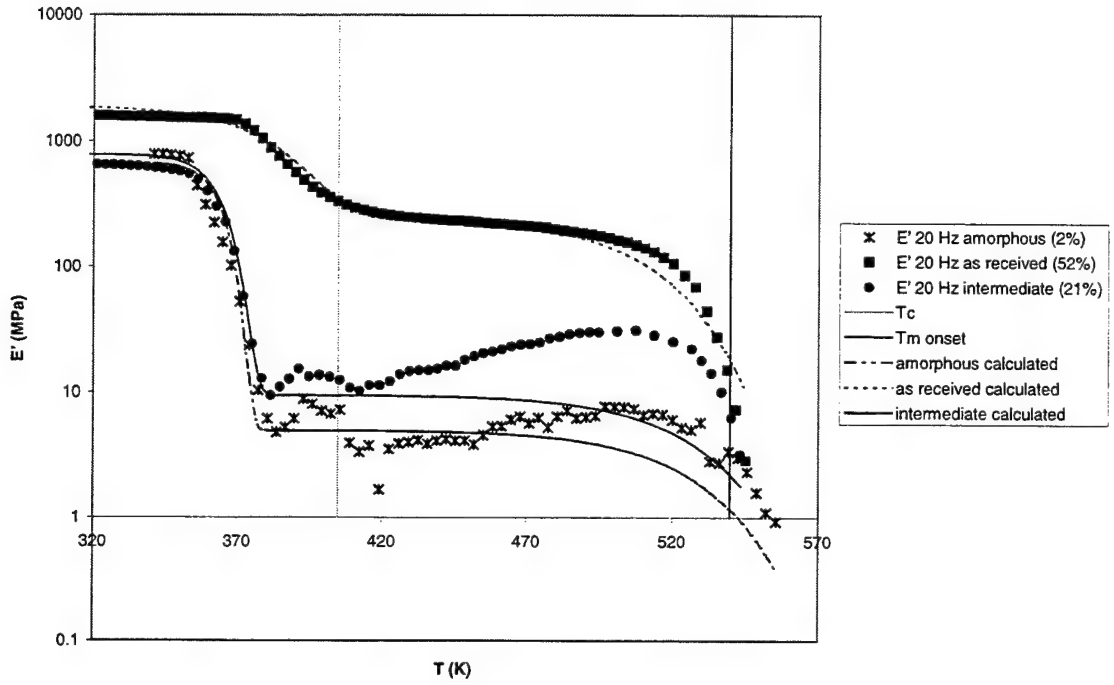

Figure 17. Experimental and theoretical results for various crystallinities of PPS PR09.

Material	T_2	T_3	E_2 (MPa)	E_3 (MPa)	m_2	m_3
PPS PR09 amorphous	365	530	682	5	60	20
PPS PR09 intermediate	365	530	780	9.5	50	20
PPS Pr09 as received	385	515	1875	240	20	20

Table 5. Parameters for PPS PR09.

5.1.1.3 PPS PR10

The PR10 samples were also studied. However, during the experiments, strange behavior of the material indicates the presence of impurity in this sample (the material was very difficult to melt, a fully transparent material could not be obtained...) Intermediate samples with low crystallinity contents could not be obtained due to a very fast crystallization of the material. Two samples with crystallinity 25% and 38% were tested. The two curves superimpose perfectly and are very close to the material as

received (47%). This might corroborate the idea that a threshold value for the crystallinity content exists, above which, the mechanical response of the polymer does not vary much. In the glass transition region, the behavior of the material as received is also surprising: the drop is very steep and a bump immediately follows. This, again, can be explained by the presence of impurities in the polymer. The different results are shown in Figure 18 and Table 6.

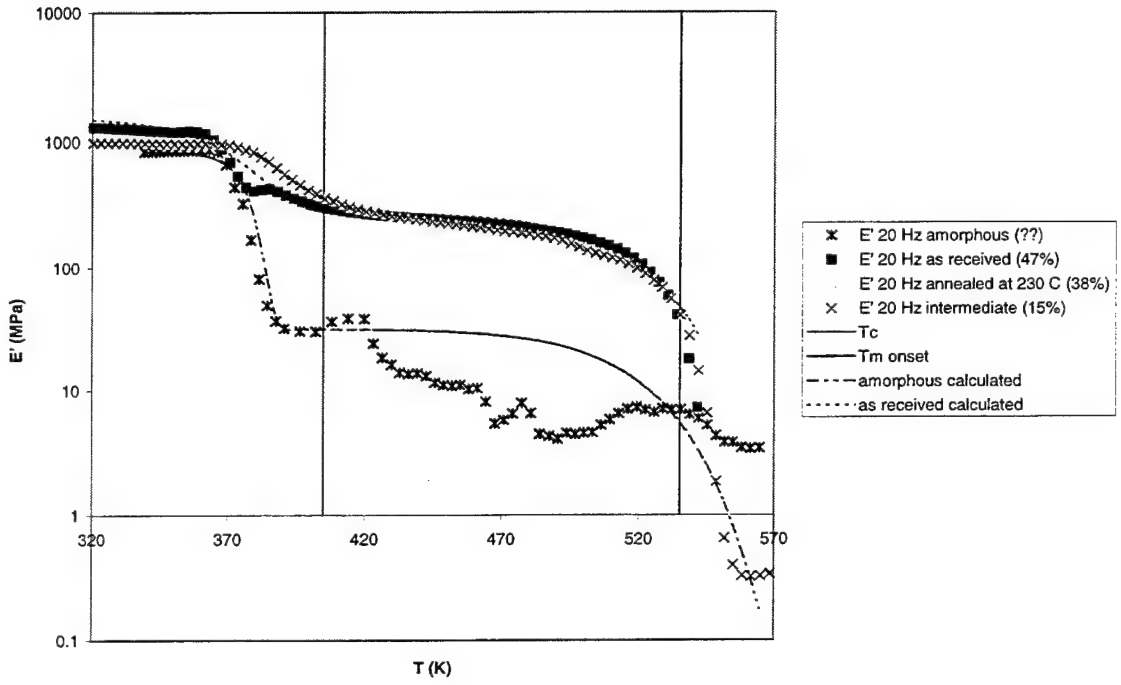

Figure 18. Experimental and theoretical results for various crystallinities of PPS PR10.

Material	T_2	T_3	E_2 (MPa)	E_3 (MPa)	m_2	m_3
PPS PR10 amorphous	373	520	1543	280	60	20
PPS PR10 as received	373	520	841	32	20	20

Table 6. Parameters for PPS PR10.

5.1.2 PEEK

5.1.2.1 PEEK 150

A similar approach was used for the different crystallinities of the PEEK 150 samples (amorphous, intermediate, as received). PEEK exhibits the presence of a secondary relaxation at low temperatures. Therefore equation (6) was used to model the mechanical response of the polymer. Similar observations to the PPS samples can be made (figure 19):

-the magnitude of the glass-transition drop increases with decreasing crystallinity,

-the transition temperatures increase with increasing crystallinity,

-the beta transition temperature varies between –60°C for the amorphous material to –30°C for a crystallized material that corresponds to values given in the literature[20],

-the glass transition is between 144°C and 157°C that also corresponds to literature data[19],

-a modulus rise can be observed for the amorphous sample at the crystallization temperature.

The different parameters are summarized in table 7.

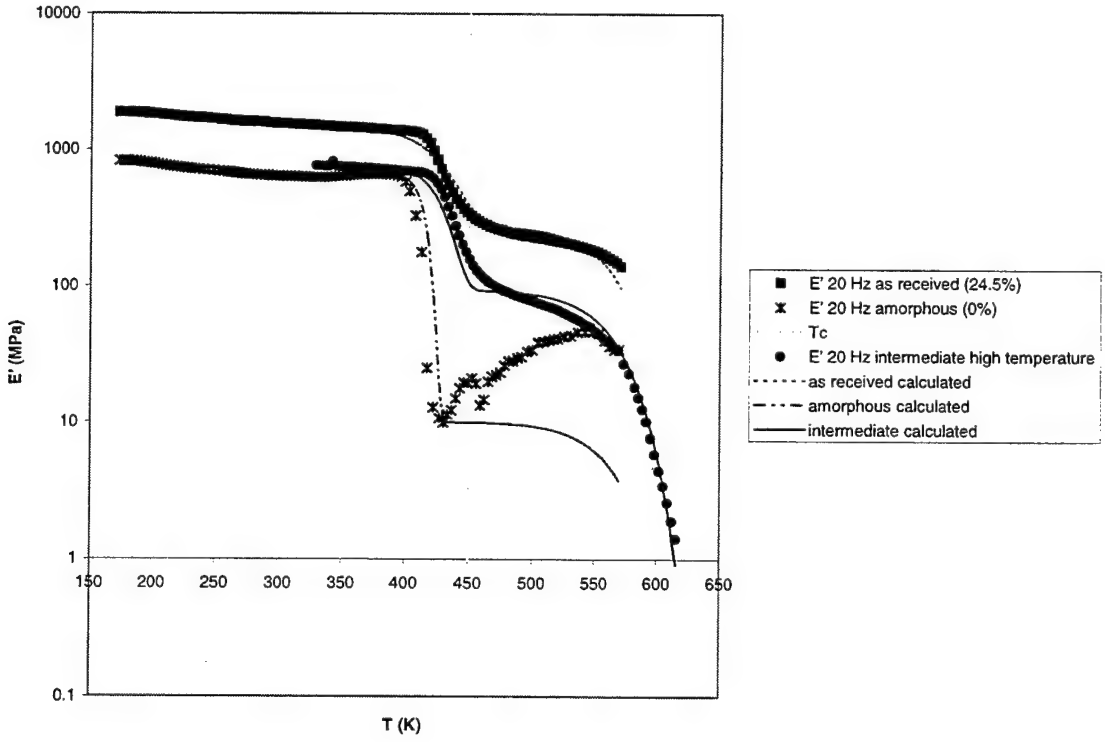

Figure 19. Experimental and theoretical results for various crystallinities of PEEK 150.

Material	T_1	T_2	T_3	E_1 (MPa)	E_2 (MPa)	E_3 (MPa)	m_1	m_2	m_3
PEEK 150 amorphous	213	417	570	824	661	10	5	60	20
PEEK 150 intermediate	230	430	570	900	780	93	5	30	20
PEEK 150 as received	254	431	570	1875	1470	275	5	20	20

Table 7. Parameters for PEEK 150.

5.1.2.2 PEEK 450

The results for PEEK 450 are shown in Figure 20 and Table 8.

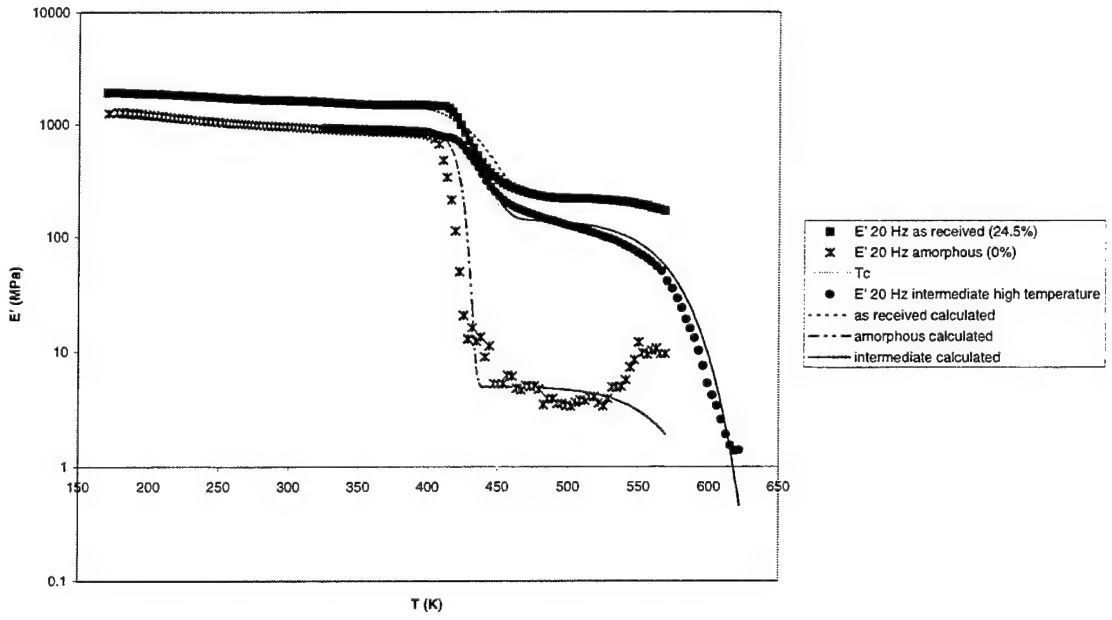

Figure 20. Experimental and theoretical results for various crystallinities of PEEK 450.

Material	T_1	T_2	T_3	E_1 (MPa)	E_2 (MPa)	E_3 (MPa)	m_1	m_2	m_3
PEEK 450 amorphous	213	422	570	934	761	5	20	60	20
PEEK 450 intermediate	230	432	570	1279	955	143	20	30	20
PEEK 450 as received	254	435	600	934	1818	220	20	20	20

Table 8. Parameters for PEEK 450.

5.1.3 Composite

The DMA was also preformed on the composite as received (almost amorphous) and crystallized. As the DMA was performed in bending, we can observe a large temperature effect. For the crystallized sample, the glass transition disappears. This behavior was observed in other studies for highly crystalline materials[32]. In this case, we only need a "one transition" model (equation 4).

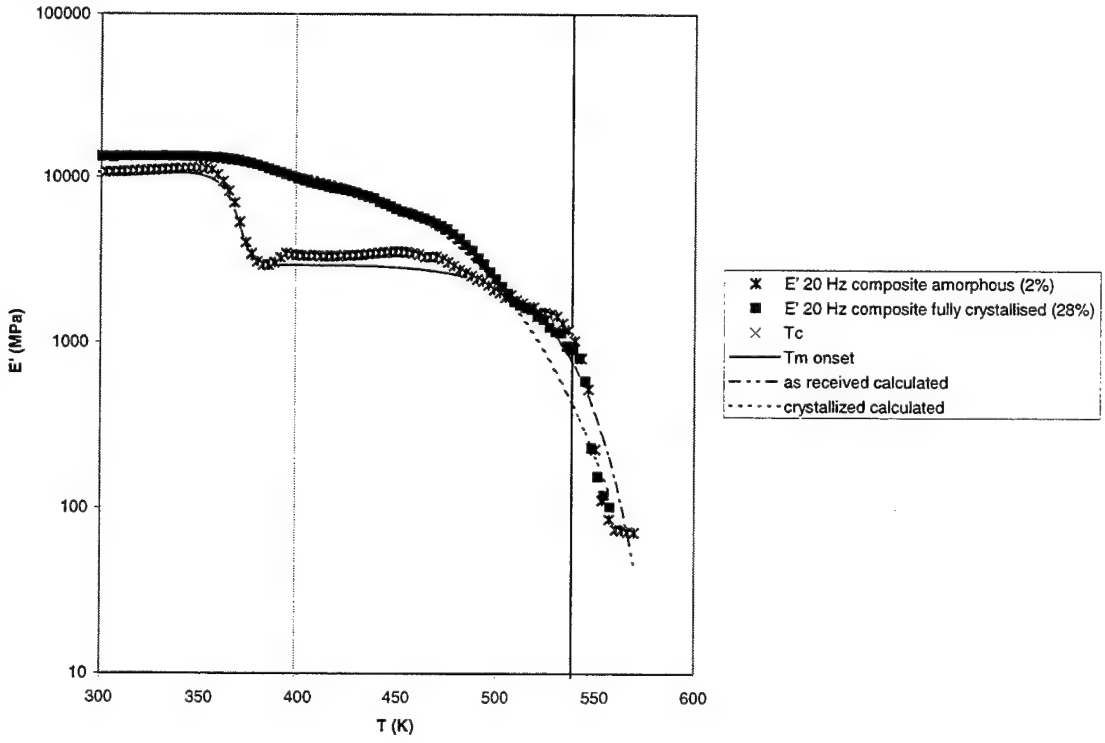

Figure 21. Experimental and theoretical results for various crystallinities of AS4/PPS composite.

Material	T_2	T_3	E_2 (MPa)	E_3 (Mpa)	m_2	m_3
PPS/AS4 composite as received	368	530	10690	2957	60	20
PPS/AS4 composite crystallized		469		11335		9

Table 9. Parameters for AS4/PPS composite.

5.2 Varying the molecular weights

We also investigated the effect of molecular weight on the different parameters by testing different grades of a same polymer.

5.2.1 PMMA

To investigate the effect of molecular weight on our model, a completely amorphous material was chosen. The two molecular weight samples of PMMA were tested and experimental results are reported in figure 22. The different parameters are summarized in table 10. As expected the high molecular weight material was slightly stiffer than the low molecular weight sample. The different transitions also occurred for higher temperatures for the high molecular weight specimen.

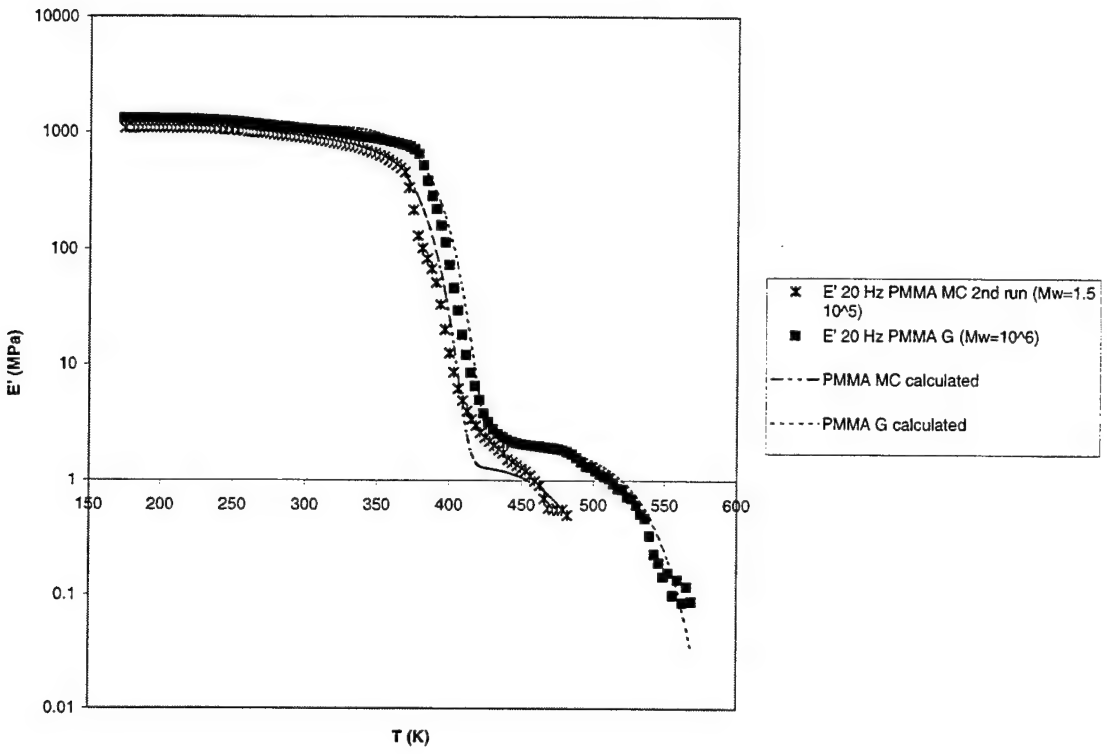

Figure 22. Experimental and theoretical results for PMMA.

Material	T_1	T_2	T_3	E_1 (Mpa)	E_2 (MPa)	E_3 (MPa)	m_1	m_2	m_3
PMMA MC (10^5 g/mol)	273	375	480	1080	867	1.4	20	20	20
PMMA G (10^6 g/mol)	273	385	530	1347	1150	2	20	20	20

Table 10. Parameters for PMMA.

5.2.2 PPS

For comparison purposes, the DMA of the PPS samples with different molecular weights were plotted on a same graph (Figure 23). The samples "as received" are being compared. One should note that the crystallinities are slightly different from one grade to the other. The higher molecular weight material is a little bit stiffer and flows for slightly higher temperatures. The PR10 grade crosses the other molecular weight curve. This phenomenon has been observed in other studies[33] but is not yet well understood.

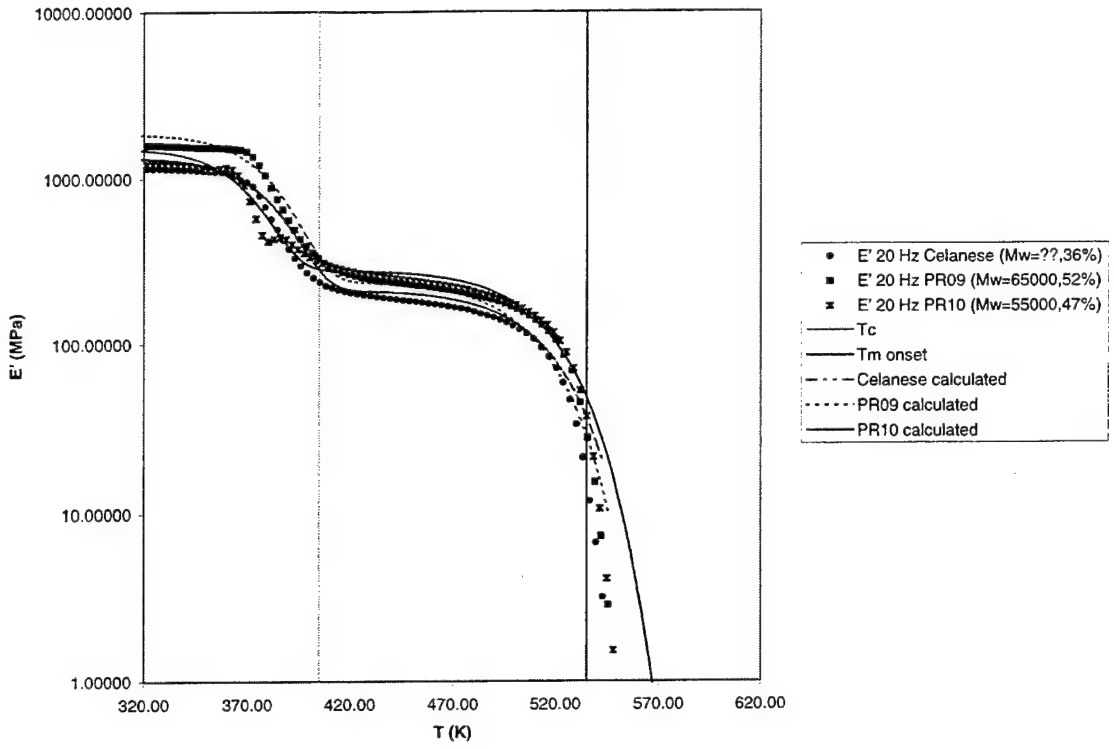

Figure 23. Experimental and theoretical results for various molecular weights of PPS.

5.2.3 PEEK

The two grades of PEEK were plotted on a same graph. The as received samples had similar crystallinities. As can be observed the higher molecular weight is slightly stiffer and flows at temperatures slightly higher than the lower molecular weight. However, the difference between these two curves is not clearly significant.

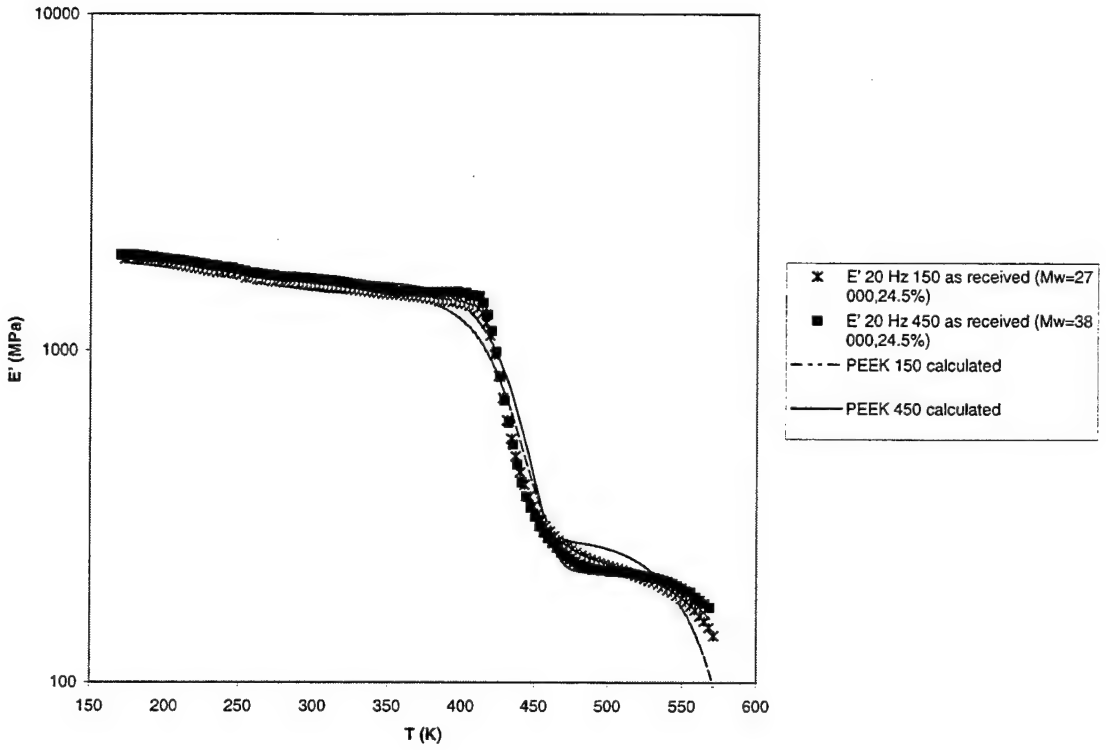

Figure 25. Experimental and theoretical results for various molecular weights of PEEK.

5.2.4 Rubber

The results of the DMA on the two grades of poybutadiene that were stiff enough to be tested are shown in figure 25. The higher molecular weight material is stiffer in the glassy region but the rubbery plateaus are not significantly different.

The glass transition temperature is around –83°C that compares well with the temperature indicated in the literature[32]. The other parameters used for the theoretical model are shown in Table 11.

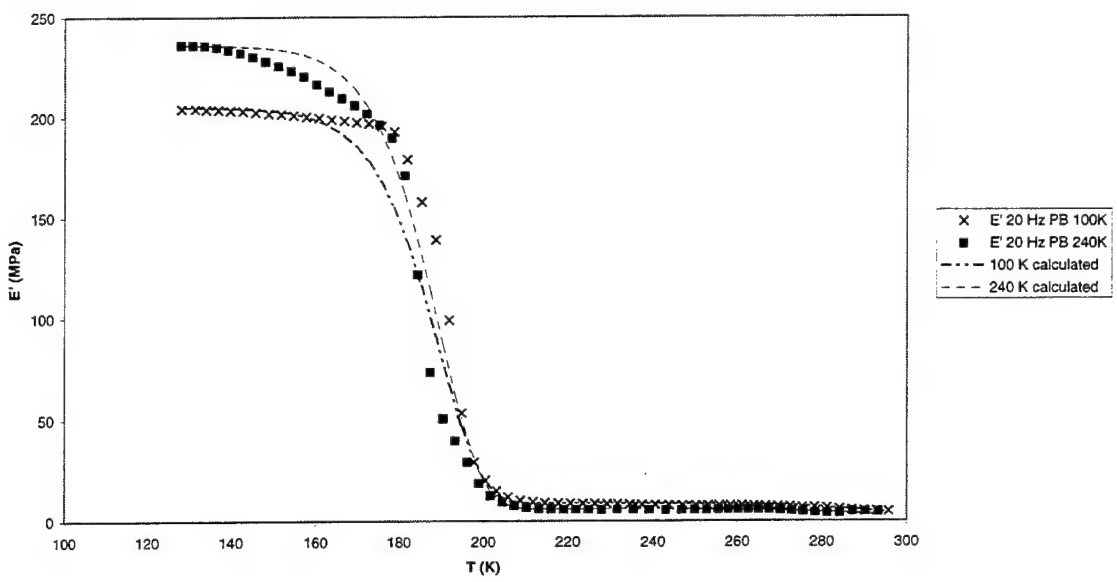

Figure 24. Experimental and theoretical results for various molecular weights of polyisobutylene.

Material	T_2	T_3	E_2 (MPa)	E_3 (MPa)	m_2	m_3
Rubber (10^5 g/mol)	190	300	205	9	20	20
Rubber ($2.4.10^5$ g/mol)	190	300	236	6	20	20

Table 10. Parameters for polyisobutylene.

6. Discussion

We were successful in representing the behavior of all our polymers using the model developed in section 2. The statistics of bond breakage was applicable to the relaxation of polymers having different chemical nature, molecular weights, and crystallinity contents. We could also successfully represent the behavior of the polymers in the different regions and transitions, from glassy state to melting and flow. The behavior of the amorphous polymers can only be analytically represented up to the crystallization

temperature. After this temperature and at low heating rates, the material recrystallizes during the measurements leading to a rise in the modulus. At the present point, our model does not allow for bond re-formation.

The parameters needed to apply this equation are of two kinds: physical parameters and the statistical parameters. All of the physical parameters can be determined by independent experiments (transition temperatures, instantaneous moduli...) and several models exist in the literature that relate these values to the microscopic details of the polymers (e.g. Tg-molecular weight relationship[18], magnitude of the glass transition drop-crystallinity relationship[34]...). The main discussion needs to focus on the statistical parameters, new characteristics of this study. The different parameters were obtained by fitting the model to the experimental data, in order to obtain the best fit for the shape of the curve (that does not necessarily correspond to the fit that minimizes the error). According to section 2, we were expecting small values of the Weibull modulus associated with the beta transition (small number of molecular segments involved in the relaxation). We find our m_1 constantly equal to 5. One needs to be careful about interpreting this result however. This coefficient might slightly vary from one polymer to the other, but the magnitude of the relaxation was so small for our polymers that not much difference could be seen for a parameter varying between 2 and 10. In the glass transition, we were expecting this number to increase, as the number of molecular segments involved increases and the distribution of bond strength broadens. The Weibull coefficients were found equal to 20 for the thermoset, amorphous PMMA and thermoplastics as received. However this coefficient increases with decreasing crystallinity: as the polymer becomes more homogenous, the distribution of bond failure mechanisms narrows, leading to higher values of the Weibull modulus. A theoretical relationship between this coefficient and the percent of crystallinity still needs to be established. The molecular weight seems to have very little effect on our polymers, and does not seem to influence the Weibull coefficients. Only the physical parameters change according to already known rules[18]. The last coefficient related to melting and flow was kept equal to 20. The flow region was not studied in detail in the present paper. However, the statistics of bond breakage seems to be applicable to this region of the

material. It is remarkable that our model enables the curves associated with the different crystallinity degrees to meet after the melting temperature of the polymer.

7. Recommendations

To be used as a prediction tool, our model needs further study in the following areas:

- literature review of the different models relating microstructure to Tg and instantaneous moduli,
- establish the theoretical models enabling the systematic computation of the Weibull coefficient associate with the glass transition as a function of crystallinity content,
- similar study of crosslinked materials,
- integrate strain rate effects (and other conditions, such as moisture, fillers effects),
- specific study of the flow region.

This model will also be easily integrated into micromechanics of composite materials and life prediction tools. Different studies have been performed on the influence of temperature on polymer matrix composites, and have been reported in the previous OSR reports[35,36]. We suggest using this model to predict the behavior of the following systems:

- unidirectional composites in tension at elevated temperatures, where a temperature dependence of strength and stiffness have been recorded (AS4/PEEK, AS4/PPS)[36],
- stress rupture of polymer matrix composites in end-loaded bending at elevated temperatures (AS4/PPS)[35,36],
- life prediction of polymer matrix composites under combined fatigue and thermal loads (AS4/PPS)[36] using MR-Life,
- all other temperature related studies of polymer matrix composites, and life prediction schemes.

8. Conclusions

A new concept used to model polymer relaxation has been established. The statistics of bond failure have been used successfully to model the behavior of various polymers with very different microstructures and properties over large ranges of temperatures. Molecular weights and crystallinity have been systematically varied for several commercial polymers. The applicability of this model to polymer matrix composites has also been established on an amorphous and cystallized AS4/PPS composite. This new model needs further study to be used as a prediction tool. It offers great potential in ultimately reducing the experimental work required to design new composites, and would enable the use of Life Prediction tools, such as MR-Life, over large temperature ranges including the matrix transitions.

9. References

1. Murayama, T., and J.P. Bell, J. Polym. Sci., 8, 437, 1970

2. Van Krevelen, D.W., "Properties of polymers," 3rd Ed., Elsevier, 1990

3. Lacks, D.J., and G.C. Rutledge, "Simultaion of the temperature dependence of mechanical properties of polyethylene," Journal of Physical chemistry, vol. 98, No. 4, Jan 1994.

4. Williams, G., D.C. Watts, Trans. Fraday Soc. 1970, 66, 80

5. Rouse, P.E., J. Chem. Phys., 21, 1272, 1953

6. Aklonis, J.J., and W.J. MacKnight, "Introduction to polymer viscoelasticity", 2nd Ed., Whiley & Sons, 1983

7. Williams, M.L., R.F. Landel, and J.D. Ferry, J. Amer. Chem. Soc, 77, 3701, 1955

8. Santangelo, P.G., K.L. Ngai, and C.M. Roland, "Distinctive manifestations of segmental motion in amorphous poly(tetrahydrofuran) and polysiobutylene," Macromolecules, Vol. 26, No. 11, 1993

9. McKenna, G.B., "Glass formation and glassy behavior," Comprehensive polymer science, Pergamon, 1989

10. Ashby, M.F. and D.R.H. Jones, "Engineering materials 2: an introduction to microstructures, processing, and design"

11. De Gennes, P-G., "Scaling Concepts in Polymer Physics," Cornell University, 1979.

12. Weibull, W., "A Statistical Theory of the Strength of Materials", Ingeniorsvertenskapsakademiens handlingar 151, 1939

13. Schmieder, K. and K. Wolf, Kolloid Z., 127, 65, 1953

14. Brennan, A.B., and Y.Q. Wang, Polymer, Vol 34, 4, pp.807-812, 1993

15. Bartolotta, A., G. Di Marco, M. Lanza, and G. Carini, Journal of Polymer Science: Part B: Polymer Physics, Vol. 33, 93-104, 1995

16. Risch, B.G., D.E. Rodrigues, K. Lyon, J.E. McGrath and G.L. Wilkes, Polymer, Vol 37, No 7, 1229-1242, 1996

17. Chanda, M., and S. K. Roy, Plastics technology handbook, Marcel Dekker, Inc., New York, 1987

18. Sperling, L. H., Introduction to physical polymer science, 2nd ed., John Wiley & Sons, Inc., New York, 1992

19. Margolis, J. M., Engineering thermoplastics, properties and applications, Marcel Dekker, Inc., New York, 1985

20. Krishnaswamy, R.K., and D.S. Kalika, "Dynamic relaxation properties of poly(ether ether ketone)", Polymer, Vol. 35, No. 6, 1994

21. Devaux, J., et al, "On the molecular weight determination of poly(ary-ether-ether-ketone) (PEEK), polymer, Vol. 26, December, 1985

22. Phillips Petroleum Company, private communication.

23. Victrex, PEEK processing guide, 1998

24. Society Plastics Engineers, ANTEC, Atlanta, 1998

25. Mettler Toledo instruction notebook, density determination kit for AT/AG and PG/PG-S/PR balances.

26. Huo, P. and P. Cebe, "Dielectric relaxation of Poly(Phenylene Sulfide) containing a fraction of amorphous phase," Journal of Polymer Science: Part B: Polymer Physics, Vol. 30, 239-250, 1992

27. Bas, C., M. Fugier and N. D. Albertola, "Reinforcement effect and molecular motions in semicrystalline PEEK films: Mechanical and Physical modelings. I," Journal of applied Polymer Science, 64, 1041-1052, 1997

28. www.shef.ac.uk/chemistry/webelements/nofr-heat/In.html

29. Mahan, B.H., Thermodynamique chimique, Intereditions, 1977

30. Lu, S.X., and P. Cebe, "Effects of annealing on the disappearance and creation of constrained amorphous phase," Polymer, Vol. 31, No. 21, 1996

31. Bas, C., and D. Alberola, Polymer Journal, Vol. 29, No. 5, 1997

32. Turi, E.A., "Thermal characterization of polymeric materials," Academic press, 1997

33. Lu, S.X., P. Cebe, and M. Chapel, "Effects of molecular weight on the structure of Poly(phenylene sulfide) crystallized at low temperatures", Macromolecules, 30, 1997

34. Khanna, Y.P., "Estimation of polymer crystallinity by dynamic mechanical techniques," J. Appl. Polym. Sci., vol. 37, No. 9, May 1989

35. Reifsnider, K.L., et. al., AFOSR Grant No. F49620-95-1-0217, Annual report, 1 September, 1996

36. Reifsnider, K.L., et. al., AFOSR Grant No. F49620-95-1-0217, Annual report, "Mechanics of long-term behavior of high temperature polymer composites," 1 September, 1997

Appendix II

Effect of Temperature on the Tensile Strength Of Unidirectional Composites

Brady Walther and K.L. Reifsnider

Effect of Temperature on the Tensile Strength of Unidirectional Composites

Brady Walther and Ken Reifsnider
Virginia Tech

In the past decade polymer based composites have provided a high strength to weight ratio. Many applications in the aerospace industry have benefited from these materials. However, in many cases the majority of the material has been placed in the structures as non-load-bearing members. In order to use composite materials as load-bearing members, the design parameters must be fully described. This description is very complex because of the nature of the composite system. Unlike steel or alloys, a composite system is anisotropic and heterogeneous material. In addition, the properties are sensitive to environmental conditions such as humidity, temperature, loading rates and aging.

However, much has been done in the area of describing such materials for design. One of the most important parameters for design is strength. This is generally defined by the condition where the material experiences a load and completely fails or fractures under that load. The micro-mechanics of this failure can be described to predict to the macro-mechanical failure strength. Two particular micro-mechanical models are described below. This paper focuses on the strength of composite systems under the effect of elevated temperature. In addition to strength, the stiffness of the system was measured at elevated temperatures. The effects on the stiffness will be reported; however, the main focus was on the strength.

Only a brief review of models is given in this document. Many other modeling approaches are available in the literature. The models discussed evaluate the system at

the micro-mechanical level, unlike traditional classical laminate theory. Some background information is given about the philosophy behind the models. However the background information is not extensive. This discussion focuses on using the existing models and comparing them to experimental data. The fundamental mathematics will not be changed in the models. However, the mathematical parameters, that are expected to be affected by elevated temperatures, will be developed to reflect this change.

The micro-mechanical parameters effected by elevated temperatures in the strength predictions are discussed with these developments. The predictions are compared to our experimental data to test their validity. The discussion of the extensive experimental program conducted to support this discussion is deferred to another opportunity for presentation. This material is extracted, for the most part, from a Thesis in satisfaction of the requirements for the degree of Master of Science in Engineering in Engineering Mechanics in the Department of Engineering Science and Mechanics at Virginia Tech. The title of the thesis is "An Investigation of the Tensile Strength and Stiffness of Unidirectional Polymer-Matrix, Carbon-Fiber Composites under the Influence of Elevated Temperatures." The entire document is available electronically at the Virginia Tech web site, www.vt.com.

1. Strength

Micro-mechanics models have evolved to predict the tensile strength of unidirectional composites. For the past two decades several researchers have studied tensile failure and strength. Weibull used the weakest link theory to predict the fracture of a single fiber. This theory was developed because Weibull discovered that the tensile strength of a single fiber was not uniform from point to point. Coleman, Rosen, and

Hahn studied the fracture of a bundle of fibers [1]. Rosen calculated the bundle strength assuming that the statistical distribution of strength of the fibers governs the failure of each fiber. Therefore, the failure of the bundle of fibers is due to the statistical accumulation of fiber fractures in the system.

Zweben and Rosen related the failure of the fiber bundles in the company of the matrix material. They used the ineffective length to estimate the tensile strength. This was based on shear lag analysis. However, this model did not consider the effects of stress concentrations in the fibers adjacent to the broken fiber [1].

Batdorf showed that the stress concentrations in the adjacent fiber would lead to the accumulation of fiber fractures and this would lead to final (ultimate) failure of the composite [1]. His model uses the argument of the accumulation of a critical number of fiber fractures called "i-plets" leads to instability. The load level at which the instability occurs is the failure strength of the laminate.

These models lead us to the point that tensile strength of unidirectional composites is based on the ineffective length and stress concentration effects near fiber fractures; both of these quantities are functions of the fiber and matrix elastic moduli. However, to this point the models do not consider the effects of the fiber-matrix interface. Resent experiments show that the strength can be improved considerably by changing the fiber matrix bonding.

Reifsnider postulated that the assumption of a perfect elastic matrix does not reflect the problem accurately. The high stress concentration in the matrix material near the broken fiber could lead to local matrix plasticity or debonding of the fiber matrix interface. Therefore, Reifsnider constructed a model that allows for elasto-plastic matrix

deformation near fiber fractures. This model predicts an optimum interfacial strength value for which the tensile strength will be maximized [1].

When bonding between the fiber and the matrix is poor, there is an inefficient load transfer between the matrix and fiber. This may cause the matrix not to completely transfer the load to the fiber. If the load remains in the matrix the ultimate strength should decrease. Experimental results demonstrate this response; Madhukar and Drzal observed over a 10% decrease longitudinal stiffness going from an untreated fiber to a surface treated fiber [1]. This indicates that varying the interface can alter the longitudinal stiffness. The data indicated that if the transfer of load is 100% efficient then the experimental strength is comparable to the role of mixtures. However 100% transfer is theoretical.

In order to allow for this transfer effectiveness, Reifsnider introduces a new variable called "efficiency" to account for the interface interaction. This variable is determined by experimental results.

General Formulation of Strength Models

This section describes the formulation of two models that are based on the shear lag approach to tensile strength in the fiber direction. It is important to understand some of the assumptions that are made in the models. The first model is similar to that developed by Reifsnider and Gao (Model 1) and is included in MRLife10 (a life prediction code developed by the Materials Response Group at Virginia Tech) [2]. Reifsnider and Subramanian (Model 2) developed the second model [1]. For the most part, each of the models derived the strength representation with the same basic

arguments. However, there are some minor differences between the two models. Let us take a look at each approach and the arguments made.

Model One

Gao and Reifsnider's model (Model 1) was derived for the unidirectional tensile strength of a polymer matrix composite material. It is based on the probability analysis that Batdorf used in 1982 [3]. Batdorf bases his analysis on the assumption that damage in the composite due to an applied load consists solely of breaks in the fibers. The composite is made of N fibers of length L that are held together by a matrix material. A single isolated break was called a singlet, pairs of breaks doublets, and in general an *i*-plet for all adjacent breaks of *i* fibers. Each of these breaks create a stress concentration factor c_i in the plane of the fiber break. That stress concentration is affected by the relative geometry of the unbroken fiber (fracture mechanics) and the material properties; however, this acts over a distance δ, called the ineffective length. Next, Batdorf assumes that the fiber failure is governed by a two-parameter Weibull representation. When a stress is applied to a fiber of length L, the probability of the failure is given by

$$P_f = 1 - \exp\left[-\frac{L}{l_0}\left(\frac{\sigma}{\sigma_0}\right)^m\right] \qquad \mathbf{1}$$

P_f = The probability of failure
L = Fiber length
σ_0 = Weibull characteristic value
m = Weibull modulus
l_o = Reference length
σ = The applied stress

However, if P_f is very small (<<1) then, Batdorf approximates the above equation by

$$P_f = \frac{L}{l_o}\left(\frac{\sigma}{\sigma_o}\right)^m \qquad 2$$

To calculate the number of singlets, Q_1, is multiplying the probability of failure given by Equation 3 so that

$$Q_1 = NP_f = N\frac{l}{l_o}\left(\frac{\sigma}{\sigma_o}\right)^m$$

$$Q_1 = \text{Number of singlets} \qquad 3$$

Next we assume that the stress concentration in the neighboring fibers varies with a linear behavior from c_1 to unity over a distance $\delta_1/2$, the ineffective length divided by two. This functional variation may be expressed as:

$$f(z) = c_1 + \frac{z}{\delta_1/2}(1 - c_1) \qquad 4$$

Reifsnider expressed the reliability of the fiber having a stress variation of this type given by:

$$R = \exp\left[-\left(\frac{\sigma}{\sigma_{ao}}\right)^m\right] \qquad 5$$

where the variable σ_{ao} is defined by intergration over the length of the fiber.

$$\sigma_{ao} = \sigma_o\left(\int_o^L [f(z)]^m \, dz\right)^{\frac{-1}{m}} \qquad 6$$

Now these relations can be combined in equation 4 to show that the probability of failure in the over-stressed region may be approximated by:

$$P_1 \approx \frac{\lambda_1}{l_o}\left(c_1 \frac{\sigma}{\sigma_o}\right)^m \qquad 7$$

where the variable λ_1 contains the distance (ineffective length) and stress concentration.

$$\lambda_1 = \delta_1 \frac{c_1^{m+1} - 1}{c_1^m (c_1 - 1)(m+1)} \qquad 8$$

Next the development considers the probability that a singlet becomes a doublet. If there are n_1 nearest neighbors, then this probability is given by:

$$P_{1\to 2} = n_1 \frac{\lambda_1}{l_o}\left(c_1 \frac{\sigma}{\sigma_o}\right)^m \qquad 9$$

Using equation 3, an estimate of the number of doublets is derived as:

$$Q_2 = Q_1 n_1 \frac{\lambda_1}{l_o}\left(c \frac{\sigma}{\sigma_o}\right)^m \qquad 10$$

Repeating this process leads to a general model to estimate the number of i-plets:

$$Q_{i+1} = Q_i n_i \frac{\lambda_i}{l_o}\left(c_i \frac{\sigma}{\sigma_o}\right)^m \qquad 11$$

or as

$$Q_i = N \frac{L}{l_o}\left(\frac{\sigma}{\sigma_o}\right)^{im} \prod_{j=1}^{i-1} c_j^m n_j \frac{\lambda_j}{l_o} \qquad 12$$

The above equations are based by Batdorf (Equations 1-12). A log-log plot of Q_i versus stress (sigma) has a slope of im [2]. This is shown in Figure 1.01.

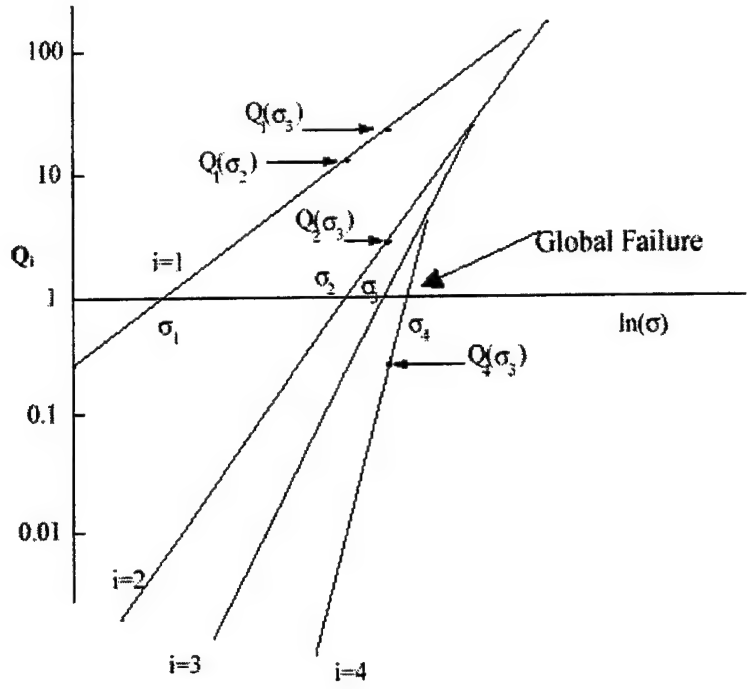

Figure 1.01 Batdorf Q-plot where composite failure occurs at the point of instability.

The failure stress is given by the lowest stress at which any unstable i-plet is formed. Therefore, the stress at which the envelope intersects the horizontal line $Q_i = 1$ or $\ln Q_i = 0$, is the failure stress. The only thing left to determine are the stress concentrations and the ineffective lengths for each number of adjacent fiber fractures. Gao and Reifsnider used a shear-lag model to determine these two values [3].

Gao and Reifsnider start by making an assumption that there is a central core of broken fibers as shown in Figure 1.02 [3]. The broken fiber are surrounded by unbroken fibers that are being strained. The core of broken fibers is assumed to be a homogeneous material whose Young's modulus is obtained by the rule of mixtures. The assumed circular cross sectional areas of the equivalent broken core is equal to the total area of the ith concentric cylinder of radius $r_f + d$.

$$\pi r_o^2 = i\pi(r_f + d)^2 = iA_f + iA_m$$

r_f = the radius of the fiber

d = half of the width of matrix region

13

The variables correspond to the concentric cylinder model given in Figure 1.02 [4].

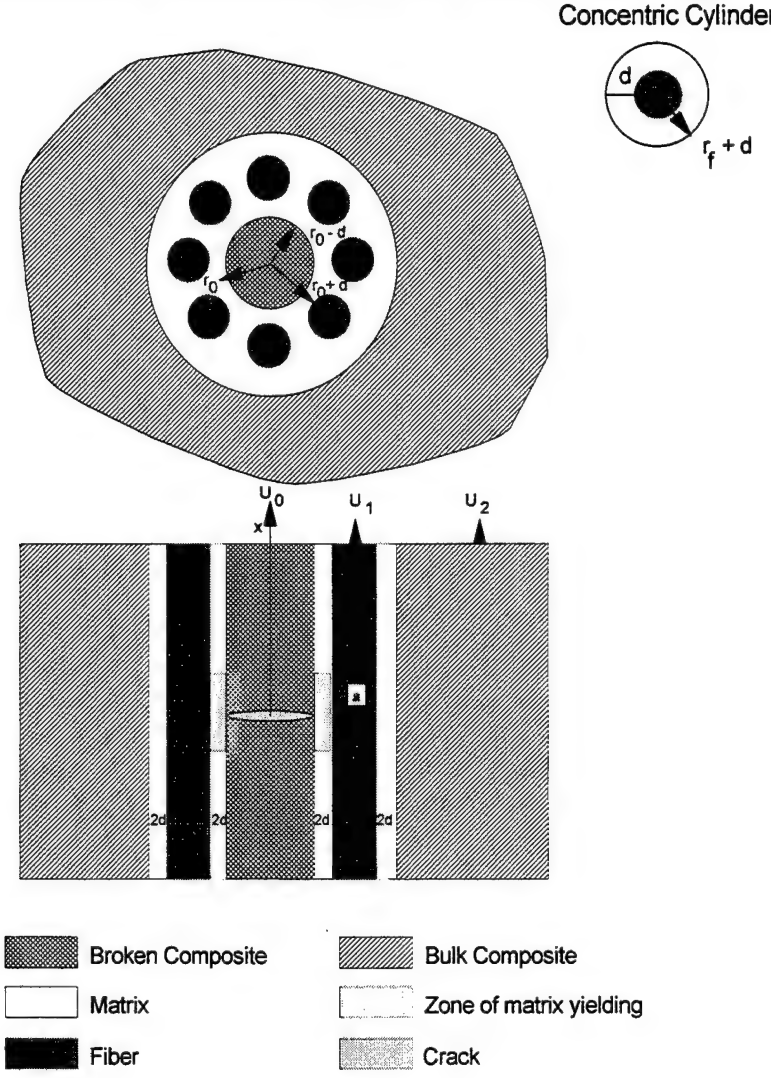

Figure 1.02 Fiber fracture of unidirectional composites used by Gao and Reifsnider.

The fiber area and matrix area are given by:

$$A_f = \pi r_f^2$$

14

$$\pi r_o^2 = i\pi(r_f + d)^2 = iA_f + iA_m$$

r_f = the radius of the fiber

d = half of the width of matrix region

13

The variables correspond to the concentric cylinder model given in Figure 1.02 [4].

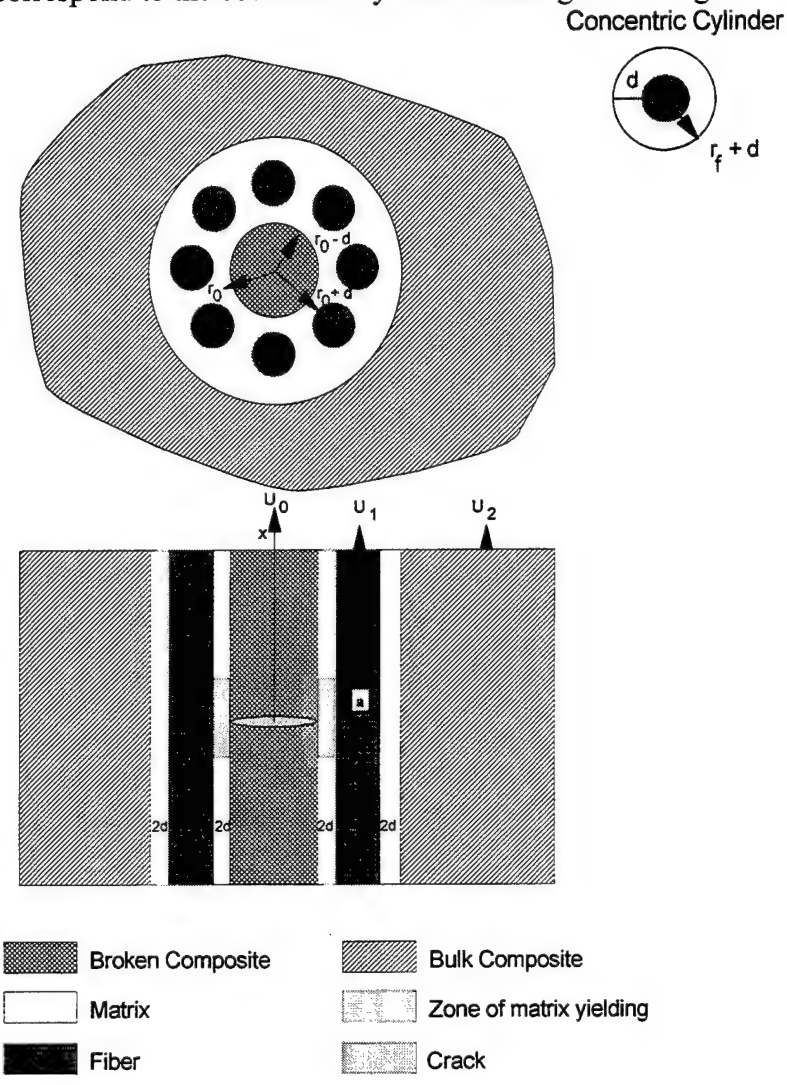

Figure 1.02 Fiber fracture of unidirectional composites used by Gao and Reifsnider.

The fiber area and matrix area are given by:

$$A_f = \pi r_f^2$$

14

$$A_m = \pi(r_f + d)^2 - \pi r_f^2 \qquad \textbf{15}$$

The number of neighboring unbroken fibers, n_i, is dependent upon the number of broken fibers, i. The assumption is made that only the fibers carry the axial stress and the matrix only supports shear (the classical shear lag assumptions). The distance measurement "*a*" gives the half-length of the region of matrix and/or interfacial yielding. The equilibrium equations for this region of the matrix and interfacial yielding are given as:

$$E\pi(r_o - d)^2 \frac{d^2U_o}{dx^2} - 2\pi r_o \eta \tau_o = 0$$

$$n_i A_f E_f \frac{d^2U_1}{dx^2} + 2\pi(r_o + 2d + 2r_f)\frac{G_m}{2d}(U_2 - U_1) + 2\pi r_o \eta \tau_o = 0$$

$$0 \le x \le a \qquad \textbf{16}$$

U_o = Displacements of the broken core
U_1 = Displacements of neighboring unbroken fiber
U_2 = Displacements of average composite
E_f = Young's modulus of the fiber
G_m = Shear modulus of the matrix
A_f = Area of the fiber
τ_o = Yielding stress of the matrix and interface
η = a shear parameter, efficiency factor

The efficiency factor parameter defines the efficiency nature of the shear transfer in the inelastic region. This parameter has the value between one and zero with zero being no shear stress transfer between broken fibers and their neighbors in the region. This is a representation of a complete fiber-matrix debonding of matrix cracking in the region.

Using the rule of mixtures, the Young's modulus of the broken core, E, is determined to be:

$$E = \frac{\mathrm{iA_f E_f} + \left[\mathrm{iA_m} - \pi(r_o^2 - (r_o - d)^2)\right]E_m}{\pi(\mathrm{r_o} - d)^2} \qquad 17$$

where E_f and E_m are the Young's modulus for the fiber and matrix. Hence,

$$E\pi(r_o - d)^2 = \mathrm{iA_f E_f} + \left[\mathrm{iA_m} - \pi(r_o^2 - (r_o - d)^2)\right]E_m$$

$$= \mathrm{iA_f} E_f \left\{1 + \frac{\left[\mathrm{iA_m} - \pi(r_o^2 - (r_o - d)^2)\right]}{iA_f\ E_f} E_m\right\}$$

$$= iA_f E_f \beta \qquad 18$$

where Beta is defined to be:

$$\beta = \left\{1 + \frac{\left[\mathrm{iA_m} - \pi(r_o^2 - (r_o - d)^2)\right]}{iA_f\ E_f} E_m\right\} \qquad 19$$

Now the equilibrium equations (equation 16) are rewritten as:

$$iA_f E_f \beta \frac{\mathrm{d^2 U_o}}{\mathrm{dx^2}} - 2\pi r_o \eta \tau_o = 0$$

$$n_i A_f E_f \frac{d^2 U_1}{dx^2} + 2\pi(r_o + 2d + 2r_f)\frac{G_m}{2d}(U_2 - U_1) + 2\pi r_o \eta \tau_o = 0 \qquad 20$$

For the region in which no interfacial yielding has occurred, the equilibrium equations are:

$$E\pi(r_o - d)^2 \frac{d^2U_o}{dx^2} - 2\pi r_o \frac{G_m}{2d}(U_1 - U_o) = 0$$

$$n_i A_f E_f \frac{d^2U_1}{dx^2} + 2\pi(r_o + 2d + 2r_f)\frac{G_m}{2d}(U_2 - U_1) + 2\pi r_o \frac{G_m}{2d}(U_1 - U_o) = 0 \qquad \textbf{21}$$

$$a \le x < \infty$$

These equations now can be rewritten as:

$$iA_f E_f \beta \frac{\mathrm{d}^2 U_o}{\mathrm{dx}^2} - 2\pi r_o \frac{G_m}{2d}(U1 - Uo) = 0$$

$$n_i A_f E_f \frac{d^2U_1}{dx^2} + 2\pi(r_o + 2d + 2r_f)\frac{G_m}{2d}(U_2 - U_1) + 2\pi r_o \frac{G_m}{2d}(U_1 - U_o) = 0 \qquad \textbf{22}$$

Gao and Reifsnider assumed that the strain in the average composite is constant, therefore

$$U_2 = \frac{\sigma}{\mathrm{E}} x \qquad \textbf{23}$$

where σ in this equation represents the remote fiber stress. Then, introducing the following normalization:

$$U_o = \sigma \mathrm{u}_o \sqrt{\frac{2dA_f}{E_f G_m r_o}}$$

$$U_1 = \sigma u_1 \sqrt{\frac{2dA_f}{E_f G_m r_o}}$$

$$x = \zeta \sqrt{\frac{2A_f E_f d}{G_m r_o}}$$

$$\tau_o = \bar{\tau}_o \sigma \sqrt{\frac{A_f G_m}{2dE_f r_o}}$$

$$a = \alpha \sqrt{\frac{2A_f E_f d}{G_m r_o}} \qquad \textbf{24}$$

We can rewrite the equilibrium equations as

$$\frac{d^2 u_o}{d\xi^2} - \frac{2\pi}{i\beta} \eta \bar{\tau}_o = 0$$

$$\frac{d^2 u_1}{d\zeta^2} - \phi t u_1 + \phi(\eta \bar{\tau}_o + t\xi) = 0$$

$$0 \le \zeta < \infty \qquad \textbf{25}$$

with

$$\frac{d^2 u_o}{d\zeta^2} + \frac{2\pi}{i\beta}(u_1 - u_o) = 0$$

$$\frac{d^2 u_1}{d\zeta^2} - \phi(1+t)u_1 + \phi u_o = -\phi t\zeta \qquad \textbf{26}$$

$$\alpha \le \zeta < \infty$$

where

$$t = \frac{r_o + 2d + 2r_f}{r_o} \qquad 27$$

$$\phi = \frac{2\pi}{n_i} \qquad 28$$

In order to solve the second order differential equations, two boundary conditions must be applied. They are as follows:

$$\frac{du_o(0)}{d\zeta} = u_1(0) = 0$$

$$\frac{du_o(\infty)}{d\zeta} = \frac{du_1(\infty)}{d\zeta} = 1 \qquad 29$$

The solution to the second order differential equation (equations 26) is as follows:

$$u_o = \frac{\pi\eta\bar{\tau}_o}{i\beta}\zeta^2 + A_1$$

$$u_1 = \frac{\eta\bar{\tau}_o}{t} + \zeta + A_2\exp(\zeta\sqrt{t\phi}) - (A_2 + \frac{\zeta\bar{\tau}_o}{t})\exp(-\zeta\sqrt{t\phi}) \qquad 30$$

The constants A_1 and A_2 will be determined from continuity conditions.

The solution to equations 27 can be written as follows:

$$u_o = \zeta + B_1(1 + t - \frac{\lambda_1}{\phi})\exp(-\sqrt{\lambda_1\zeta}) + B_2(1 + t - \frac{\lambda_2}{\phi})\exp(-\sqrt{\lambda_2\zeta})$$

$$u_1 = \zeta + B_1\exp(-\sqrt{\lambda_1\zeta}) + B_2\exp(-\sqrt{\lambda_2\zeta}) \qquad 31$$

where B_1 and B_2 are constants with

$$\lambda_1 = \left\{ n_i + i\beta(1+t) + \sqrt{n_i^2\ 2i\beta n_i(1-t) + (i\beta)^2(1+t)^2} \right\} \frac{\pi}{i\beta n_i}$$

$$\lambda_2 = \left\{ n_i + i\beta(1+t) - \sqrt{n_i^2\ 2i\beta n_i(1-t) + (i\beta)^2(1+t)^2} \right\} \frac{\pi}{i\beta n_i} \quad \textbf{32}$$

The stress concentration on the unbroken fibers is expressed as;

$$C_i(\zeta) = \frac{du_1(\zeta)}{d\zeta} \quad \textbf{33}$$

and the dimensionless shear stress is expressed as:

$$\bar{\tau}(\zeta) = u_o - u_1 \quad \textbf{34}$$

The finial equation used to predict the strength of the composite is shown below.

$$X_t = V_f \bullet \hat{\sigma}_c + (1 - V_f) E_m \bullet \frac{\hat{\sigma}_c}{E_f}$$

V_f = Fiber Volume Fraction **35**
$\hat{\sigma}_c$ = Critical Stress
E_m = Stiffness of Matrix
E_f = Stiffness of Fiber

Case and Reifsnider have developed a computer code based on the above arguments for strength with a polymer matrix composite. This code (MRLife) is written in "C++" and the results from this code will be used to compare with the experimental results [2].

Model Two

The Subramanian and Reifsnider model is based on many of the same assumptions that model 1 is based on [1]. The broken fibers are assumed to form a central core with a layer of matrix material around the fiber. The broken fiber(s) is assumed to have the neighbors of fibers arranged in a concentric cylinder with the broken fiber(s) in the center, as shown in Figure 1.03. These assumptions are based on the work of Gao and Reifsnider described previously. The equilibrium equations for the central core of broken fibers and the adjacent fibers are written in the differential equation with the dependent variable of displacement in this form

$$E_{f1}\pi \, r_{f1}^2 \frac{d^2 u_{f1}}{dx^2} + 2\pi \, r_{f1}\tau_{m1} = 0 \qquad \textbf{36}$$

$$n_i E_{f2}\pi \, r_f^2 \frac{d^2 u_{f2}}{dx^2} + 2\,\pi r_m \tau_{m2} + 2\pi \, r_{f2}\tau_{m3} = 0 \qquad \textbf{37}$$

where the shear stress is defined by

$$\tau_{m1} = \left(\frac{u_{m2} - u_{m1}}{b} \right) G_m \qquad \textbf{38}$$

$$\tau_{m2} = \left(\frac{u_{m1} - u_{m2}}{b} \right) G_m \qquad \textbf{39}$$

$$\tau_{m3} = \left(\frac{u_c - u_{m2}}{b} \right) G_m \qquad \textbf{40}$$

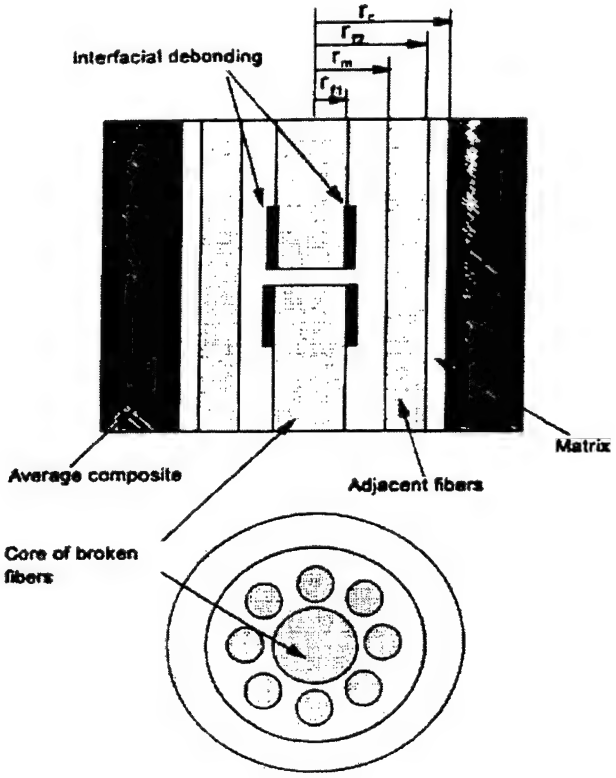

Figure 1.03 Schematic of concentric cylinder model with a core of broken fibers with the neighboring fibers.

These equations are based on the assumption that the displacement varies linearly in the radial direction in the matrix material. The fibers are also assumed to carry all the axial load with the matrix around the fibers acting only to transfer the load between the fibers through a shear transfer mechanism. Assuming that the displacement in the fiber and matrix at the fiber-matrix interface is discontinuous, and that the displacement in the average composite is uniform, the following expressions can be written

$$u_c = \frac{\sigma_a x}{E_x} \qquad 41$$

$$u_{f1} = \eta u_{m1} \qquad 42$$

$$u_{f2} = \eta \, u_{m2} \qquad 43$$

Again, the efficiency factor is used to determine how well the load is transferred from the matrix into the fiber. If the value is one, then this indicates perfect bonding of the interface and a good load transfer. A value of zero indicates no transfer of load from the matrix into the fiber.

The equilibrium equations may then be rewritten as follows:

$$\frac{d^2 u_{f1}}{dx^2} + k_1 u_{f1} + k_2 u_{f2} = 0 \qquad 44$$

$$\frac{d^2 u_{f2}}{dx^2} - k_3 u_{f2} + k_4 u_{f1} + k_5 x = 0 \qquad 45$$

where

$$k_1 = -\frac{2 r_{f1} G_m}{b E_{f1} \eta \, r_{f1}^2}$$

$$k_3 = \frac{2 r_m G_m}{n_i b E_{f2} \eta \, r_{f2}^2} + \frac{2 r_{f2} G_m}{n_i b E_{f2} \eta \, r_{f2}^2}$$

$$k_4 = \frac{2 r_m G_m}{n_i b E_{f2} \eta \, r_{f2}^2}$$

$$k5 = \frac{2 r_{f2} G_m \sigma_a}{n_i b E_{f2} \eta \, r_{f2}^2 E_x} \qquad 46$$

The following boundary conditions are used to solve the differential equations (44 and 45).

$$\left(\frac{du_{f1}}{dx}\right)_{x=0} = 0$$

$$(u_{f2})_{x=0} = 0 \qquad \textbf{47}$$

Solving the differential equations yields:

$$[D^4 + D^2(k_1 - k_3) - (k_2k_4 + k_1k_3)]u_{f2} - k_2k_5x = 0 \qquad \textbf{48}$$

The homogenous solution to the differential equation requires that

$$u_{f1} = C_1e^{-\alpha x} + C_2e^{-\beta x} + C_3x + C_4e^{\alpha x} + C_5e^{\beta x}$$

$$u_{f2} = D_1e^{-\alpha x} + D_2e^{-\beta x} + D_3x + D_4e^{\alpha x} + D_5e^{\beta x} \qquad \textbf{49}$$

where

$$\alpha, \beta = \left[\frac{(k_3 - k_1) \pm \sqrt{(k_1 + k_3)^2 + 4k_2k_4}}{2}\right]^{1/2} \qquad \textbf{50}$$

The following constants must be zero in order for the fiber strains to be finite at regions far away from the fiber fracture; C_4 , C_5, D_4, and D_5. Next the assumed displacement functions are substituted into the equilibrium equations and the remaining constants are determined.

$$C_3 = \frac{-k_2 k_5}{k_1 k_3 + k_2 k_4}$$

$$D_3 = -C_3$$

$$C_1 = \left(-\frac{k_2}{\alpha^2 + k_1} \right) D_1$$

$$C_2 = \left(-\frac{k_2}{\beta^2 + k_1} \right) D_2$$

$$D_1 = \frac{C_3}{\left[\frac{\beta k_2}{\beta^2 + k_1} - \frac{\alpha k_2}{\alpha^2 + k_1} \right]}$$

$$D_2 = -D_1 \qquad \textbf{51}$$

Now the solution to the displacements is obtained

$$u_{f1} = C_1 e^{-\alpha x} + C_2 e^{-\beta x} + C_3 x$$

$$u_{f2} = D_1 e^{-\alpha x} + D_2 e^{-\beta x} + D_3 x \qquad \textbf{52}$$

The strains and stresses in the central core and the adjacent fibers are derived using the strain-displacement and constitutive relationships of mechanics of materials.

$$\varepsilon_{f1} = \frac{du_{f1}}{dx}; \quad \sigma_{f1} = E_{f1} \varepsilon_{f1}$$

$$\varepsilon_{f2} = \frac{du_{f2}}{dx}; \quad \sigma_{f2} = E_{f2} \varepsilon_{f2} \qquad \textbf{53}$$

The stress concentration factor in the adjacent fiber for the elastic case is written as

$$C_i = (\sigma_{f2})_{x=0} / (\sigma_{f2})_{x\to\infty} \qquad 54$$

In the elastic case, the ineffective length is obtained by determining the length over which the inner core recovers 99% of the applied stress [1].

$$\sigma_{f1}(x) = 0.99\,\sigma_a \qquad 55$$

In the plastic case, the stress concentration factor Ci* and the ineffective length delta I* are obtained using the following approximation. It is assumed that the matrix exhibits an elastic-perfectly plastic behavior. If the average shear stress in the matrix exceeds the interfacial shear strength, the interface is assumed to debond. Once debonding occurs, the shear stress in the matrix is assumed to be constant over the region defined as the plastic ineffective length, and zero elsewhere [1]. The plastic stress concentration factor is estimated by calculating the average stress in the adjacent fiber as follows:

$$\overline{\sigma_{f2}} = \frac{1}{\delta}\int_0^{\delta} \sigma_{f2}\,dx$$

$$\overline{\sigma_{f2}} = \frac{E_{f2}}{\delta}[D_3\delta - D_1 - D_2]$$

$$C_i^* = \frac{\overline{\sigma_{f2}}}{E_{f2}D_3} \qquad 56$$

For the elastic-perfectly plastic case, the stress concentration factor will be equal to one. The force balance argument is used to estimate the plastic ineffective length as follows:

$$\delta_i^* = \frac{\overline{\sigma}_{fl} r_{f1}}{2\eta \tau_i} \qquad 57$$

where the average stress in the inner core is given by

$$\overline{\sigma}_{fl} = \frac{E_{f1}}{\delta} \int_0^{\delta} \varepsilon_{fl} dx$$

$$\overline{\sigma}_{fl} = \frac{E_{f1}}{\delta} (C_3 \delta - C_1 - C_2) \qquad 58$$

When writing the force balance equation, it was assumed that due to interfacial debonding the shear stress in the matrix is not equal to the interfacial shear strength, but is multiplied by the efficiency factor. Once debonding has occurred the transfer of stress is done with a mechanism of friction. After debonding it is assumed that the stress transfer will not be perfect. The shear stress is multiplied by the efficiency factor to reflect this behavior [1].

Now that the stress concentration factor and the ineffective lengths have been derived for both cases of plastic and elastic local behavior for different fiber breakages, the tensile strength is predicted following Batdorf's analysis. As previously discussed, Batdorf showed that the stress level at which the first fiber fracture occurs is expressed as:

$$\sigma_1 = \left(\frac{1}{NL}\right)^{1/m} \sigma_o$$

N = *total* number of fibers in the specimen
L = normalized length of the specimen
m = Weibull strength shape factor for the fiber
σ_o = Weibull strength location parameter for the fiber **59**

The stress level at which the next fiber fractures occur is given by

$$\sigma_i = \left(\frac{1}{NL\pi\, n_{i-1}\lambda_{i-1}}\right)^{1/m} \sigma_o \quad i = 2,3,... \qquad \textbf{60}$$

and

$$\lambda_i = 2\delta_i \left[\frac{C_i^{m+1} - 1}{(C_i - 1)(m+1)}\right] \qquad \textbf{61}$$

The average shear stress in the matrix region is estimated as follows

$$\overline{\tau_m} = \frac{1}{\delta}\int_0^{\delta}\left(\frac{u_{2m} - u_{1m}}{b}\right) G_m dx$$

$$\overline{\tau_m} = \frac{G_m}{\delta b \eta}\left[\frac{(D_1 - C_1)}{\alpha} + \frac{(D_2 - C_2)}{\beta}\right] \qquad \textbf{62}$$

It is assumed that interfacial debonding occurs when the average shear stress in the matrix exceeds the interfacial shear strength. At each load level, calculations are made to see if the interfacial failure occurs. Once the interfacial failure occurs then the plastic stress factor and ineffective lengths are used to predict fiber fractures. However,

if there is no interfacial failure until instability occurs, then the final failure is classified as elastic failure. If the debonding occurs before the final failure, the failure is termed plastic.

Model 2 can be used to predict failure of an unidirectional laminate for tensile strength. A computer code that makes the looped calculations of this model is written in Pascal.

Quantitative Differences between the Models

As previously mentioned, both of the models are based on the classical shear lag arguments. However there are some differences between the two models. Model 1 assumes that the displacement in the fiber and matrix outside the yielding region to be continuos at the fiber-matrix interface. Model 2 admits displacement discontinuities between the fiber and matrix outside the yielding zone. Model 1 uses the maximum shear stress value in the matrix to determine if yielding occurs. Model 2 uses the average shear stress value in the matrix to determine if yielding occurs. Other differences maybe between the assumed geometry of the fiber matrix regions.

Temperature Effects on the Strength

Many researchers have tried to understand the effects of elevated temperatures on composite materials. Many questions still remain about the effect. For example, how does the temperature affect the material system with respect to creep recovery and visco-elastic-plastic behavior. More important is how we express these behaviors in terms of known constitutive equations [5].

The approach to these questions has been to identify the failure mode(s) that control fracture, and to set up a boundary value problem that represents the micro-details in terms of the constituents and geometry. The simplest example of this is the rule of mixtures:

$$X_t = v_f X_f + v_m X_m$$

X_t = Composite strength **63**
X_f and X_m = Fiber and matrix strength
v_f and v_m = Fiber and matrix volume fraction

However this model is limited as a one-dimensional model and not considered sufficiently rigorous. An alternative model represents the tensile strength and performance of the constituents and the interphase regions between [5]. This model includes more of the physical factors and effects that control tensile strength:

$$X_t = \sigma^{\frac{m}{m+1}} \left(\frac{2\tau_0 L}{\overline{D}}\right)^{\frac{1}{m+1}} \left(\frac{2}{m+2}\right)^{\frac{1}{m+1}} \left(\frac{m+1}{m+2}\right) \frac{(1+m)^{\frac{1}{m}}}{[C_n^m + C_n^{m-1} + \ldots + 1]^{1/m}}$$

64

$\overline{D}$ = Fiber diameter
σ = Characteristic strength of the fibers
τ_o = Interfacial shear strength
L = Characteristic length of the material
C_n = Local stress concentration numbers when neighboring fibers are broken
m = Weibull shape parameter of the statistical distribution of fiber strengths

The above models are useful and if we examine them we can see that there are several parameters that are influenced by temperature. Reifsnider and Case state that the yield strength of the matrix (or interphase region between the fiber and the matrix) can be expected to decrease with increasing temperature [5]. Also, the stiffness of the components will, in general, be a function of temperature. For a polymer matrix material, for example, the shear stiffness will often be strongly temperature dependent [5].

Furthermore, temperature also effects the ineffective length. As discussed, the ineffective length is created in the region of a fiber fracture. When a fiber breaks, the stress is transferred back into a neighboring fiber by the surrounding matrix in a manner that is controlled by the stiffness of the surrounding material. As the surrounding material becomes less stiff, the ineffective length becomes larger. If the ineffective length is large, then the fiber fracture regions will interact more easily and may connect together to cause complete failure [5]. However, if the matrix material and surrounding composite is very stiff, then the stress is transferred back into the fiber over a small distance and the ineffective length is small. In this case, the stress concentration in the material next to a fiber break is very high. This greatly increases the chance of one fiber fracture causing an unstable sequence of neighboring fiber fractures resulting in complete failure. A shear lag equation for the ineffective length is as follows:

$$\delta = \frac{1}{2}\left[\frac{1}{2}\left(\frac{1-v_f^{0.5}}{v_f^{0.5}}\right)\left(\frac{E_f}{G_m}\right)\right]^{\frac{1}{2}} \ln\left(\frac{1}{1-\phi}\right)$$

δ = Ineffective length
v_f = Volume fraction of the fiber **65**
G_m = Matrix stiffness
E_f = Stiffness of the fibers
ϕ = Efficiency factor for the stress transfer

Case and Reifsnider pointed out that elevated temperature reduces the stiffness of the matrix and with this reduction the ineffective length will increase. Under this assumption, the strength equation should express what happens to the composite strength. If the increase in temperature causes the ineffective length to increase, then the composite strength may respond with an increase or decrease. The basic assumption is that as the

temperature is elevated, the polymer matrix stiffness will reduce and with this phenomena the ineffective length will increase. The effect of the ineffective length on the strength is demonstrated in the following figure (Figure 1.04) [5].

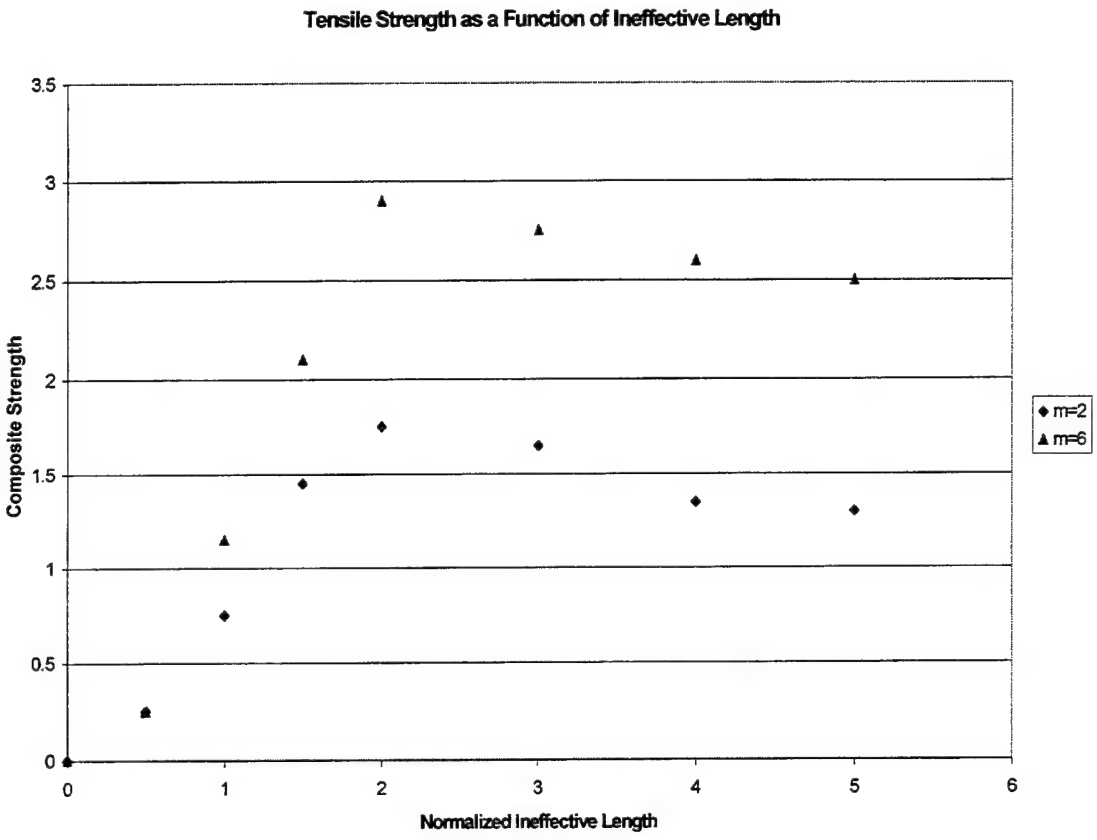

Figure 1.04 Tensile strength as a function of local ineffective length.

This figure (Figure 1.04) is generated for different ineffective length values with two different Weibull shape factors (m). Clearly, this figure indicates that there is a location were the strength is maximum. To the left of the maximum, strength is reduced by a stress concentration due to the small ineffective length that causes a brittle fracture. To the right of the maximum, the strength is reduced by the greater ineffective length because of the coupling of fiber fracture zones. Therefore, as the elevated temperatures

cause the ineffective length to change, the strength may increase or decrease based on the position of the value for the ineffective length [5].

Using some data we can demonstrate the strength increases and decreases with the change of elevated temperature (Figure 1.05). The IM7/K3B system was tested in our laboratory and the Graphite/Epoxy system was tested by Haskins [6].

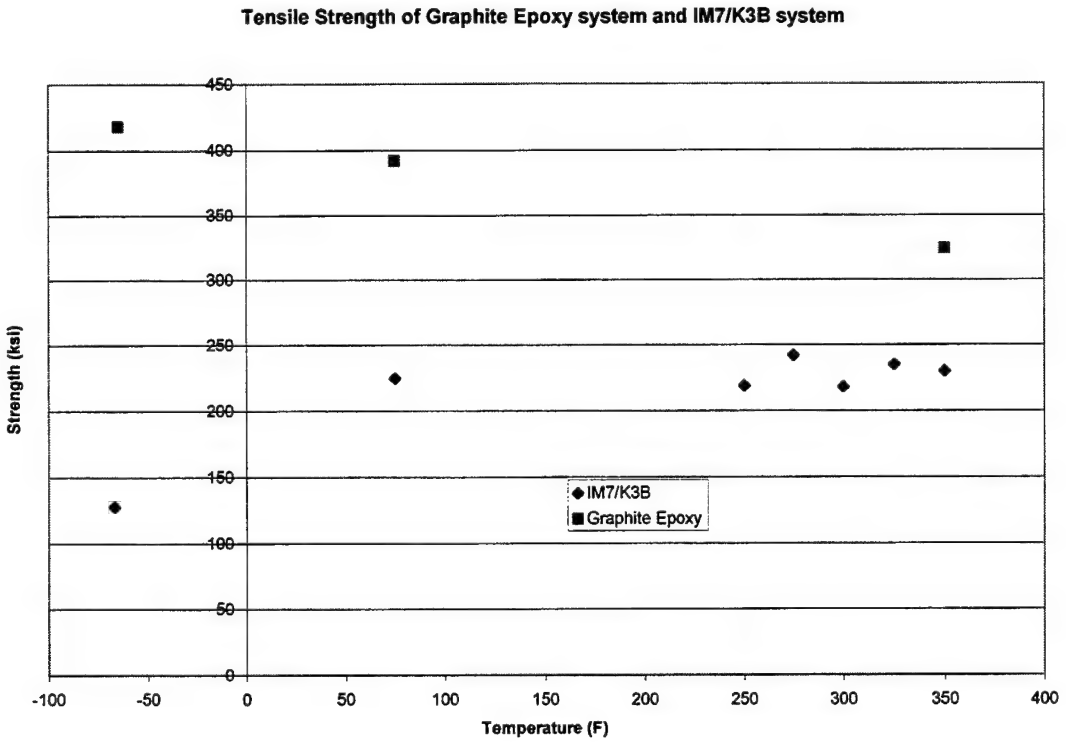

Figure 1.05 Unidirectional tensile strength as a function of temperature for two polymer carbon fiber composites.

This figure indicates that, depending on the matrix material, we can be to the left of the ineffective length temperature maximum or to the right of this maximum. Observing the Graphite/Epoxy system in Figure 1.05, the indication is that this system is

to the left of the maximum in Figure 1.04. However the IM7/K3B system indicates that the strength is to the right of the maximum in Figure 1.04.

Interfacial Shear Strength at Elevated Temperatures

Both of the above models use the interfacial shear strength as a parameter in the formulation of the strength. Many researches have spent time investigating the fiber-matrix shear strength. The matrix polymer adhering to the fiber surface produces this strength. An investigation was performed on the interfacial adhesion on carbon fiber at elevated temperatures by H. Zhuang and J.P. Wightman [7]. This evaluation is also known as single fiber fracture testing.

The testing was conducted on various carbon fibers in a single "dog bone" specimens of epoxy matrix. Preparation of the single fiber composite was as follows: a silicone rubber mold with a dog-bone-shaped cavity was used to give the composite its shape during cure of the epoxy. A single fiber was fixed on both ends with the middle suspended in the mold. Epoxy resin was poured in the mold with the fiber embedded in the epoxy. The cure schedule was 75 degrees C for 2 hours and then 125 degrees C for another 2 hours. Then the specimens were allowed to cool overnight and removed from the mold [7].

The fragmentation test was preformed as follows: the single fiber specimens were mounted in a hand operated loading fixture one at a time. The specimens were observed with a transmitting-light microscope. The specimens were then pulled in tension at a speed of 1 mm/min and the fiber fractures were observed during this process. The tension on the specimen was stopped after no further breaks were observed with

increasing load. The fragment lengths then were measured with the aid of the microscope and recorded.

The same procedure was used for the elevated temperature fragmentation tests. However, the fixture was placed in a hot oil bath with the oil at the desired temperature. The specimens were given 10 minutes in the oil bath to allow for the heat transfer [7].

The equation used to determine the interfacial shear strength was as follows.

$$\tau = \frac{\sigma_f}{2}\frac{d}{l_c}$$

τ = interfacial shear strength **66**
σ_f = fiber strength at the critical length
d = fiber diameter
l_c = critical length

Figure 1.06 and Figure 1.07 show the response of the interfacial shear strength as a function of temperature. Three different fibers were used to examine the adhesion process on the fibers for a single matrix material. The carbon fibers were AS-4, AU-4 and Panex 33 (S) and the epoxy was Epon 828. Two different curing agents were used on the epoxy. Figure 1.06 shows the response with the Jeffamine DU-700 curing agent and Figure 1.07 shows the response with mPDA curing agent [7].

The results show that the interfacial shear strength decreases as a function of temperature. The trend from one carbon fiber system to another system can vary, and the curing agent can also effect the strength value.

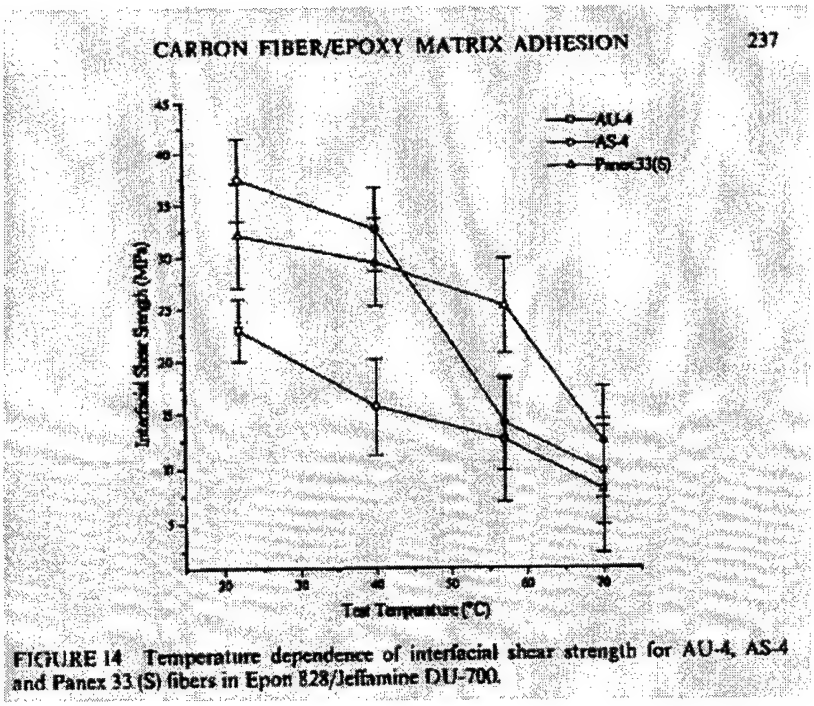

FIGURE 14 Temperature dependence of interfacial shear strength for AU-4, AS-4 and Panex 33 (S) fibers in Epon 828/Jeffamine DU-700.

Figure 1.06 Interfacial shear strength as a function of temperature from single fragmentation test/ Epon 828 DU-700 [7].

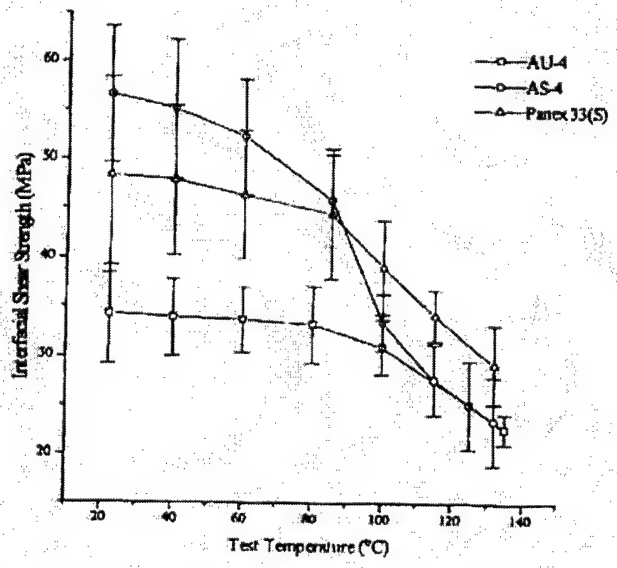

FIGURE 13 Temperature dependence of interfacial shear strength for AU-4, AS-4 and Panex 33 (S) fibers in Epon 828/mPDA.

Figure 1.07 Interfacial shear strength as a function of temperature from single fragmentation test/ Epon 828 mPDA [7].

Bulk Polymer Stiffness at Elevated Temperatures

The other variable known to be affected by the elevated temperature is the matrix stiffness. Most polymers become less stiff as their temperature is increased because the polymer chains are given more freedom to move and bonding is reduced. At melt temperature, most polymers act as a fluid; therefore, as the temperature approaches the glass transition temperature of the polymer, the stiffness is effected. An example of this behavior is found in Figure 1.08 [8]. This figure is a collection of stress-strain curves for epon 828 epoxy.

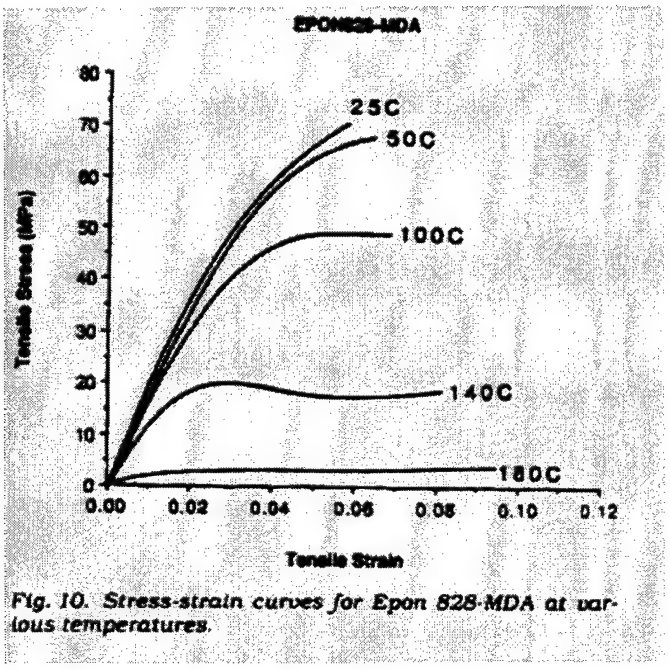

Fig. 10. Stress-strain curves for Epon 828-MDA at various temperatures.

Figure 1.08 Bulk Epon 828 stress-strain curves at elevated temperatures [8].

Mechanical Properties for Materials

Mechanical properties for AS-4 carbon fiber are give in Table 1.01. The source of the property is also given in the table. In addition to the carbon fiber, properties of

PPS and PEEK polymers are given in Table 1.02. These properties will be used in the models.

Table 1.01 Summary of mechanics parameter for AS-4 carbon fiber.

AS-4 Carbon Fiber Properties	**Value**
Young's Modulus E_f [8]	241 (Msi)
Weibull location parameter [8]	5.25
Weibull shape factor [8]	10.65
Radius of a single fiber [8]	1.378x10-4 (in)
Fiber strength location Parameter [8]	786000 (psi)

Table 1.02 Properties of thermoplastics PEEK and PPS.

Property at 23 degrees C	**PPS**	**PEEK**
Tensile Modulus	480 (ksi) [9]	470 (ksi) [10]
Poisson's ration	0.35	0.40 [10]
Melt Temperature	285-290 (C) [9]	370-400 (C) [10]
Glass Transitional Temp.	88 (C) [9]	143 (C) [10]

4. Changes to Model Parameters for Elevated Temperature

As Figure 1.06 indicated, the interfacial shear strength is known to be some function of temperature. No specific measurement was made of the interfacial shear strength with PPS and a carbon fiber at elevated temperatures. Assuming the trend shown in Fig. 1.06 would apply to the PPS system, an approximation was generated of the interfacial shear strength as a function of elevated temperatures. This is shown in Figure 4.02. The approximation used a value of room temperature interfacial shear strength for PPS with a carbon fiber found in the literature [13]. Using the room temperature as one reference point and the melt temperature of PPS as the other reference

point, a straight line was fitted. At melt temperature, the interfacial shear strength was assumed to be zero.

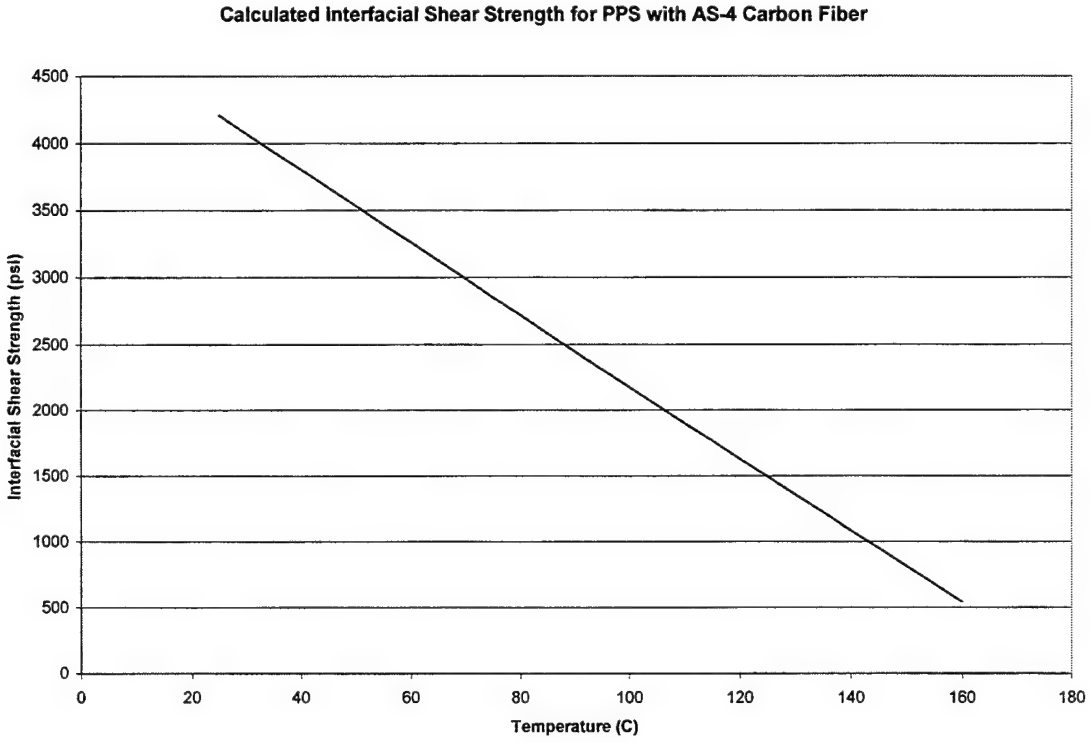

Figure 4.02 Approximation of the interfacial shear strength as a function of temperature for a PPS composite system.

In addition to the interfacial shear strength, Figure 1.08 indicated that the stiffness of the matrix material should be some function of temperature. No specific measurement was made on the stiffness of the PPS polymer as a function of temperature. Assuming this trend from Fig. 1.08 would apply to the PPS polymer, an approximation was generated of the stiffness as a function of elevated temperatures. This is shown in Figure 4.03. The approximation used a value of the stiffness at room temperature of the PPS found in the literature [9]. Using the room temperature of PPS as one reference point and

the melt temperature of PPS as the other reference point a straight line was fitted. At melt temperature, the stiffness of PPS was assumed to be zero.

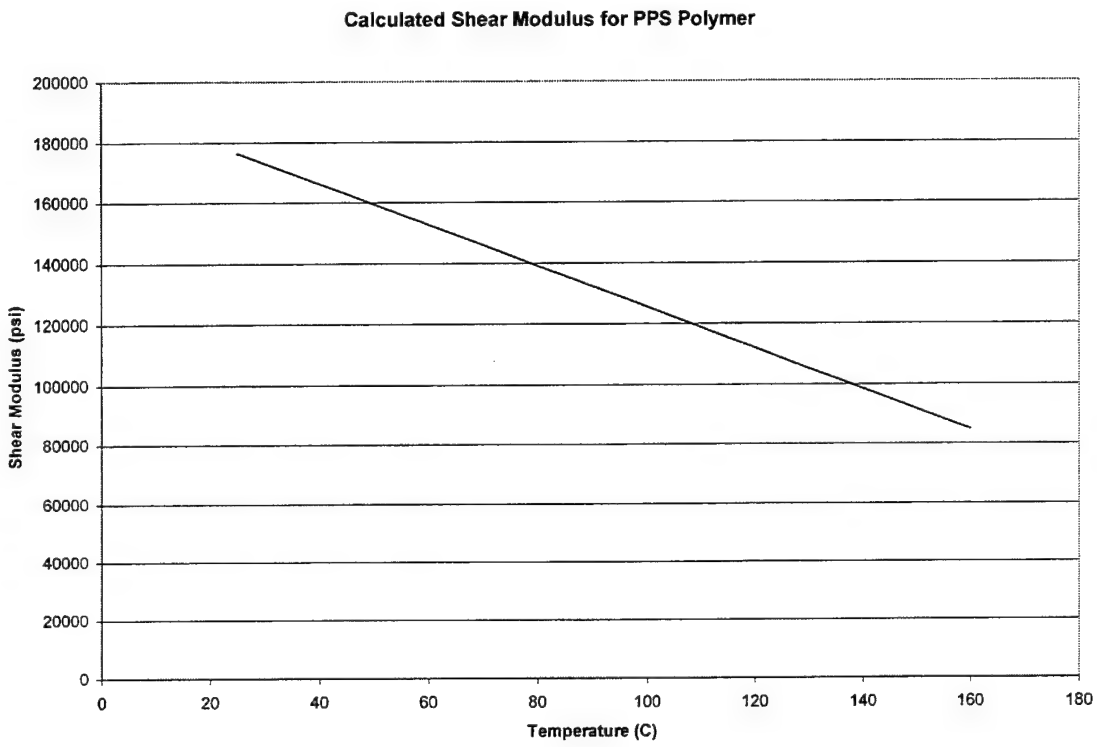

Figure 4.03 Approximation of the shear modulus as a function of temperature for the PPS matrix.

In addition to the PPS system, the interfacial shear strength of the PEEK system should be some function of temperature. No specific measurement was made of the interfacial shear strength with PEEK and a carbon fiber at elevated temperatures. So assuming that a trend similar to Fig. 1.06 applies to the PEEK system, an approximation was generated of the interfacial shear strength as a function of elevated temperatures. This is shown in Figure 4.04. The approximation was generated by using a value of interfacial shear strength at room temperature for PEEK with a carbon fiber found in the literature [13]. Using the room temperature as one reference point and the melt temperature of the PEEK matrix as the other reference point a linear line was fitted as the

approximation. At melt temperature, the interfacial shear strength was assumed to be zero.

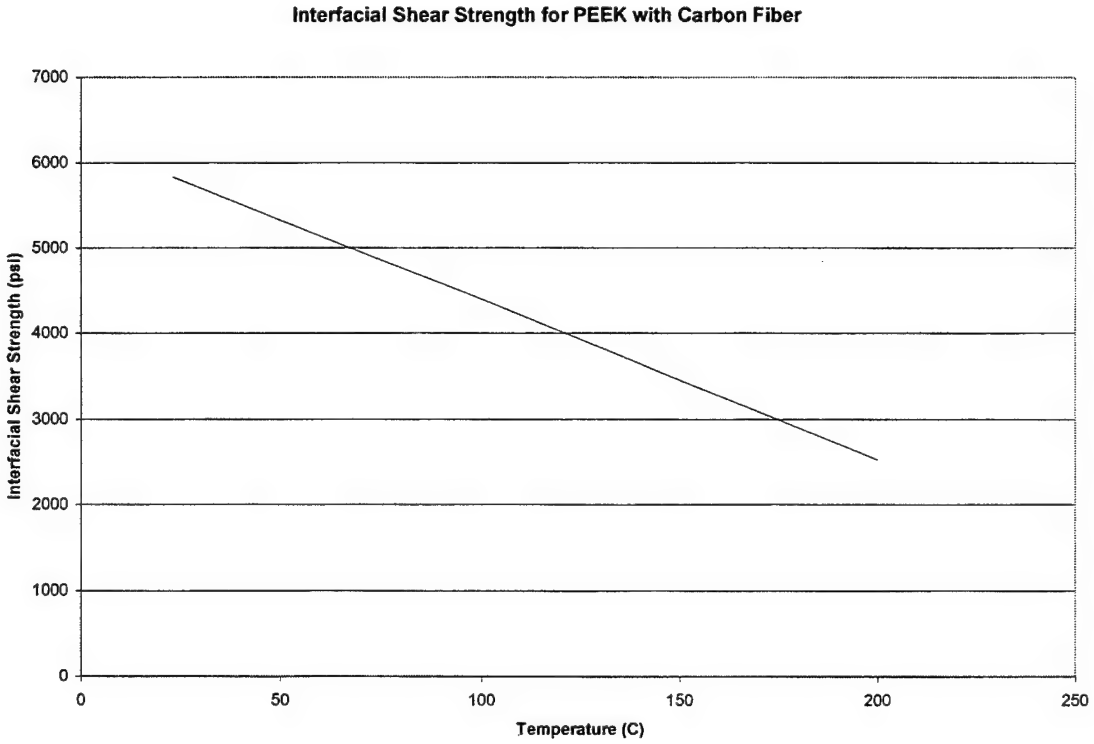

Figure 4.04 Approximation to the interfacial shear strength as a function of temperature for PEEK composite system.

As mentioned above, Figure 1.08 indicated that the stiffness of a polymer material should be some function of temperature. No specific measurement was made on the stiffness of PEEK at elevated temperature. However, by using the room temperature value found in the literature, an approximation was generated assuming the trend indicated by Figure 1.08 [10]. A linear fit was used as the trend with one reference point at room temperature and the other at melt temperature. At melt temperature, the stiffness of the PEEK was assumed to be zero. This approximation is shown in Figure 4.05.

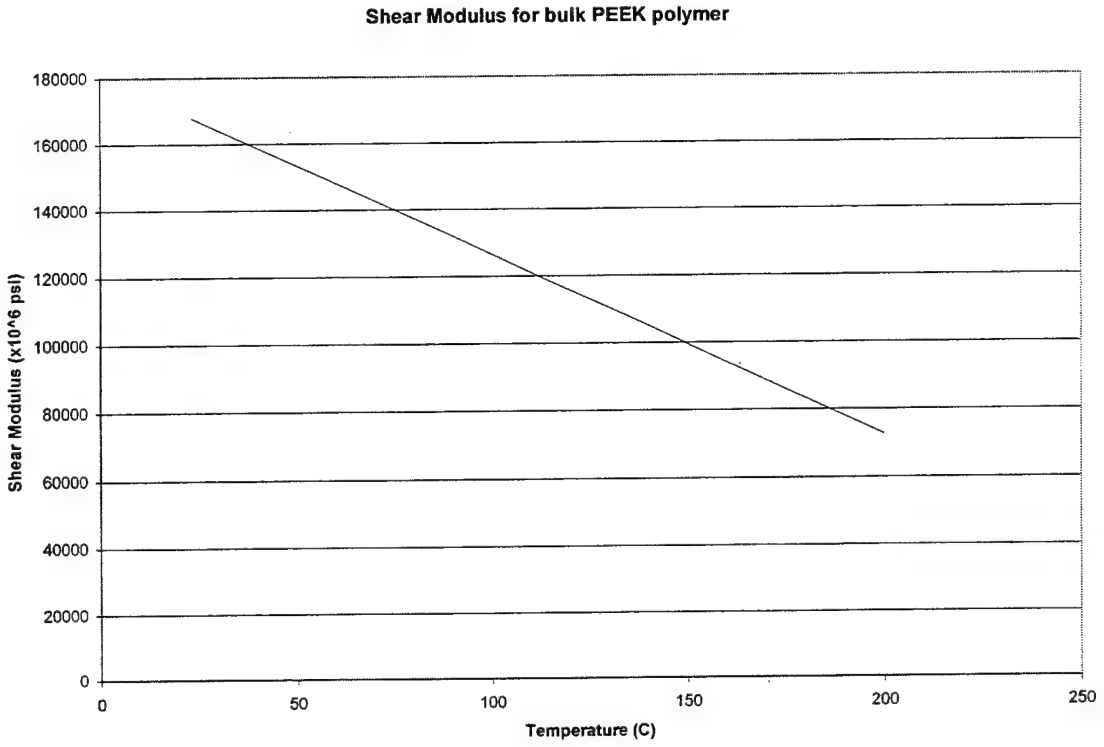

Figure 4.05 Approximation of the shear modulus for PEEK as a function of temperature.

Model Predictions of Strength at Elevated Temperatures

The above variables were entered into both models as a function of temperature. The other variables for the PPS and PEEK systems that were used in the models are given in Table 4.01 and 4.02 (also given in Table 1.02). The fiber properties used in the models are given in Table 4.01 and 4.02 (also given in Table 1.01). These are the main variables that must be determined and inserted into both models. The predicted results from the models are shown in Table 4.03 and 4.04 for both the PPS and PEEK systems.

Table 4.01 Input variables for the micro-mechanical models for PPS composite.

Variable Description	Variable Symbol	Value
Matrix Shear Modulus	G_m	180,000 PSI at Room Temperature; Then the function developed above
Interfacial Shear Strength	Tau_m	4407 PSI at Room Temperature; then

		the function developed above
Fiber Modulus	e_{f2}	34x10^6 PSI
Fiber Volume Fraction	v_f	0.40
Radius of a Single Fiber	r_f	1.378 x 10^-4 in
Total # of Fibers in Composite	n	83627
Fiber Strength Location Parameter	Sig_o	786000 PSI
Efficiency Factor	η	1
Fiber Strength Shape Factor	M	10.65

Table 4.02 Input variables for the micro-mechanical models for PEEK composite.

Variable Description	Variable Symbol	Value
Matrix Shear Modulus	G_m	167,825 PSI at Room Temperature; Then the function developed above
Interfacial Shear Strength	Tau_m	5831 PSI at Room Temperature; then the function developed above
Fiber Modulus	e_{f2}	34x10^6 PSI
Fiber Volume Fraction	v_f	0.39
Radius of a Single Fiber	r_f	1.378 x 10^-4 in
Total # of Fibers in Composite	n	231,329
Fiber Strength Location Parameter	Sig_o	786000 PSI
Efficiency Factor	η	1
Fiber Strength Shape Factor	M	10.65

These inputs were used in the two models along with the derived temperature functions for the interfacial shear strength and the stiffness of the matrix. The predictions from both models can be found in Table 4.03 and 4.04.

Table 4.03 Model strength results for the PPS composite system.

Test Temperature (C)	Average Strength from figure 3.xx (ksi)	Predicted Strength (Model 1 Reifsnider and Gao) (ksi)	Predicted Strength (Model 2 Reifsnider and Subramanian) (ksi)
23-30	241	221	213

60	223	216	208
80	221	213	205
100	220	209	201
120	212	204	198
140	198	197	191

Table 4.04 Model strength results for the PEEK composite system.

Test Temperature (C)	Average Strength from figure 3.xx (ksi)	Predicted Strength (Model 1 Reifsnider and Gao) (ksi)	Predicted Strength (Model 2 Reifsnider and Subramanian) (ksi)
23-27	333	393	367
60	308	389	363
80	317	386	361
100	296	383	359
120	301	381	357
160	299	374	349

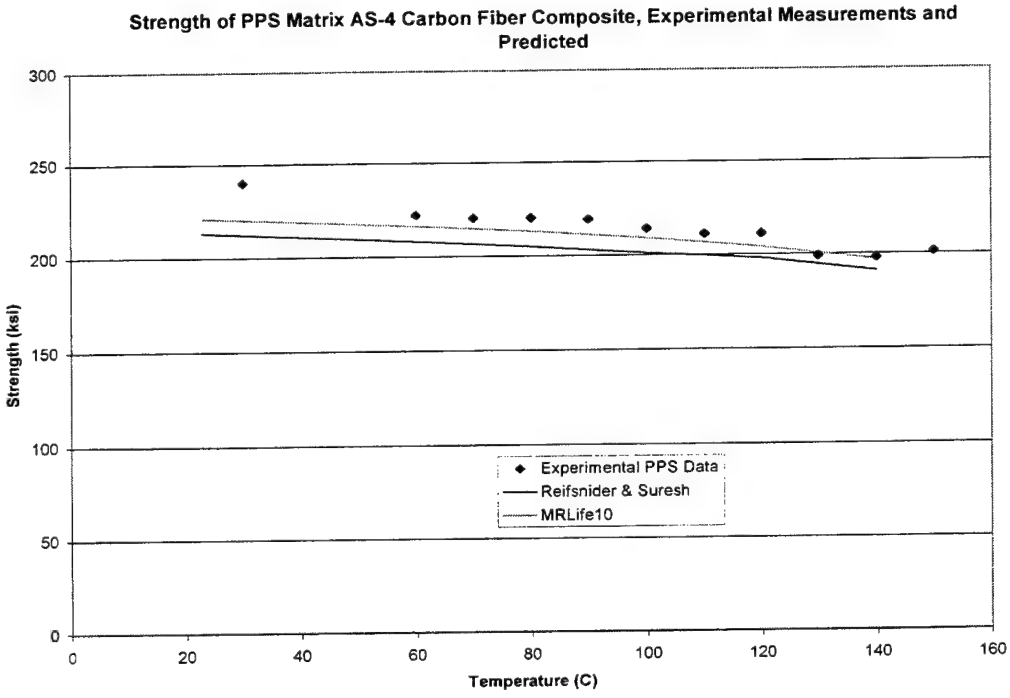

Figure 4.06 Experimental data for PPS compared to model predictions of strength.

As shown in Figure 4.06, both models slightly under-predict the average strength of the PPS composite system. However, both of the models' predictions are within the experimental scatter of this system. Both models predict a 10 percent decrease in

strength from room temperature to 140 degrees Celsius. An R-squared linear fit for model #2 gave a slope of -0.18 and a R-square value of 0.96. The same fit for model #1 gave a slope of -0.19 and a R-square value of 0.96. The experimental results showed a 17 percent decrease in this temperature range for the PPS composite system. An R-squared linear fit for the average experimental data gave a slope of 0.32 and a R-square value of 0.93. This difference could be a result of several factors. One such factor is that the interfacial shear strength and the shear modulus assumptions in Figures 4.02 and 4.03 are not accurate. More information must be determined to eliminate the guesswork for these variables. Another factor could be due to the fact that the temperature is effecting more variables than the interfacial shear strength and the matrix stiffness. Maybe the models have not taken into account all the variables that control the strength.

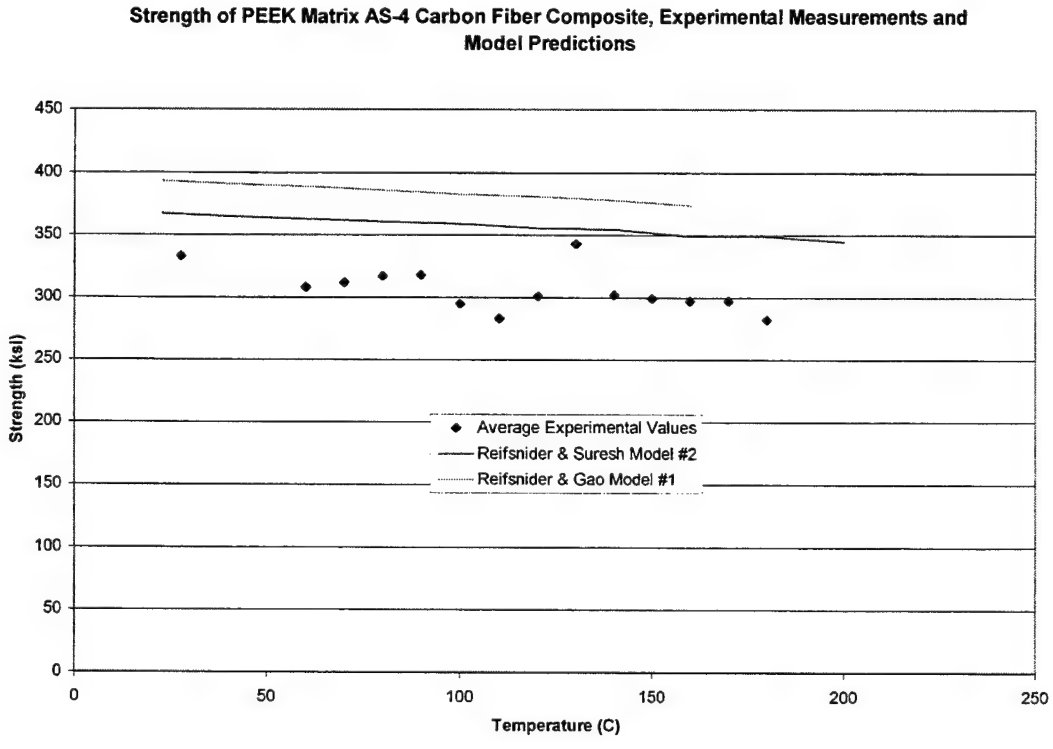

Figure 4.07 Experimental data for PEEK composite compared to model predictions of strength.

For the PEEK, both models over estimated the average experimental strength value (Figure 4.07). Both of the models' predictions did not fall within the experimental values for this system. Additionally, both models predict a 5 percent decrease in strength from room temperature to 160 degrease Celsius for this system. An R-squared linear fit for model #2 gave a slope of -0.12 and an R-square value of 0.98. The same fit was applied to model #1 gave a slope of -0.13 and an R-square value of 0.99. The experimental results showed a 10 percent decrease in strength. An R-squared linear fit for the average experimental data gave a slope of -0.20 and an R-square value of 0.29. This could be due to the same factors discussed for the PPS system.

Summary of Method

In order to predict the strength of a polymer composite in an environment of elevated temperature using the models discussed, the temperature dependence of the two main variables must be determined. These variables are the interfacial shear strength and the shear modulus of the matrix material. If the information is not available, then an approximation can be used for these values. After these variables are determined, the micro-mechanical models can be used to predict the temperature response of the composite system.

Conclusions

For the three material systems examined, the strength of unidirectional polymer composite systems can be expected to decrease with elevated temperatures between room temperature and the glass transitional temperature. In addition to the strength, the

stiffness of these systems was also found to decrease. The strength decrease is generally more than the stiffness decrease. At the fiber-matrix level, for each of these materials, the ineffective length is being increased as the temperature is elevated. This is concluded because the matrix stiffness decreases. The change in the fracture mode of vinyl ester also leads to this conclusion.

The vinyl ester system at the lower temperatures failed with more of the fibers grouped together. At the higher temperatures, the fracture was less clumped with groups of fibers and consisted more of single fibers. In this case, ineffective lengths were larger and fiber fracture regions connected more readily to cause global failure.

Based on recent research efforts, the interfacial shear strength of a polymer matrix and a carbon fiber can be expected to decrease with elevated temperatures. The interfacial strength and stiffness also controls the ineffective length. In addition to the interfacial shear strength, the stiffness of a polymer can be expected to decrease with elevated temperatures. The combination of these effects can be placed in micro-mechanical models to give a reasonable predictions. The models that we have developed showed good agreement with observations. Therefore, this method is viable for predicting the failure strength of unidirectional polymer carbon fiber composite systems, and opens the door to the construction of robust engineering design models that can be used for the estimation of strength, stiffness and life of polymer based composite systems over a wide range of use temperatures. The construction of such design models is the ultimate goal of this work.

REFERENCES:

1. Subramanian, S., Reifsnider, K.L., and Stinchcomb, W.W., "Tensile Strength of Unidirection Composites: The Role of Efficiency and Strength of Fiber-Matrix Interface," *Journal of Composites Technology & Research,* JCTRER, Vol.17,No. 4, October 1995, pp. 239-300.

2. MRLife10, *"A Strength and Life Prediction Code for Laminated Composite Materials,"* S. Case and K.L. Reifsnider, Materials Response Group, Virginia Polytechnic Institute and State University, 1997.

3. Gao, Z., and Reifsnider, K.L., "Micromechanics of Tensile Strength in Composite Systems," *Composite Materials: Fatigue and Fracture, Fourth Volume,* ASTM STP 1156, W.W. Stinchcomb and N.E. Ashbaugh, Eds., American Society for Testing and Materials, Philadelphia, 1993, pp. 453-470.

4. Reifsnider K.L., ESM 6104 Class Notes, Department of Engineering Science and Mechanics, Virginia Polytechnic Institute & State University.

5. Reifsnider, K.L., Case, Scott, "Mechanics of Temperature-Driven Long-Term Environmental Degradation of Polymer-Based Composite Systems," Department of Engineering Science and Mechanics, *Virginia Polytechnic Institute and State University*, Blacksburg, Virginia.

6. NASA Contractor Report # 178272, *"Time-Temperature-Stress Capabilities of Composite Materials for Advanced Supersonic Technology Application,"* J.R. Kerr and J.F. Haskins, NASA, May 1987.

7. H. Zhuang and J.P. Wightman, "The Influence of Surface Properties on Carbon Fiber / Epoxy Matrix Interfacial Adhesion," *Journal of Adhesion,* 1996, Vol. 62, pp. 213-245.

8. A.S. Wimolkiatisak and J. P. Bell, "Interfacial Shear Strength and Failure Modes of Interphase-Modified Graphite-Epoxy Composites," *Polymer Composites,* June 1989, Vol. 10, No.3, pp. 162-172.

9. Charles A. Harper, "Handbook of Plastics, Elastomers, and Composites," Third Edition, McGraw-Hill Companies, Inc., 1996.

10. P.K. Mallick, "Fiber-Reinforced Composites," Second Edition, Marcel Dekker, Inc., 1993.

11. A.J. Kinloch, *"Adhesion and Adhesives,"* Chapman & Hall, London, 1987

12. ASTM Designation D 3039/D 3039M - 93, "*Standard Test Method for Tensile Properties of Polymer Matrix Composite Materials,*" 1993

13. S. L. Chuang and Ning-Jo Chu, "Effect of Polyamic Acids on Interfacial Shear Strength in Carbon Fiber / Aromatic Thermoplastics," *Journal of Applied Polymer Science,* Vol. 41, 1990, pp. 373-382.

Appendix III

Life Prediction of PPS Composites Subjected to Cyclic Loading at Elevated Temperatures

James Loverich and K.L. Reifsnider

Life Prediction of PPS Composites Subjected to Cyclic Loading At Elevated Temperatures

James Loverich and Kenneth Reifsnider
Virginia Polytechnic Institute and State University
Blacksburg, Virginia 24060

ABSTRACT

Combinations of failure mechanisms are frequently encountered in the life prediction of composite materials. MRLife, a well established performance simulation code for material systems developed by the Materials Response Group at Virginia Tech, is applied to one such failure mechanism combination. This program uses experimental data and analytical tools to predict the long-term behavior of a composite. The MRLife prediction scheme is based on the assumption that damage accumulation progressively reduces the remaining strength of a composite. An overview of the fundamental concepts of the MRLife code including several modifications designed to better represent the loading and material under study is presented. The code is used to model the elevated temperature fatigue behavior of a unidirectional AS-4 carbon fiber / PolyPhenylene Sulfide (PPS) matrix composite material. The nonlinear combined effects of time at elevated temperature and fatigue are taken into account by considering elevated temperature tensile rupture and room temperature fatigue behavior. The MRLife prediction for the combined loading is compared to 90°C tensile-tensile fatigue data. This comparison shows good correlation between the prediction and data and demonstrates the code's effectiveness in life prediction modeling.

INTRODUCTION

Life prediction of composite materials subjected to combined loading is a common occurrence in design situations. Combined loads may be comprised of quasi-static mechanical loads (tension, compression, shear, etc.), mechanical fatigue, elevated temperatures, thermal cycling and chemical degradation. It is usually not possible to include all of these factors and

their variations in a single test. Therefore it is necessary to have a method for combining the applicable conditions to predict the life of composites.

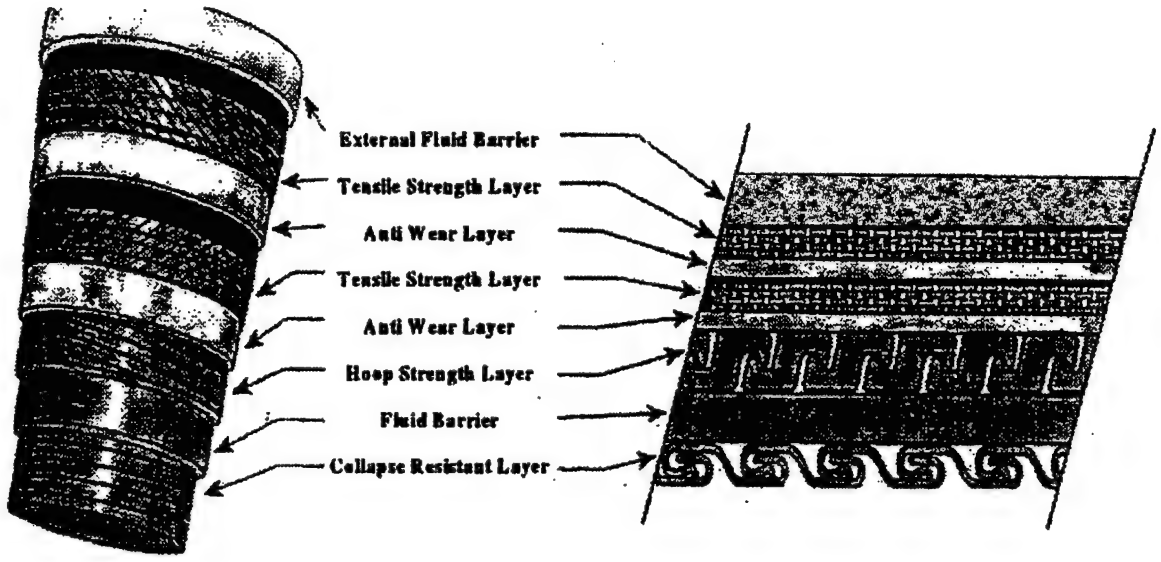

Figure 1 Typical flexible pipe schematic

The analysis and results of the current study were conducted to characterize and predict the life of a unidirectional AS-4 carbon fiber / PolyPhenylene Sulfide (PPS) matrix composite material. This material's intended application is helical tensile armor in flexible pipe used by the offshore oil industry. A typical flexible pipe design is shown in Figure 1. In order to reduce the weight of flexible pipes, replacement of the standard steel tensile layer with composite materials is being considered. A weight reduction of 30% and increased corrosion resistance is expected for a composite armor pipe designed to the specifications of a comparable conventional flexible pipe.

In order to use this material for this application, the life prediction must include better represent the loading and material under study. The code is verified for the current material via comparison of experimental data to the predicted life.

MRLife OVERVIEW

The MRLife life prediction scheme is based upon damage accumulation in composites. The basic principles of this scheme are described as follows. We begin our analysis by postulating that remaining strength may be used as a damage metric. We next assume that the remaining strength may be determined (or predicted) as a function of load level and some form

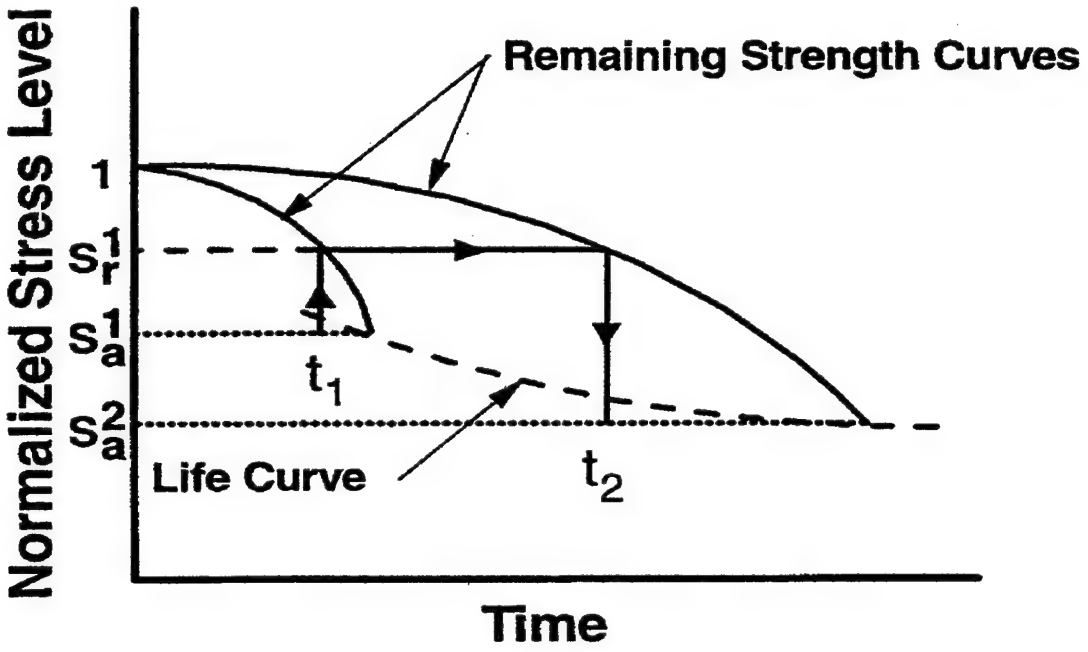

Figure 2 The use of remaining strength as a damage metric

of generalized time. For a given load level, a particular fraction of life corresponds to a certain reduction in remaining strength.

We claim that a particular fraction of life at a second load level is equivalent to the first if and only if it gives the same reduction in remaining strength, as illustrated in Figure 2. In the case of Figure 2, time t_1 at an applied stress level S_a^1 is equivalent to time t_2 at stress level S_a^2 because it gives the same remaining strength. In addition, the remaining life at the second load level is given by the amount of generalized time required to reduce the remaining strength to the applied load level. In this way, the effect of several increments of loading may be accounted for

by adding their respective reductions in remaining strength and life calculations are path dependent.

Our next step in the analysis is to postulate that normalized remaining strength (our damage metric) is an internal state variable for a damaged material system. This normalized remaining strength is based upon the selection of an appropriate failure criterion (such as maximum stress or Tsai-Hill) which is a scalar combination of the principal material strengths and applied stresses in the critical element. In this way we are able to consider a single quantity rather than the individual components of the strength tensor. We denote this failure function by *Fa.* We next construct a second state variable, the continuity [5], defined as *(1-Fa)* and denote it by V. We shall attempt to define our remaining strength and life in terms of V. To do so, we assume that the kinetics are defined by a specific damage accumulation process for a particular failure mode, and assign different rate equations to each of the processes that may be present.

As an example, let us consider a common kinetic equation (a power law) such that

$$\frac{d\Psi}{d\tau} = A\Psi^j \tag{1}$$

where

Ψ = continuity , c = generalized time variable, A,j = material constants

The generalized time, r , is defined by

$$\tau = \frac{t}{\hat{\tau}} \tag{2}$$

where t is siderial time and $\hat{\tau}$ is the characteristic time, in the sense of relaxation times.

The characteristic time could be a creep rupture life, a creep time constant, or even a fatigue life, in which case

$$\tau = \frac{n}{N} \tag{3}$$

where

n = number of fatigue cycles

N = number of cycles to failure for the applied loading conditions

It is also possible to combine time dependent and cycle dependent processes utilizing the R-Ratio, R, by expressing the characteristic time as

$$\frac{1}{\hat{\tau}} = R\frac{1}{t_{rupture}} + (1-R)\frac{1}{t_{fatigue}} \tag{4}$$

where

$t_{fatigue} = \frac{N_{fatigue}}{\nu}$, $R = \frac{\sigma_{min}}{\sigma_{max}}$, ν =fatigue frequency, $N_{fatigue}$= number of cycles to fatigue failure, and $t_{rupture}$= time to failure for the time dependent process.

It can be seen that this concept is correct in its limits; when R is 1 (pure rupture) $\hat{\tau}$ is the time to rupture failure and when R = 0 (pure fatigue) $\hat{\tau}$ is the time required for fatigue failure to occur at the given frequency. This concept was added to the code to model the combined effects of fatigue and time at elevated temperature on the current material under study.

Next, we rearrange equation (1) and integrate so that we obtain

$$\int_{\Psi_0}^{\Psi_i} d\Psi = A\int_0^{\tau_i} (\Psi(\tau))^j \, d\tau \tag{5}$$

If we set A = -1 and **j = 1**, we arrive at

$$\Psi_i - \Psi_0 = 1 - Fa_i - (1 - Fa_0) = -\Delta Fa = -\int_0^{\tau_i} (1 - Fa(\tau)) d\tau \tag{6}$$

Then we define our normalized remaining strength, **Fr** so that

$$Fr = 1 - \Delta Fa = 1 - \int (1 - Fa(\tau)) d\tau \tag{7}$$

In such a form, failure is predicted at the point at which the remaining strength equals the applied load (Fr = Fa).

CODE VALIDATION

We will now apply the damage accumulation scheme previously described to predict the elevated temperature fatigue behavior of the material under study and then compare these predictions to experimental data.

Tensile Rupture

The first step in implementing the code for this task is to characterize the time dependent behavior of the failure process. In our case this is tensile rupture at an elevated tem erature of 90'C.

The general representation for strength reduction as a function of time in MRLife is

$$R = 1 + A\log(t) + B\log(t)^2 + C\log(t)^3 + D\log(t)^4 \tag{8}$$

where R= remaining strength fraction, t = elapsed time in hours, and A,B,C,D = material constants determined via curve fitting. Due to the inherent shape of this curve, it could not adequately represent the rupture data; consequently, MRLife was modified to use a strength reduction equation presented by Kachanov [5] of the form

$$t_{rupture} = \frac{1}{(n+1)A\sigma^n} \tag{9}$$

where σ = normalized initial stress
σ $t_{rupture}$=time to rupture in hours
A, n = constants determined through curve fitting.

Setting σ equal to R (the remaining strength fraction), equation (9) can be rewritten in the form used in MRLife

$$R = \left[\frac{1}{(n+1)At_{rupture}}\right]^{\frac{1}{n}} \tag{10}$$

Equation (10) is then fit, using a least squares method, to 90'C tensile rupture data. The values of A and n were determined to be 2467 and 36.7, respectively. The tensile rupture curve fit and data are shown in Fig. 3.

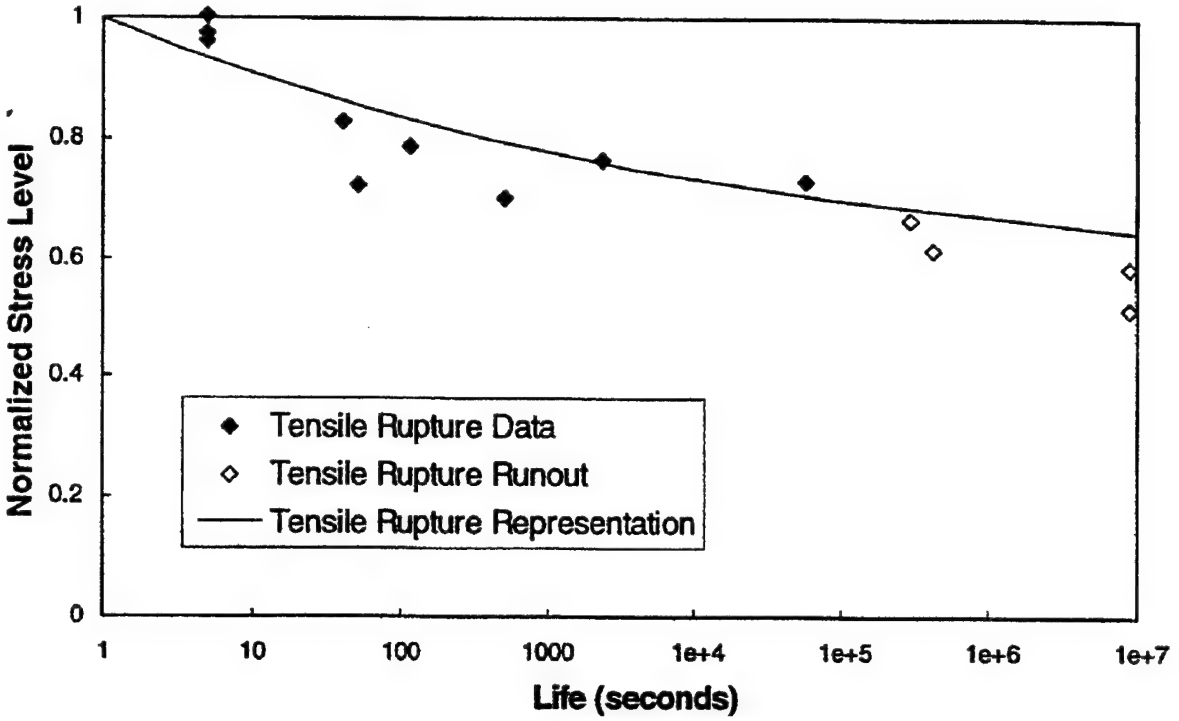

Figure 3 Tensile rupture curve fit and data

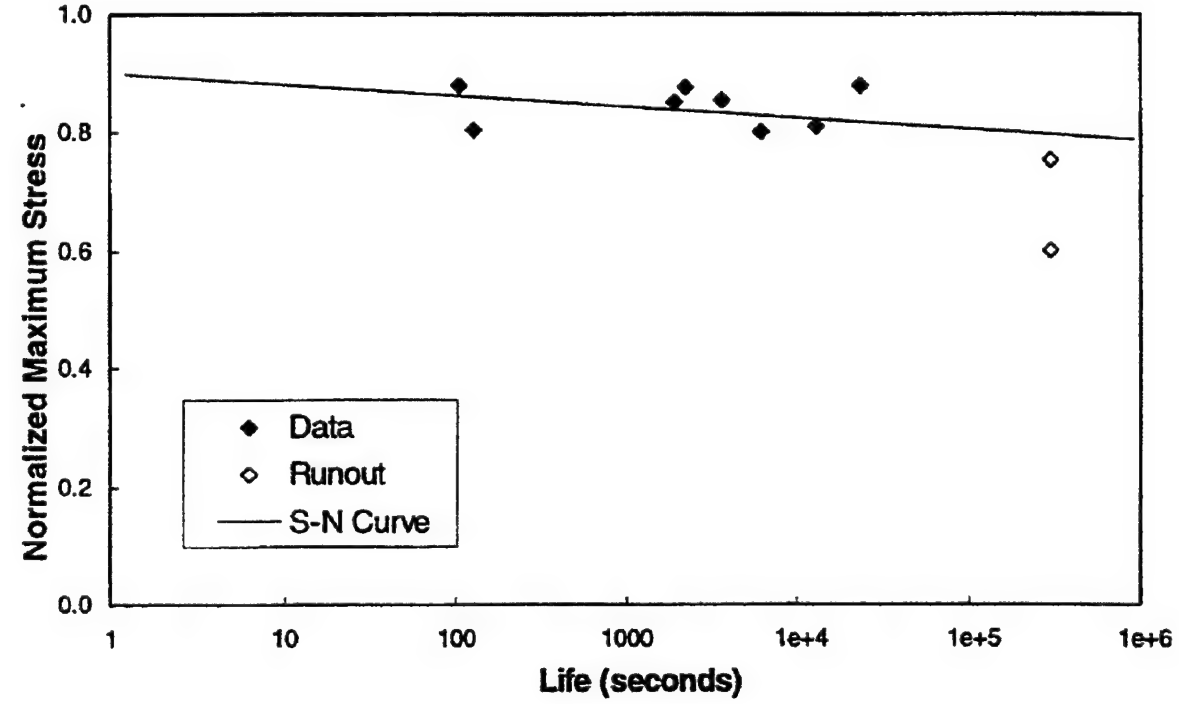

Figure 4 Room temperature fatitgue data and S-N curve fit.

Fatigue

Next, the fatigue effect of the combined loading was characterized. The room tempeerature fatigue data were fit with a conventional curve of the form

$$\frac{S}{S_{ULT}} = A_n + B_n(\log(N))^{P_n} \tag{11}$$

where S/S_{ULT} = normalized maximum stress, N = number of cycles to failure, and
A_n, B_n, P_n = material constants.

The data and curve are shown in Figure 4. The constants were found to be: A_n=0.9207, B_n=-*O.O* 1 89, and P_n= *I*.

Finally, the effects of time at elevated temperature and fatigue were combined by defining a characteristic time as described previously. For any given normalized stress level, a rupture time and a fatigue time can be determined from the two previous curve fits. These times in conjunction with the R-ratio of the process are then used to compute the characteristic time with Equation (4). The generalized time is in turn then computed with Equation (2) and input into the evolution equation (7) to predict time to failure for the given stress level.

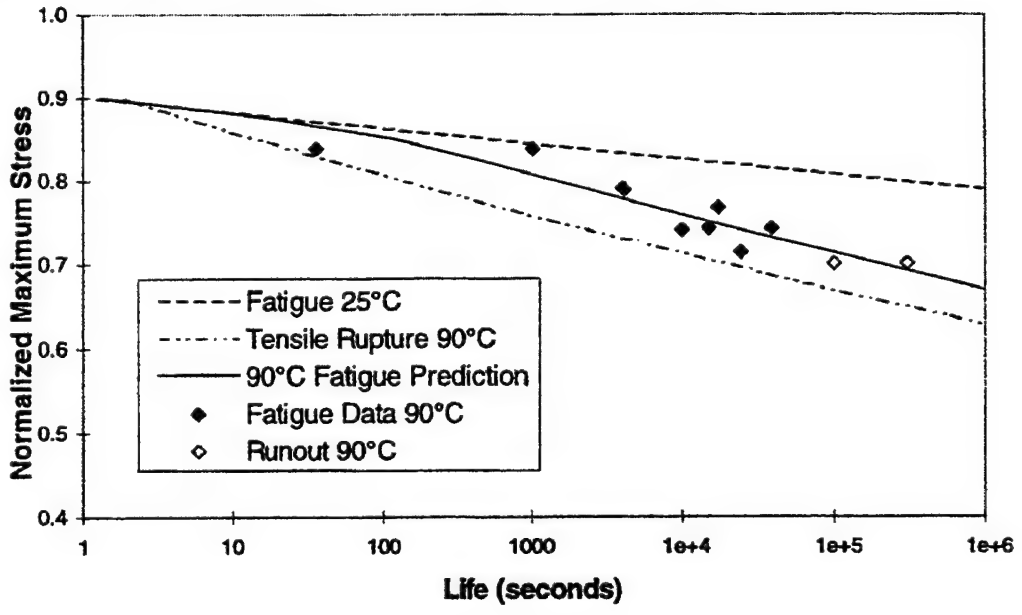

Figure 5 Comparison of elevated temperature fatigue prediction and

90 ^{0}C fatigue data.

The MRLife prediction for the combined loading and the 90'C fatigue data, shows a good correlation between the prediction and data (Figure 5). This verifies the technique for predicting the combined effects of time and cyclic processes for the material and conditions under study.

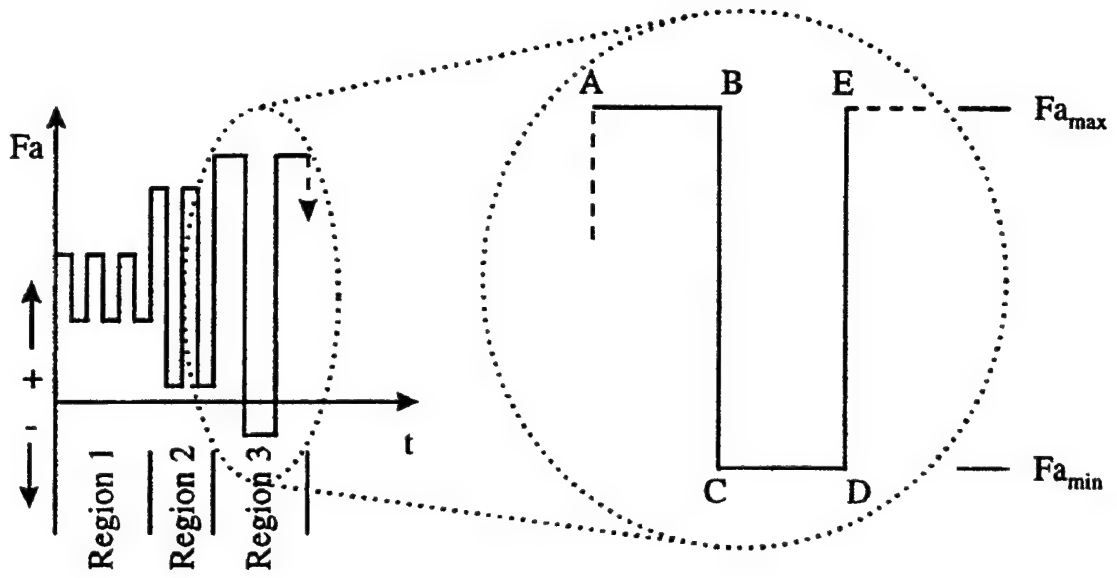

Figure 6 Approximated helical armor stress with respect to time.

NEGATIVE R-RATIOS

As can be seen, the case studied above appears to match the data well. However, for some instances, it was found that the described methodology was not applicable and a variation in the technique is necessary. The limiting factors were found to be related to the R-Ratio. If the R-Ratio is less than 0.3 and/or the stress drops below zero, a more complex strength reduction procedure must be employed.

In the following discussion all references are made to Figure 6. We found that, for R-Ratios less than 0.3 (e.g. Region 2), the rupture and fatigue combination scheme described

previously will produce non-conservative results. Also, for wave patterns which contain negative stresses (e.g. Region 3) this technique is not applicable at all since negative R-ratio values can not be evaluated with Equation (4). As a result, the following concept was devised to reduce the strength over each cycle.

On the interval between A and B the strength is reduced for a constant applied tensile rupture loading of $Fama_{,}$ for a duration equal to one half of the period. From B to C the reduction is due to one half cycle of fatigue. If Famin is positive from C to D the strength will be reduced in the same a fashion as from A to B. However, if Famin is compressive, the strength will be reduced for a constant applied bend-compression loading for a duration of one half period. The strength is then reduced again for one half cycle of fatigue for the interval D to E. This process is repeated for each cycle of fatigue over the expected lifetime of the material.

It is obvious that this second technique is considerably more involved since the strength must be reduced four times for a single wave cycle, whereas the first technique calculates the reduced strength for one intire time interval (which may consist of many wave cycles). However, the second technique does provide a method to evaluate the life for a wider variety of loading conditions.

CONCLUSION

The life prediction model presented is based on an iterative strength reduction scheme which allows for the consideration of several types of combined loads. This paper studied only environmental conditions and variable cyclic loading; however any number of other load types should be able to be combined using a similar technique. Comparison of experimental data with the life prediction results displayed the model's effectiveness for the material under study. Future work for this study includes: modeling the applied stress wave form with a more realistic sine wave form instead of the square wave pattern and expanding the model to accommodate

experimental data for the behavior of the material at lower operating temperatures and in environmental conditions such as corrosive gasses and sea water.

REFERENCES

1. Case, S.W., Xu, Y.L. and Reifsnider, K.L., *MRLife9 TM A strength and Life Prediction Code for Laminated Composite Materials,* Materials Response Group, Virginia Tech, (I 996).
2. Reifsnider, K.L., "Use of Mechanistic Life Prediction Methods for the Design of Damage-Tolerant Composite Material Systems," *Advances in Fatigue Lifetime Predictive Techniques: Second Volume, ASTM STP 1211,* (1993), pp. 3-18.
3. Reifsnider, K.L., Case, S. and lyengar, N., "Recent Advances in Composite Damage Mechanics," *European Space Agency,* Nordijk, Holland, 1996.
4. Personal Communication, Case, S., Virginia Tech, 3-5-97.

   Kachanov, L. M., *Introduction to continuum damage mechanics.* Martinus Niihoff Publishers, Boston. (1986).

Appendix IV

Strain Rate and Temperature Effecfs In Polymeric Matrices for Composite Materials

K.L. Reifsnider and Feng Sun

Strain Rate and Temperature Effects in Polymeric Matrices for Composite Materials

Ken Reifsnider and Feng Sun
Professor and Post-Doctoral Fellow
Virginia Polytechnic Institute and State University

Abstract

The effect of the rate of strain during deformation on the properties and performance of materials has been a long-standing subject of engineering interest, driven by the observation that significant differences in strength, stiffness and life can be induced by these effects. In polymer-based materials, the discussion of such effects usually centers on viscoelastic response and changes in stiffness. The present paper examines subjects that are related to strength, life, and to accelerated testing. Micromechanical effects are identified and discussed, and new concepts are introduced to assist in the interpretation and representation of physical behavior, over ranges of strain rate from impact to quasi-static testing. A strain rate-temperature equivalence principle is introduced.

Introduction

The behavior of materials, especially polymeric matrices in composites under dynamic loads, is a very important issue in practical engineering, essential for any work involving polymeric composite materials and structures in aerospace and ocean applications (1). Most of the prior research dealing with the dynamic properties of composites has concentrated on the strain rate dependent behavior of composite laminates and structures, and on macro-mechanics analysis (2-4).

In order to fully understand the strain rate dependent mechanisms and to develop better impact-tolerant composites through a micro-mechanics approach, it is necessary to know the strain rate dependent properties of the constituents, i.e., the fibers and matrices. It is only in fairly recent years that tensile impact techniques for fiber bundles and matrix have been established (5-7). There are some tensile impact data showing that the strength of epoxy, widely used as a matrix in polymeric composites, increases with strain rate (8,9). However, few quantitative analyses for the strength variations and rate dependent mechanisms for this material have been found so far, and few explanations of strain rate effects on polymeric matrices have been offered.

On the other hand, it is common knowledge that the mechanical properties of polymeric matrices change with strain rate as well as with ambient temperature. For very long-loading-time deformations, such as creep and relaxation, there is a time-temperature equivalence, e.g., WLF superposition principles may apply (10). Mechanical properties of polymers at times over several decades of significance can be predicted by the data at a higher temperatures and over short times. But this equivalence is not generally valid at temperatures below Tg, and few data support the application of WLF principles to the relationship between temperature and strain rate for polymeric matrices. It is only reported qualitatively that there exists an "equivalence" between strain rate in

impact process and temperature, for polymeric resins (11,12), and for elastomers within the range of rubbery behavior (13); but, there are no quantitative descriptions regarding this equivalence.

In this paper, for polymeric matrices in high strain rate processes, theoretical models of strain rate dependent properties and temperature effects are discussed. Then, a quantitative equivalence equation between strain rate and temperature effects is proposed. Finally, comparisons between numerical results and experimental data are shown and the applications / validations of the proposed equivalence are discussed.

Models for Strain Rate and Temperature Effects

In this paper, "material properties" refers mainly to mechanical properties, especially, strength, stiffness, strain to failure and time to failure of epoxy, in the temperature range below Tg.

It is reported that Young's modulus, strain to failure and strength for epoxy (18, 27) are proportional to the log (strain rate), as follows:

$$\begin{aligned} E &= B_1 \cdot \log \dot{\varepsilon} + C_1 \\ \varepsilon_b &= B_2 \cdot \log \dot{\varepsilon} + C_2 \\ \sigma_b &= B_3 \cdot \log \dot{\varepsilon} + C_3 \end{aligned} \qquad (1)$$

Data from references 17-28 were used to construct examples of such variations in Figs. 1 and 2, below.

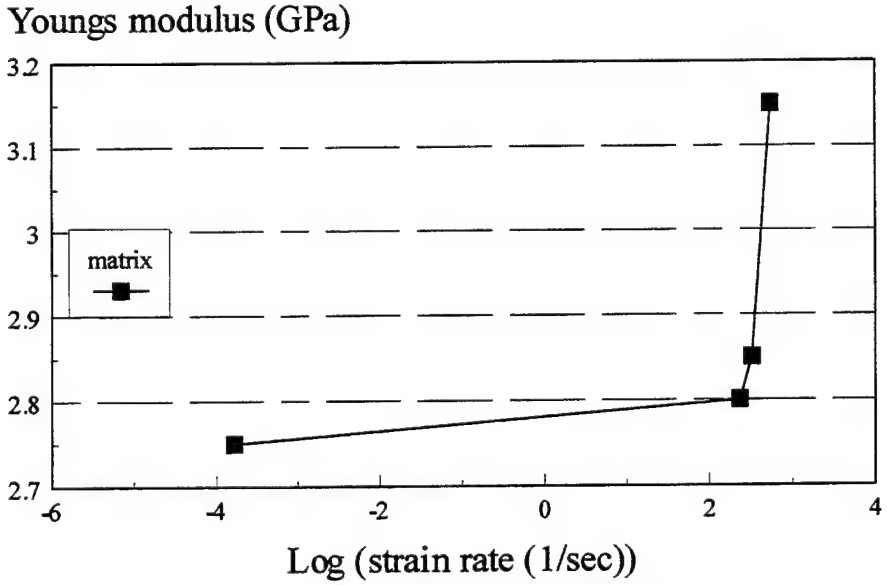

Figure 1 Variation of the stiffness of epoxy with strain rate

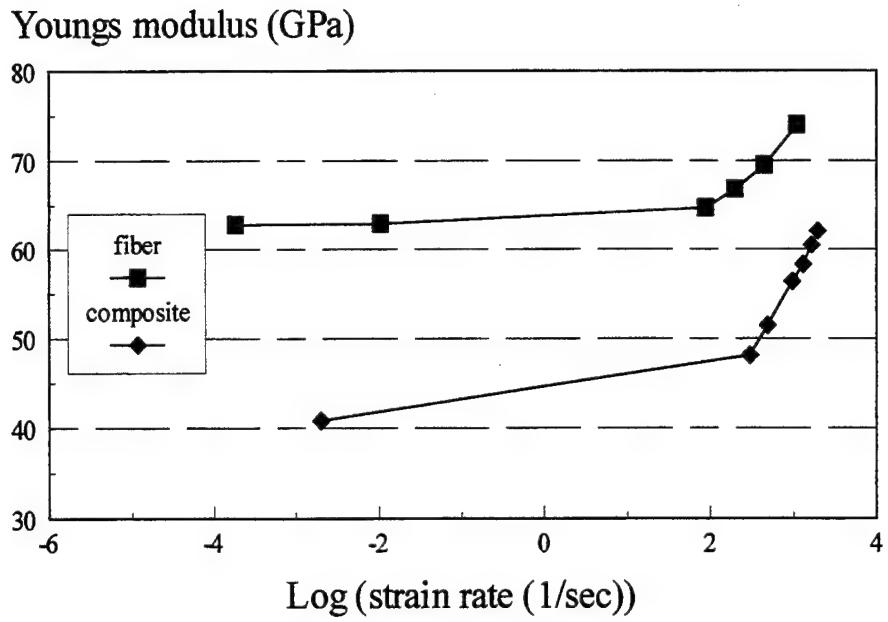

Figure 2 Variation of stiffness of glass fiber and glass-reinforced epoxy composite, as a function of strain rate.

These data indicate several important and typical features. The fiber, matrix and composite show little strain rate dependence for low strain rates. At high strain rates there is a strong dependence, which seems to be linear or nearly linear. It is also seen that the strain rate dependence of the composite stiffness follows the form of the epoxy behavior. It should be noted that the significance of high strain rates is not limited to engineering situations involving impact or other high deformation rates at the macroscopic level. Local fracture events (driven by fiber fracture or the fracture of fiber tows) are high-rate deformation events. In general, progressive damage processes in high-stiffness, low strain to failure composites are high strain rate events.

Models for strain rate effects

Various investigators have discussed material property - strain rate relations and several models have been proposed (17, 19, 20). For the present case, we propose to use a relationship developed in another (related) context.

For the relationship between time to failure and strain rate, there is a simple and widely used equation for creep of metals, polymers and other materials. It is usually refered to as the Monkman-Grant equation (23,24), as expressed by:

$$t_b \cdot \left(\varepsilon^{\bullet}\right)^m = C \qquad (2)$$

Here, for creep, t_b is time to failure, $\dot{\varepsilon}$ is the steady-state strain rate and C is a material constant. We have applied the Monkman-Grant equation to the impact process and fit the experimental data in refs.17,19, 20 and 26 by equation 2, treating t_b as the time to failure and $\dot{\varepsilon}$ as the constant strain rate in the impact process.

For impact processes under constant strain rate conditions:

$$t_b \cdot \dot{\varepsilon}^{\bullet} = \varepsilon_b$$

Using the same data sets used in equation 2 for fiber, matrix, and Figs. 1 and 2, the validity of composite over the entire range of strain rates is evaluated, in Figs. 3-5.

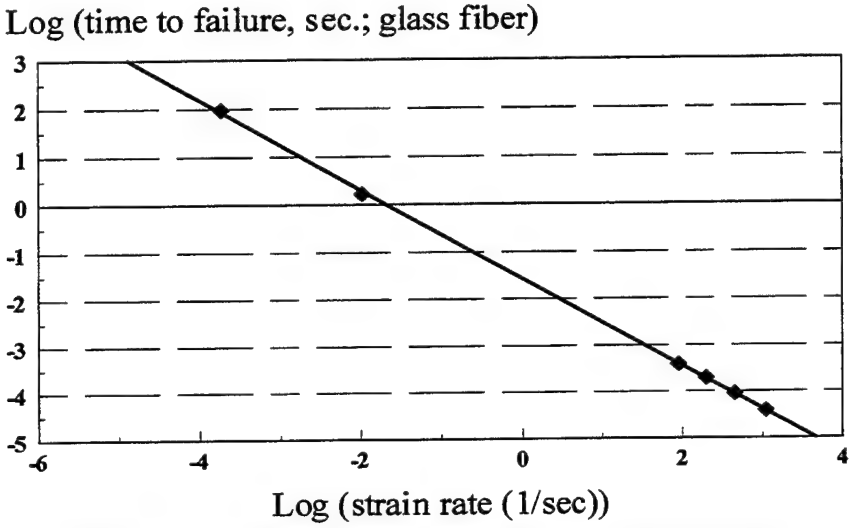

Figure 3 Variation of time to failure with strain rate for glass fibers.

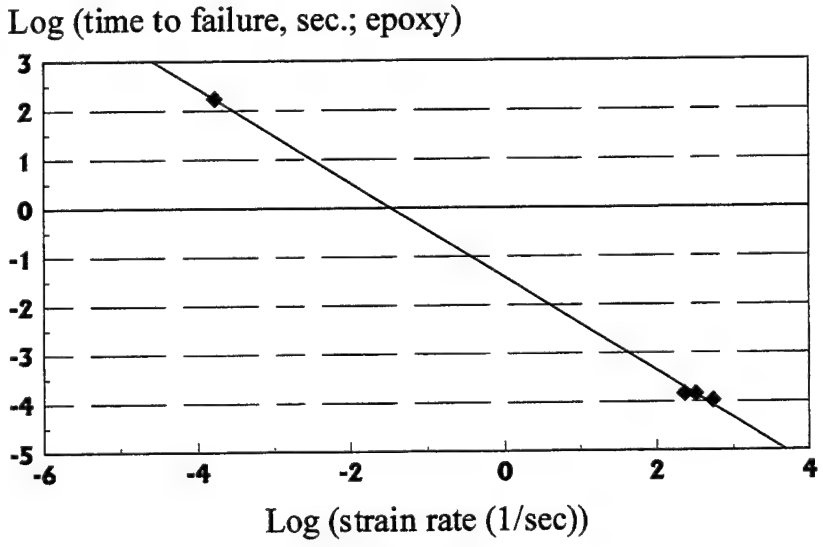

Figure 4 Variation of time to failure with strain rate for epoxy matrix.

It can be seen that the equation fits the data for epoxy at strain rates from the quasi-static to very high strain rate ranges (up to 10^3 1/sec) almost perfectly. The constants for the three conditions are:

Fiber:	$C_1 = 0.0273$	$m = 0.935$	correlation = 0.999
Matrix:	$C_1 = 0.0377$	$m = 0.908$	correlation = 0.999
Composite:	$C_1 = 0.0419$	$m = 0.908$	correlation = 0.999

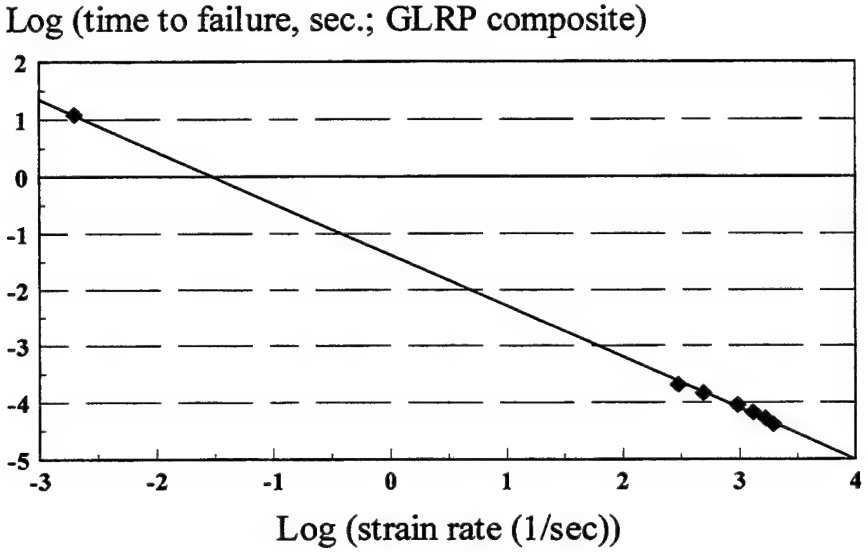

Figure 5 Variation of time to failure with strain rate for Glass-reinforced epoxy composite.

The applicability of this relationship to such a wide range of conditions is quite surprising. It raises several possibilities for predictive models when strength, strain to failure, and time to failure must be estimated in composites, and when testing or characterizations are available for one strain rate but applications require different strain rate conditions.

Over ranges of linear stiffness variation, one can substitute equation 2 into equations 1, to express those variables as a function of time to failure, as follows:

$$\begin{aligned} E &= b_1 \cdot \log t_b + c_1 \\ \varepsilon_b &= b_2 \cdot \log t_b + c_2 \\ \sigma_b &= b_3 \cdot \log t_b + c_3 \\ \left(b_i = -\frac{B_i}{m}, c_i = \frac{B_i}{m} \cdot \log C_2 + C_i, i = 1,2,3,\ldots,n \right) & \end{aligned} \qquad (3)$$

The experimental data in ref. (17, 19, 20 and 28) can be fit by the above equations with almost perfect goodness of fit for strain rates from quasi-static up to very high strain rate values.

Models for Temperature Effects (below Tg)

It is common knowledge that the state of materials, especially, polymeric matrices, fibers and composites are functions of temperature. Those temperature effects on the material state can be generally expressed as:

$$P = f(T) \tag{4}$$

Here, P expresses the material state for polymeric matrices, fibers and their composites. In the discussions below, mechanical properties for epoxies are used.

Several investigators have reported that the instantaneous tensile and shear moduli of epoxy and other resin dominated composite properties are linear functions of temperature, over various ranges of temperature. Equations such as the following are typically used.

$$E_m = E_m(T_0) + D|T - T_0| \tag{5}$$

The constant, D, in the above equation is determined by fitting the experimental data in figure 3 of ref.(28), for example; for a linear function, the fit is almost perfect for temperatures below room temperature. As the shear modulus is calculated by multiplying Young's modulus by 1 / 2(1+v), the temperature effect on the shear modulus of epoxy is also a linear function of temperature change with a different slope.

It can be seen that the temperature effects on the moduli of epoxy and resin-dominated properties of composites, both in the temperature range below and above room temperature, are linear functions of the absolute temperature.

The temperature effects on the moduli (tensile and shear) for polymeric matrices, below room temperature, have also been found to be linear functions of the absolute temperature.(26, 27) For epoxy, the Young's modulus is typically given as

$$E_m = E_m(T_0) + 20 \cdot (T_0 - T) \tag{6}$$

Equivalence between Strain Rate in Impact Process and Temperature Effects

From the above sections, it can be seen that the material state (reflected in mechanical properties) of some polymeric matrices, especially epoxy in the present example, is a function of strain rate (time to a certain state of material at various strain rates) and a function of temperature. An equivalence between strain rate effects (or time to a certain state of material at various strain rates) in impact processes and the temperature effect on the same state of materials can be proposed for such matrices, similar to that for creep and relaxation. This could be done by combining equations such

as (2) and (5). The objective would be to specify the equivalent temperature, T, for a strain rate or time to a certain state of material at that strain rate, or inversely, to specify the equivalent strain rate or time to a certain state of material at that strain rate for a specified temperature T.

In the following, some examples of the equivalence between strain rate and temperature effects on tensile and shear moduli (below Tg) of polymeric matrices are shown. For the situations examined, it can be seen from previous sections that both strain rate and temperature effects on Young's modulus are linear functions of strain rate, the time to a certain strain (on a log scale), and temperature. So, the equivalence between strain rate and temperature effects on longitudinal and shear moduli of the polymeric matrices can be quantitatively expressed as follows:

$$\left|T - T_0\right| = \frac{B_1}{D}\log(\dot{\varepsilon}) + \frac{1}{D}\left(C_1 - E_m(T_0)\right) \tag{7}$$

$$\left|T - T_0\right| = \frac{B_1}{D}\log(t) + \frac{1}{D}\left(C_1 - E_m(T_0)\right) \tag{8}$$

Numerical Examples for the proposed Equivalence

In the present paper, an empirical superposition principle was employed to calculate equivalent temperatures for different strain rates, especially for impact processes. Here, the time to break, t_b, which is a function of strain rate is used in the calculation. The time corresponding to low temperatures can be arbitrarily chosen at a convenient strain rate for experiment. For the present example, it is set to t_S, the time to break in a quasi-static test.

Then, the room temperature data for very short-time fracture (high strain rate) is converted to the data at long fracture times (quasi-static test) and low temperature, by a shift factor a_T, along the time scale.

Here,

$$a_T = \frac{t_S}{t_b} \tag{9}$$

In order to calculate Log (a_T), the following Arrhenius relationship is employed (30):

$$\log(a_T) = \frac{\Delta H}{2.303G}\left[\frac{1}{T} - \frac{1}{T_0}\right] \tag{10}$$

Here, the activation energy is ΔH =219 for epoxy.

Therefore, the temperature for the quasi-static test, which is equivalent to high strain rate, can be calculated by combining equations (7) and (10) as follows:

$$T = \left[\frac{2.303G \log\left(\frac{t_S}{C_1(\dot{\varepsilon})^{-m}} \right)}{\Delta H} + \frac{1}{T_0} \right]^{-1} \qquad (11)$$

Comparisons between the experimental data of longitudinal and shear moduli at various strain rates and the calculated values at equivalent temperatures are carried out for epoxies in refs. 17, 26 and 28.. Some examples of the results are shown in Figure 6. It can be seen that the calculated results corresponding to the equivalent temperature (lower temperature) at a reference strain rate agree, quite well, with the experimental data at higher strain rates and temperatures over seven orders of strain rate. (Calculations for two reference values of the activation energy are shown.)

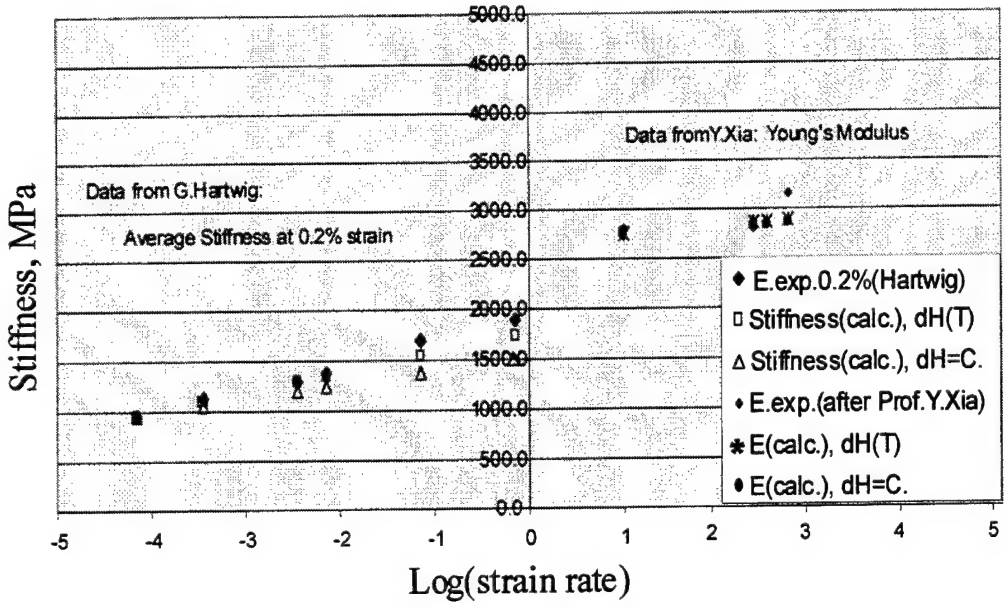

Figure 6 Predicted (from quasi-static tests) and observed stiffness values as a function of strain rate for epoxy, using two different activation energy values.

It can be seen that the calculated stiffness values match the measured values very closely over a wide range of strain rates.

Conclusions

Based upon the above discussion and data, it can be concluded that:

(1) The Monkman – Grant relationship in creep may be applicable to the description of the relationship between time and strain rate processes, not only for the time to failure and strain to failure, but also for the time to a certain material state as a function of strain rate for epoxy. This suggests that there may exist a common

mechanism between creep and rate processes such as impact in this material, and also suggests that relationships of this type may be developed for similar materials.

(2) Relationships between mechanical properties in an impact process and log(strain rate) or log(time) were postulated. Predictions of stiffness as a function of strain rate from such equations agree with experimental data very well for epoxy.

(3) An equivalence between strain rate effects and temperature effects on material states was proposed. A quantitative equivalence equation was obtained for the longitudinal and shear moduli of epoxy, as an example. It was found that an empirical superposition approach based upon an Arrhenius equation is an effective method for predicting the equivalent temperatures for various strain rates. Predicted values of stiffness for different strain rates (corresponding to impact conditions) based on values obtained from quasi-static testing at room temperature (obtained by predicting an equivalent lower temperature for which the stiffness should match the experimental value obtained at a rapid strain rate at room temperature) matched observed values well for epoxy over seven orders of magnitude of strain rates.

Several distinctive features of this work should be emphasized. First, we have addressed the effect of temperature and strain rate on failure, specifically the time to failure and the strain to failure. And second, we have developed a simple concept and equations that make it possible to calculate values of stiffness, strain to failure, and time to failure as a function of temperature and strain rate, based on one set of reference data at a given temperature and strain rate and knowledge (or estimate) of the activation energy. It is expected that this equivalence is applicable to other temperature and strain rate dependent properties for not only polymeric materials but also for matrix-controlled composite properties and performance. Some evidence of the carry-over to composite behavior was shown in Fig. 2.

Expected applications of these concepts are numerous. An especially important one, at the global level, is the construction of algorithms that can be used in predictive analysis codes to estimate stiffness (and, thereby, stresses and strains, strains to failure, and time to failure) as a function of strain rates and temperature for materials used in dynamic loading situations, especially impact conditions. Another global use is the "acceleration" of testing, in the sense that test results under very difficult (and expensive) test conditions (such as very high strain rates or very high or low temperatures) can be estimated from more easily obtained room temperature quasi-static test data. And at the local level, micromechanical analysis of fiber / matrix / interface behavior depends on a firm knowledge of stiffness as a function of strain rate and temperature, since events like fiber fracture are inherently high-strain-rate processes. If we have any hope of getting the local stress state correct for such events (and estimating composite strength using micromechanics), we must get the local stiffness correct under those conditions. The present approach offers an approach to that objective.

Acknowledgements

The authors gratefully acknowledge the support of the Air Force Office of Scientific Research (grant no. F49620-95-1-0217) for the research on high temperature polymer composites, and the National Science Foundation under grant no. DMR9120004 for support of the micromechanical modeling.

References

1. Robert L. Sierakowski and Shive K. Chaturvedi, Dynanic Loading and Characterization of Fiber-Reinforced Composites, Published by John Wiley & Sons, Inc.,1997.
2. C.A.Ross and R.L.Sierakowski, " Studies on the Impact resistance of Composites", Composites, July 1973, pp.157-161..
3. S.R.Finn and G.S.Springer, " Composite Plates Impact Damage", Technomic publishing Co., Inc., 1991.
4. D.Hull, " A Unified Approach to progressive Crushing of Fiber- reinforced Composite Tubes", Composites Science and Technology, 40, pp.377-421, 1991.
5. J.Harding and L.M. Welsh, " Impact testing of Fiber – Reinforced Composite materials", Proc. ICCM 4, pp.845-852, Tokyo, Japan, 1982.
6. K.Kawata, S.Hashimoto and N.Takeda, " Mechanical Behaviors in High Velocity Tension of Composites", Proc. ICCM 4, pp.829-836, Japan, 1982.
7. Y.Xia, B.Yang L.Dong and D.Jia, " Experimental Study of Constitutive Relation for Unidirectional Glass Fiber Reinforced Resin under Tensile Impact", Proc. of ISCMS, Beijing, China, pp.997-1002,1986.
8. J.Harding and L.M. Welsh, A Testing Technique for Fiber – Reinforced Composites at Impact rates of Strain", J. of Materials Science, 18, pp.1810-1826, 1983.
9. L.Dong, Y.Xia and B.Yang, " Tensile Impact Testing of fiber Bundles", ICSTAD proceedings, India, pp.184-189, July 29 – Aug.3,1990.
10. M.L.Williams, R.F.Landel and J.D.Ferry, The temperature Dependence of Relaxation Mechanisms in Amorphous Polymers and Other Glass-Forming Liquids", J. American Chemical Society, 77, pp.3701-3707,1955.
11. L.E.Nielsen and R.F.Landel, Mechanical Properties of Polymers and Composites, 2nd ed., Published by Marcel Dekker, Inc., pp.256, 1994.
12. C.Hall, Polymer Materials, Published by John Wiley & Sons, pp.73,1981.
13. T.I.Smith and P.J.Sterdy, " Time and Temperature Dependence of the Ultimate Properties of an SBR Rubber at Constant Elongations", J.of Applied Physics, 31, No.11, pp.1892-1898, 1960.
14. L.Dong, Y.Xia and B.Yang, Tensile Impact Testing of Fiber Bundles, ACTA MATERIAE COMPOSITAE SINICA, pp.9-14, Dec. 1990 (in Chinese).
15. D.R.Hartman, M.E.Greenwood and D.M.Miller, Technical Paper-High Strength Glass Fibers, Published by Owens-Corning Fiberglass Corparation, (Figure 2), Mar. 1994.
16. Y.Xia, L.Dong, S.Rao and B.Yang, "Energy Transition of Fiber-Bundle and Their Unidirectional Composites under Tensile Impact", Proc. ICCM 8, Hawaii, pp.29-O-1-8, 1991.

17. T.S.Gates, " Matrix-Dominated Stress/Strain behavior in Polymeric Composites : Effects of Hold Time, Nonlinearity, and Rate Dependency", ASTM STP 1206, E.T.Camponeschi, Jr., Ed., Philadelphia, pp.177-189, 1993.
18. Y.Xia, B.Yang and M.Li, "Tensile Impact Response of Resin Matrices and their composites", ACTA MATERIAE COMPOSITAE SINICA, Vol. 4, No.2, pp.59-65, 1987 (In Chinese).
19. M.F.Ashby and D.R.H.Jones, Engineering Materials 2, Pergamon Press, pp.226-231,1986.
20. Y.Xia, J.Yuan and B.Yang, " A Statistical Model and Experimental Study of the Strain – Rate Dependence of the Strength of Fibers", Composites Science and Technology, 82, pp.499-504, 1994
21. Y.Xia, and W.Xing, " Constitutive Equation for Unidirectional Composites under Tensile Impact", Composites Science and Technology, 56, pp.155-160, 1996.
22. G. Carrington, Basic Thermodynamics, 2nd ed., Oxford Science Publications, pp.275-280, 1994.
23. S. L. Rosen, "Fundamental Principles of Polymeric Materials", John Wiley and Sons, Inc., P242, 1982.
24. H.E.Evans, "Mechanisms of Creep Fracture", Elsevier Applied Publishers, p.20,1984.
25. G.M.Bartenev and Yu.S.Zuyev, translated by F.F. and P. Jaray, Strength and Failure of Visco-elastic Materials, Pergamon Press, p.102, 1968.
26. Y.Xia, X.Wang and B.Yang, " Brittle-ductile-brittle transition of glass fiber-reinforced epoxy under tensile impact", J.Materials Sci.Lett., Vol.12, pp.1481-1484, 1993.
27. G.Hartwig, "Mechanical and Electrical low temperature properties of high polymers", Nonmetallic Materials and Composites at Low Temperatures, edited by A.F.Clark, R.P.Reed and G.Hartwig, Plenum Press, 1978, pp.33-50.
28. P.K.Dutta, K.L.Faran and D.Hui, "Influence of Low Temperature on Energy Absorption in Laminated Composites", Proc. ICCM 9, 1993, pp.311-320.
29. K.Padmanabhan, "Time-Temperature Failure Analysis of Epoxies and Unidirectional Glass/Epoxy Composites in Compression", Composites, Part A, Vol.27A (1996), pp.585-596.
30. Y. Miyano and M.Kanemitsu, "Time and Temperature Dependence of Flexural Strength in Transversal Direction of Fibers in CFRP", Fiber Science and Technology, Vol.18, pp.65-79, 1983.

Appendix V

Influence of Polymer Network Structures On Mechanical Response

Lu Shan, C.G. Roberstson, K.N.E. Verghese, E. Burts
J.S. Riffle, T.C. Ward, and K.L. Reifsnider

Influence of Polymer Network Structure on Mechanical Response

Lu Shan, C. G. Robertson, K. N. E. Verghese, E. Burts, J. S. Riffle, T. C. Ward
and K. L. Reifsnider
NSF Science and Technology Center:
High Performance Polymeric Adhesive and Composites
Virginia Polytechnic Institute and State University, Blacksburg, VA

Abstract

Vinyl ester and epoxy network polymers were studied for two tasks. Vinyl ester resins were studied for the influence of the network structure on their viscoelastic, physical and mechanical properties. The crosslink density of the resins was altered by changing the molecular weight of the vinyl ester oligomer and by varying the styrene used during the crosslinking reaction. The glass transition temperatures of the polymers and the breadth of the glass transition regions were found to increase systematically with the increase of crosslink density without additional influence of the composition. Cooperativity studies were also performed in the glass formation temperature region of the networks. The cooperativity of the systems seemed to be influenced by both the crosslink density and the styrene content. A linear correlation was found between the fracture toughness of the networks and the cooperative domain size at the glass transition temperature normalized by the crosslink density. The crosslink density of the epoxy resins was varied with three different molecular weights of the crosslinking agent poly(oxypropylene)diamine. The tensile stress-strain behavior of the polymers due to the change in the crosslink density was studied. Ultimate tensile properties of the systems were also obtained to re-examine the existence of a proposed master failure envelope.

Introduction

Network polymers are highly intractable crosslinked resins made through irreversible curing processes from fusible, soluble products. They have been widely used in many applications due to their outstanding stability characteristics and combined properties of toughness, chemical resistance, and flexibility. Typical applications of crosslinked polymers include surface coatings, adhesives, and composite matrix materials used in aerospace, construction, tire and many other industries. The task of linking macroscopic properties to molecular structure continues to be a research focus for network polymers.

The majority of the fundamental studies on crosslinked polymers involve varying the molecular weight between crosslinks by changing the density of crosslink junctions with different crosslinking agents without altering the chemical composition of the network chains. The properties that were investigated were consequently dependent on the functional characteristics of the crosslinking agents. There are two major methods of changing the molecular weights: changing the length of the crosslinking agent, as well as changing the backbone chain length. A study of the influence of the mechanical response by the crosslink density changes with both of the crosslinking methods can determine more accurately whether

the effects are due to the general trend of the crosslink density variation or due to the individuality of certain components. In this contribution, this current study investigates vinyl ester resins, a widely used type of composite matrix materials, under the influence of the change in crosslink density. The crosslink density of vinyl ester is systematically varied by using two different vinyl ester oligomer molecular weights and two weight percentages of styrene as a crosslinking component.

The work is particularly interested in the role of the network density on secondary relaxation and glass-to-rubber transition for the vinyl ester polymers. As observed previously,[1, 2] nearly all tough ductile glassy polymers and those with high impact strength have prominent secondary peaks. The secondary relaxation for the vinyl ester resins is examined for possible reflection of their crosslink densities and fracture toughness properties. A careful study on the influence of the crosslink density on the glass transition temperatures, and the breadth of the glass transition regions will be performed. Moreover, viscoelastic properties such as the loss modulus and damping are investigated for the influence of these crosslinked polymers.

A closer examination of the glass transition region of the vinyl ester materials will be afforded by cooperativity studies. The glass transition involves a long range of cooperative motions of molecular segments. Some neighboring segments are close enough to restrain the movements of other segments. The intermolecular cooperativity model describing the degree of intermolecular interactions was first proposed by Adam and Gibbs.[3] This cooperative domain was visually described by Matsuoka and his coworker.[4] Plazek and Ngai[5] further correlated the polymer segmental chain cooperativity with the relaxations of the neighboring segments using their coupling model of relaxations. Several studies have been done using the concept of the cooperative relaxation motions. Connolly and Karasz[6] studied the chemical structural effects on cooperativity for a series of thermoplastic polymers. Roland and Ngai[7, 8] investigated the cooperativity change due to various chemical structures of the semicrystalline polymers. Previous research using the cooperativity model has found accurate indications of the intermolecular coupling on the molecular level. This study of the crosslinked polymer materials utilizes the cooperativity approach to correlate the effects of both chemical structure and crosslink density with the cooperativity of the network polymers. Since glassy state properties reflect how the polymer is packed and frozen into the glassy state, it is valuable to seek for connections between the intermolecular cooperativity and packing in the glass transition and the mechanical and physical properties. One further interest of the study is to examine the effects on the fracture toughness for the glassy state vinyl ester polymers.

The failure properties of the polymers, as well as many other mechanical properties are of special interest to researchers. The kinetic theory[9] predicts a directly proportional relationship between the stress at break, σ_b and ν_e, or the crosslink density. van der Sanden and Meijer,[10] in their studies of rubber-modified polymers, noticed a constant strain-to-break (ε_b) independent of the amount of the core-shell rubber present. They also observed an increase in the strain-to-break as the molecular weight between crosslinks, M_c, increases. This trend is in agreement with the studies conducted by Landel et al.[9] A great discovery was made, after Landel, etc. collected the break stress and strain data for elastomers including EPDM, SBR, poly(vinyl ethyl ether) and butadiene, the normalized σ_b with the temperature and the crosslink density shows a clear relationship with ε_b in a failure envelope.[9] This failure envelope is able to describe the relationship between the ultimate strain and stress per crosslinked chain normalized by the

testing temperature, without the influence of the testing rate. If such a failure master curve does exist for most crosslinked polymers, the tremendous amount of the information the master curve provides, as well as the simplicity it introduces in assessing the ultimate tensile properties of numerous materials, can be of great contribution to engineering applications. This work takes the curiosity for such a master curve to re-examine and further investigate the master curve on more chemically complicated systems, epoxy DGEBA-poly(oxypropylene)diamines.

Experimental

Materials

The two different oligomer molecular weights of vinyl ester neat resins were supplied by the Dow Chemical Company. The vinyl esters are a group of epoxide resins from bisphenol-A, epichlorohydrin, and methacrylic acid. The average oligomer molecular weights are 1000g/mol and 690g/mol. Both of these resins were crosslinked with two different styrene contents, 20% and 35%. The chemical structure of the vinyl ester neat resin is shown in Figure 1.

Structure of Vinyl Ester (M_n = 700, 1000g/mol)

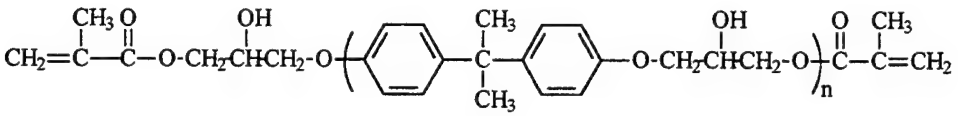

Figure 1 – Chemical structures of the vinyl ester neat resin.

The epoxy neat resin is a type of diglycidyl ether of bisphenol A (Epon 828) supplied by the Shell Chemical Company. Epon 828 has with two epoxide groups with an epoxy equivalent weight of 192 g/mol for each epoxide group. The epoxy neat resins are then crosslinked by the poly(oxypropylene)diamines (Jeffamine) with the different molecular weights of 230, 400, 2000 g/mol. The chemical structure of epoxy resin is shown in Figure 2.

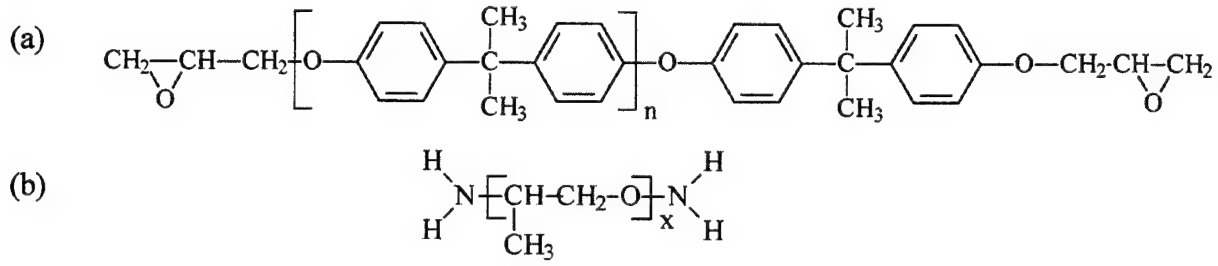

Figure 2 – Structure of components of the epoxy resins. (a) Epoxy Epon 828 neat resin (b) Jeffamines

Sample Preparation

In preparation of the vinyl ester resins with systematically varied crosslink densities, styrene monomer was mixed with the vinyl ester neat resins, either 1000g/mol or 690g/mol, at mass ratios of 20% and 35%. After the styrene dissolved the resin at 70°C, 1.1% of benzoyl peroxide

as an initiator was added into the mixture. Constant stirring was carried out till a homogeneous mixture was formed. The resin was then poured into silicone rubber molds and then placed in an oven at 150°C for 1 hour to reach a complete cure.

The Epon 828 resin was mixed with stoichiometric amounts of the three types of Jeffamines. After a steady stir for 15 minutes, the mixture was degassed in a vacuum oven at 60°C for about 20 minutes to allow all visible air bubbles to escape. The degassed resin mixture was poured into preheated silicone rubber molds. The molds were then placed into an oven at 80°C for 2 hours followed by 3 hours at 125°C for a full cure. The size of the tensile samples was determined by the mold side that had been cast out according to the ASTM standard.

Characterization

The glass transition temperatures of the vinyl ester resins were measured through differential scanning calorimetry (DSC) using a Perkin Elmer DSC 7. The heating rate was 10°C/min and two heating cycles were used with a hold for 10 min at 200°C. The DSC scans for the epoxy resins were performed on a SEIKO-Instruments DSC 210 at a heating rate of 10°C/min. All samples were measured under a nitrogen purge. The samples were taken up to 40°C above their estimated glass transition temperatures, T_g, to eliminate any possible physical aging occurring in the glassy state, except for the epoxy prepared from Epon 828 and Jeffamine D2000 since it is in a rubbery state at room temperature. The T_g was determined at the inflection point of the glass transition. No thermodynamic transitions were detected on the spectra of both sets of resins, verifying the completeness of the curing reactions. *Table 1* and *Table 2* list the determined glass transition temperatures.

Vinyl Ester Oligomer Weight (g/mol)	Styrene Content (%)	Calculated M_c (g/mol)	Measured M_c (g/mol)	T_g Onset (DSC,°C)	T_g End (DSC,°C)	DSC T_g (°C)	ΔC_p (J/g°C)
700	20	292	300	136	164	152	0.269
700	35	359	569	124	145	136	0.244
1000	20	417	812	115	133	125	0.322
1000	35	513	969	110	126	118	0.298

Table 1 – Characterization of the vinyl ester resins: the DSC analysis and M_c measurements

	Epon/D230	Epon/D400	Epon/D2000
Tg (°C)	80	47	-38
ν_e (mole of chains/cm^3)	1.3E-3	9.6E-4	2.8E-4

Table 2 - Glass transition temperatures and the crosslink densities of the epoxy resins

The molecular weights between crosslinks of the vinyl ester resins were calculated from the elastic rubbery modulus and the density using:

$$M_c = \frac{3RT\rho}{E} \qquad (1)$$

The elastic moduli of the vinyl esters were obtained using a Dynastat in a small load mode at 40°C above T_g. The crosslink density, ν_e, of the epoxy resins were determined from the elastic rubbery moduli obtained from tensile testing at 40°C above their T_g's, using

$$\nu_e = \frac{\rho}{M_c} = \frac{E}{3RT} \qquad (2)$$

The average molecular weights between crosslinks of the vinyl ester systems were also calculated from the chemical compositions of the resins and the number average molecular weights of the oligomers. This method has been widely applied for polymer systems that are considered fully cured and reasonably homogeneous.[11, 12] The crosslink density characterization results of the polymers are also listed in *Table 1 and 2*.

Room temperature densities of the samples were obtained on a Mettler-Toledo AG204 balance with a Mettler-Toledo density determination kit.[11] The densities at 40°C above T_g were further calculated with the coefficients of thermal expansion below and above T_g. The coefficients of linear thermal expansion were measured by thermal mechanical analysis (TMA).

Dynamic Mechanical Analysis

Dynamic mechanical thermal analysis of all samples was performed on a Seiko DMS 210 in tensile mode. The operating temperature range was from around -150°C to 220°C. Viscoelastic responses measured at 13 different frequencies, from 0.02Hz to 20Hz, were obtained simultaneously throughout the temperature ramp.

Mechanical Tests

Fracture toughness properties of the vinyl ester resins were determined in terms of the critical-stress intensity factor K_{Ic}. According to ASTM Standard D 5045-91, three-point bend tests were performed with the single-edge notch bending method. Some literature values are available and referenced for the current study.[11]

Ultimate tensile tests on the epoxy resins were performed on an Instron 4505 equipped with a temperature-controlled chamber. The network samples were tested at both 40°C above and below their T_g's at a crosshead displacement speed of 2.5mm/min. 4 or 5 runs were done for each sample.

Results and Discussion

(1) Vinyl Ester Studies

The crosslink density of the vinyl ester resins was varied by both changing the oligomer molecular weights and styrene content for each sample (Figure 3). This provides an efficient set of samples for the study.

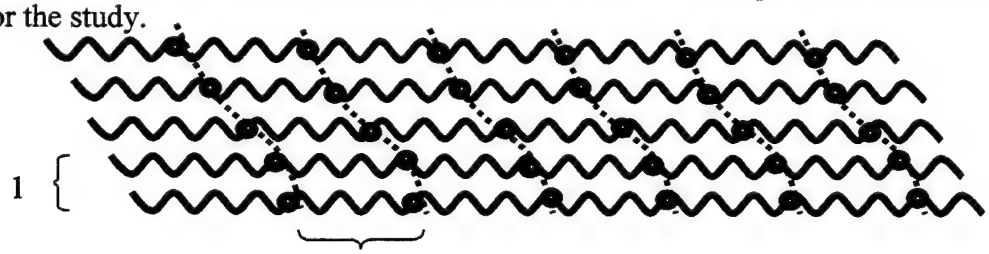

Figure 3 – Network structure of a crosslinked polymer. Note:
1. Length of the styrene chain between crosslinks 2. Length of the vinyl ester chain between crosslinks

The differential scanning calorimetry spectra of the resins are shown in Figure 4. The two DSC heating cycles for each network were nearly identical, indicating stability of the networks even after they were held at 200°C for 10 minutes. No indication of additional curing was seen on the DSC curves.

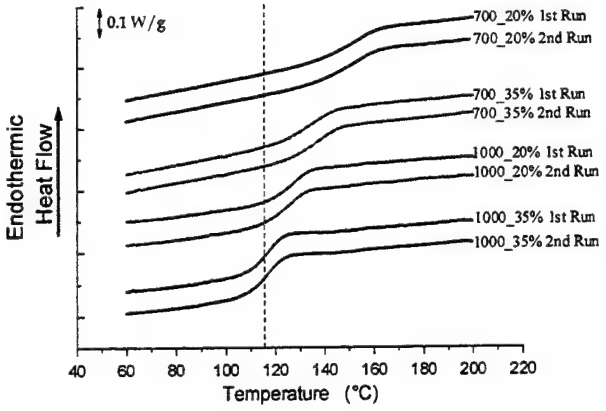

Figure 4 – Differential scanning calorimetry plots for the vinyl ester resins. The numbers on the left of the data labels represent the oligomer molecular weight of the vinyl ester samples. The right numbers represent the styrene content present in the cured resins.

The dynamic mechanical loss spectra of the networks over a wide range of temperatures are shown in Figure 5. The secondary relaxations of the polymers are observed in the loss modulus spectra. Previous research done by Heux and coworkers[13] showed significant variation of the secondary relaxation by the effects of antiplasticizer of aryl-aliphatic epoxy resins. The vinyl ester polymer systems, however, do not exhibit any marked changes in the secondary relaxations. In the current study the vinyl ester polymers do not exhibit any marked change with the various amount of styrene, reasonable for the relatively small range of the variation of the styrene content.

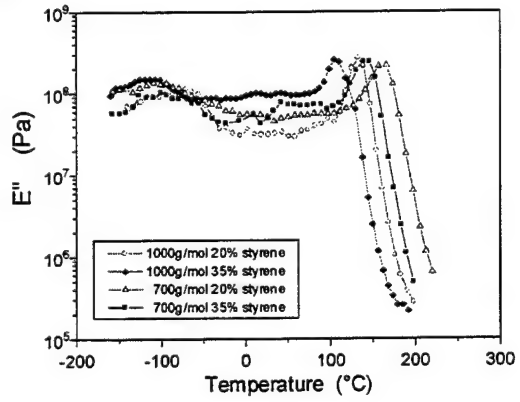

Figure 5 – Dynamic mechanical loss modulus spectra through a wide range of temperature.

Role of Network Density on Glass Transition and Viscoelastic Relaxations

The T_g increases as the network density increases. Fox and Loshaek[14] first described a direct relationship between T_g and M_c:

$$T_g = T_{g\infty} + \frac{B}{M_c} \qquad (3)$$

This relationship is verified with the vinyl ester systems (Figure 6). The linear relationship holds true for the T_g's indicated both by the DSC and dynamic tanδ peak. The calculated M_c from the chemical structures, however, shows a better fit than the measured ones. The correlation is

excellent despite the fact that the crosslink densities were varied by two distinct methods, which indicates the styrene content does not further affect the linear variation of T_g with respect to $1/M_c$.

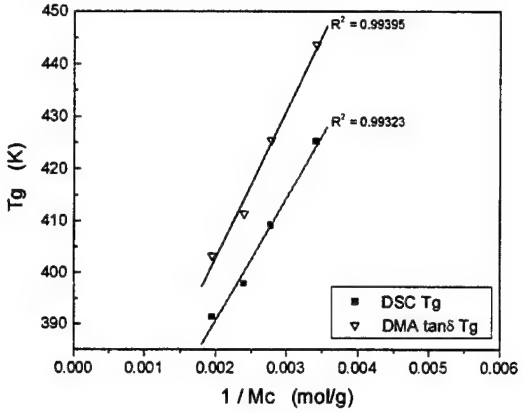

Figure 6 –T_g as a function of 1/ Mc for vinyl ester networks varied in oligomer molecular weights from 700g/mol to 1000g/mol, and styrene contents from 20% to 35%

The dynamic mechanical tanδ peak, related to the damping properties of a material, exhibits a systematical change with the change in the crosslink density shown in Figure 7a. The magnitude of the tanδ peak is found to decrease as the crosslink density increases, thus the polymer damping diminishes as the network structure tightens. As the M_c increases, the damping levels off and reaches a maximum value that is no longer affected by the opening of the network structure.

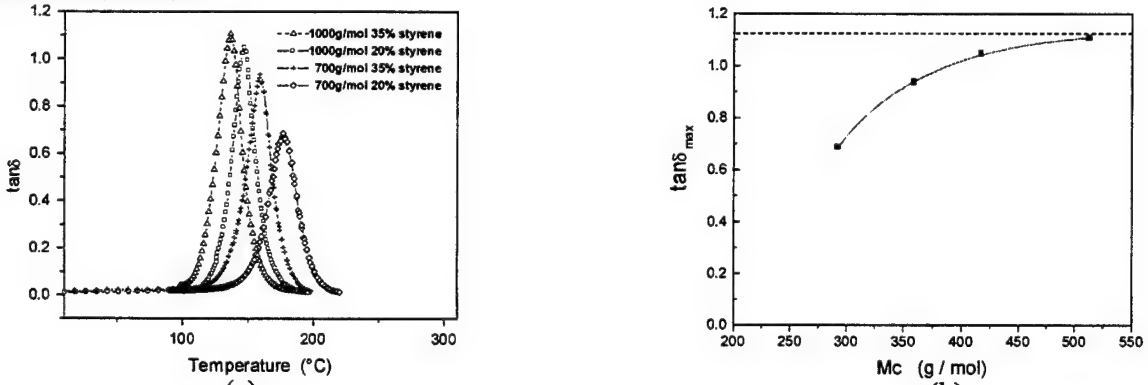

Figure 7 – The tanδ damping peaks of the vinyl ester networks as a function of crosslink density. (a) The tanδ spectra for the four networks over the glass transition regions (b) The magnitude of the maximum damping vs. M_c.

A closer examination of the glass transition shows the breadth of the glass transition is also influenced by the network density. The breadth of the glass transition is represented by the difference between the onset T_g and end T_g determined by the DSC technique explained in the experimental section above (see Table 1). The denser network has a broader glass transition (Figure 8). This effect does not seem to be affected by the different crosslinking techniques used.

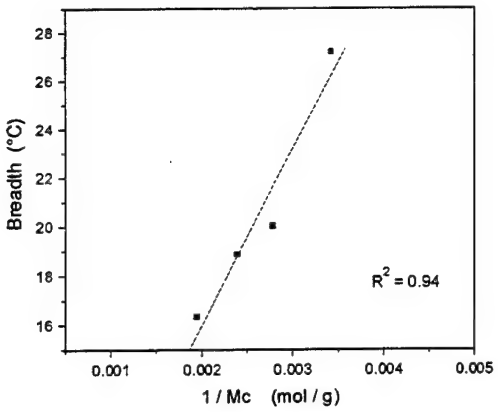

Figure 8 – The breadth of the glass formation as a function of $1/M_c$ for the vinyl ester networks. The breadth is the difference between the end and onset T_g determined from the DSC measurement.

Intermolecular Cooperativity in the Glass Formation Region

To thoroughly understand the dynamics of the glass formation region as influenced by the change in the network structure, the temperature and frequency dependence of the dynamic mechanical spectra were determined. The frequency and temperature-dependent mechanical loss moduli of the vinyl ester materials are combined into a master curve, using the time-temperature superposition principle.[15, 16] The loss moduli at each temperature T are corrected vertically to the reference temperature T_o (T_o is chosen to be T_g) by multiplying by the ratio T_g/T. The E" curves are then shifted horizontally to the alignment with the one at T_g (Figure 9a and 9b).

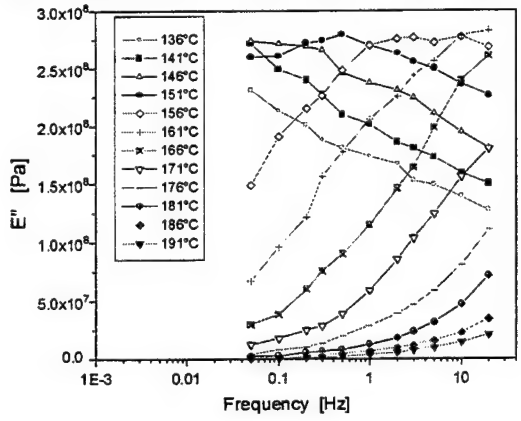

(a)

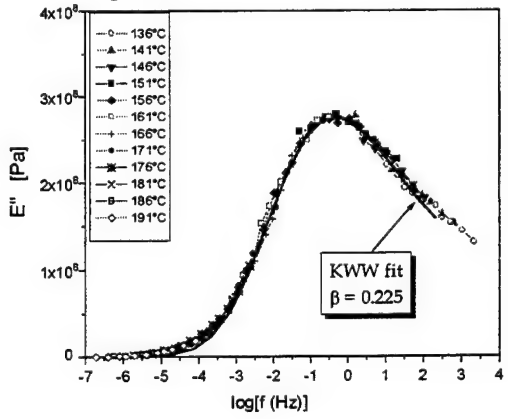

(b)

Figure 8 – Time-temperature superposition of the loss modulus. (a) The mechanical loss moduli as a function of time and temperature, for vinyl ester (M_n = 1000 g/mol) with 20% styrene (b) The superimposed master curve shifted on a log time scale.

Since the superposition occurs on the log time scale, the shifting implies a multiplication of the original time by a shift factor, known as the temperature shift factor, a_T,

$$a_T = \tau_T / \tau_{To} \qquad (4)$$

where τ_T is the relaxation time at temperature T and τ_{To} is the relaxation time from the same response at the reference temperature. The temperature dependence of viscoelastic relaxation times for a single relaxation mechanism system has been described by the Williams-Landel-Ferry (WLF) equation:[17]

$$\log a_T = \frac{-C_1(T-T_0)}{C_2+T-T_0} \qquad (5)$$

where a_T is the temperature shift factor described above, T represents the temperature corresponding to the shift factor, T_o is the reference temperature chosen to be T_g in the study, and C_1 and C_2 are WLF constants. The temperature dependence of the temperature shift factor a_T, obtained from the superposition, is plotted in Figure 10 for each vinyl ester network. The WLF fitting of each curve provides the values of C_1 and C_2 for each network, listed in Table 2. From the fitting, the slope at the glass transition temperature T_g of the $\log a_T$ temperature dependence curve for each network, which represents the cooperativity of the network, is derived from the WLF equation[17], that is,

$$m = \left.\frac{d(\log a_T)}{d(T_g/T)}\right|_{T=T_g} = \frac{C_1 T_g}{C_2} \qquad (6)$$

where the cooperativity is denoted as m, C_1 and C_2 are the constants in the WLF equation, and T_g is used if it is chosen to be the reference temperature.

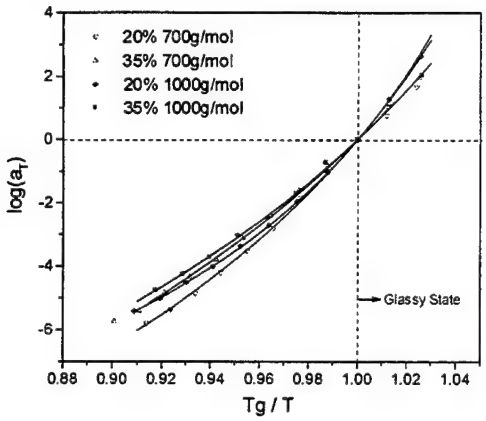

Figure 10 – The temperature shift factor as a function of 1/T normalized by T_g. The data are fitted by the WLF equation.

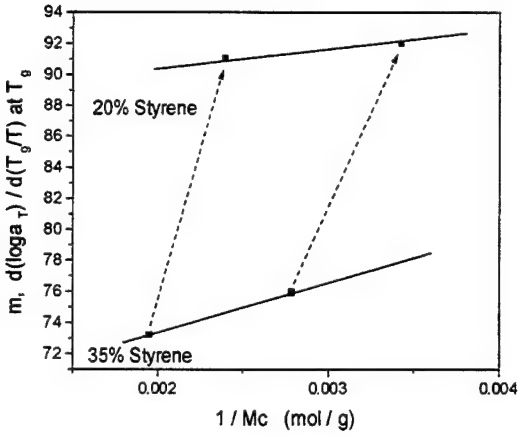

Figure 11 – Plot of the cooperativity as a function of the as $1/M_c$. The non-linear relationship indicates multiple factors exist to influence the cooperative motions at the molecular level when the crosslink density is varied.

The relationship between the cooperativity, m, and crosslink density was plotted in Figure 11. The two crosslink-density variation methods, though both have effectively changed the crosslink density, have different effects on the cooperativity of the molecular segments during the glass formation. The varied styrene content has a larger impact on the change of the intermolecular cooperativity that the changed oligomer molecular weight of the vinyl ester resins. The figure shows a shift of the trend between the cooperativity and the crosslink density, when the styrene starts to vary. This feature points out the fact that the molecular level of the segmental cooperative motion is not only dependent on the number of chains between crosslinks, but also differences in packing effects and other intermolecular constraints that are caused by the changes in chemical compositions. It is worth noting that on the other hand, the composition effects showed almost no additional influence at all on the location and the breadth of the glass transitions.

Correlation between Cooperativity and Glassy State Fracture Toughness

The fracture toughness data obtained from a previous paper[11] are plotted versus the cooperativity parameter m for the vinyl ester networks, and no simple correlation is found (see Fig.12). As shown in the figure, as the crosslink density is increased by changing the oligomer molecular weight, the fracture toughness of the resins decreases. On the other hand, if the crosslink density is increased by the variation of the amount of the styrene content, the fracture toughness decreases. The two effects of crosslink constraint and chemical play different roles of influencing the fracture toughness property.

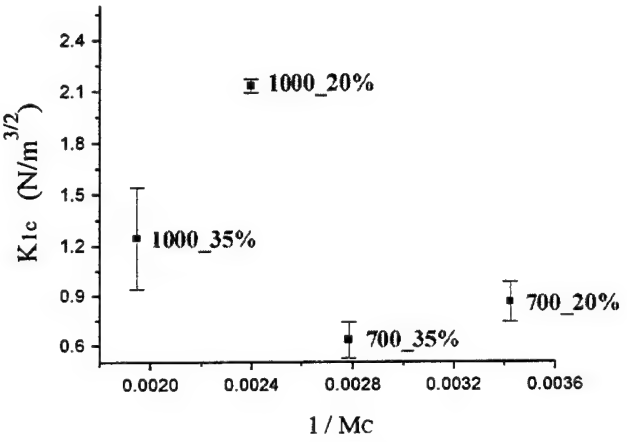

Figure 12 – Plot of fracture toughness K_{Ic} as a function of $1/M_c$ for the four vinyl ester systems. The left-hand numbers in the data labels represent the oligomer molecular weight in the vinyl ester resins, and the right-hand numbers represent the styrene content present in the resins.

The cooperative domain size at the glass transition temperature, which can be expressed as[18]

$$z_g = (T_g / C_2)^2 \qquad (7)$$

where C_2 is the WLF constant, and z_g represents the number of conformers in an hypothetical domain that are required to relax in a cooperative mode at the glass transition temperature. The domain size at a certain temperature is influenced by the degree of cooperativity among the molecular segments. While no correlation was found between the fracture toughness and the domain size at T_g (Figure 13 a), a linear relationship does exist between the fracture toughness of the vinyl ester resins and their domain sizes at T_g when they are normalized by the crosslink densities (Figure 13 b). This correlation may be because when the domain size, reflecting all constraints, was accounted for the crosslink effects, other intermolecular constraints were distinguished and found directly related to the fracture toughness property of the four networks.

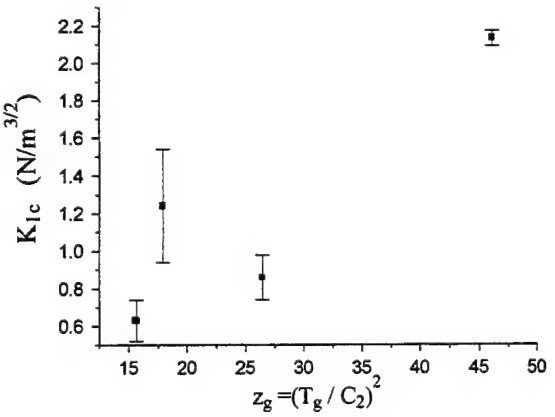

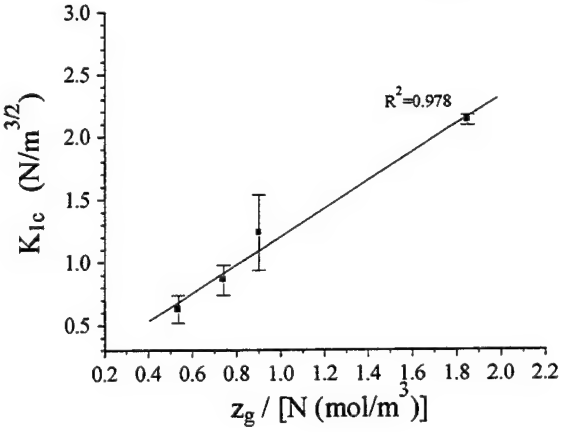

Figure 12 – Plots of the fracture toughness K_{Ic} values as a function of z_g. (a) z_g is not normalized by the crosslink density. (b) z_g is normalized by the crosslink density, N, as $N = \rho/M_c$.

(2) Epoxy Studies

Stress-Strain Behaviors of the Networks

The stress-strain curves for the networks are plotted in Figures 13 and 14. The glass stress-strain relationship was measured at 40°C below the T_g of the sample, and the rubbery stress-strain was obtained at 40°C above the T_g's.

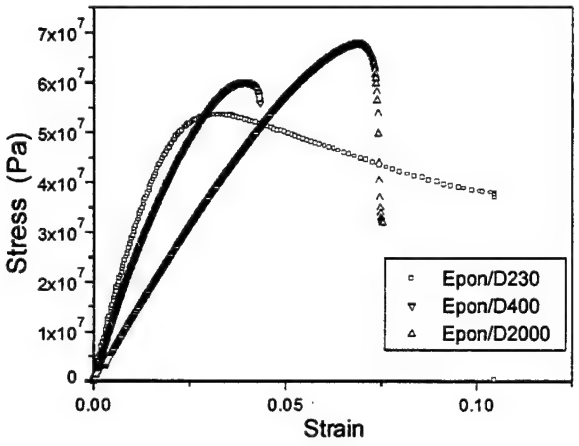

Figure 13 – Stress-strain relationship at the glassy state for Epon/D230, Epon/D400, and Epon/D2000. Strain rate = 2.5 mm/min. Testing temperature are 40, 7, -78°C, respectively.

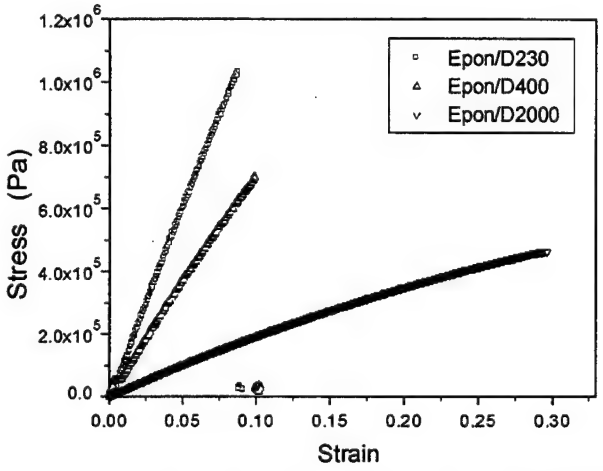

Figure 14 – Stress-strain relationship at the rubbery state for Epon/D230, Epon/D400, and Epon/D2000. Strain rate = 2.5 mm/min. Testing temperatures are 120, 87, and 8°C, respectively.

The figures show clearly the variation of the slopes of the curves in the low strain regions. This variation is due to the change of the crosslink densities of the resins, with the changing length of the Jeffamine diamines.

Elastic Moduli and Glassy Ultimate Strengths

The Young's moduli can be determined by obtaining the slope values of the elastic regions of the stress-strain curves.[15] The strengths of the glass network resins are determined from the highest peak in the stress-strain curves. As shown in Figure 13, there is also a change of the tensile strength of the resins due to the change in their crosslink densities. *Table 3* lists the values of the calculated elastic moduli and tensile strength.

	Glass Modulus (GPa, T_g - 40°C)	Rubber Modulus (MPa, T_g +40°C)	Tensile Strength (MPa, T_g - 40°C)
Epon/D230	3.1 ± 0.2	12.7 ± 2.0	51.2
Epon/D400	2.4 ± 0.1	8.7 ± 0.8	60.0
Epon/D2000	1.3 ± 0.7	2.0 ± 0.0	67.6

Table 3 – Elastic Moduli and Tensile Strength of the Epoxy Resins (strain rate = 2.5mm/min)

Ultimate Stress-Strain Properties

The tensile failure properties of the Epon/Jeffamine copolymer epoxy resins were studied. The data fit very well on the flow of the failure envelope plotted with the data examined by Landel, etc. More interestingly, the epoxy resins extend the failure envelope down to a more highly crosslinked region (Fig. 15). The previous literature data were able to fit the failure envelop from above 40% strain at break ($\log 100\varepsilon_b >= 1.6$). The lower region of the strain-to-break is extended by the epoxy resins. Another striking feature of the results is that the scattering of the data due to experimental errors also falls on the flow of the master failure envelope.

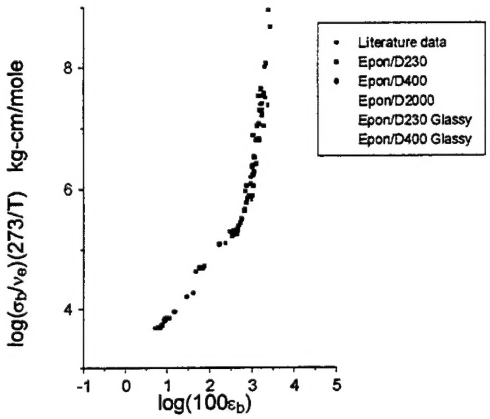

Figure 15 – The ultimate tensile properties of the epoxy resins in the context of the literature data obtained for the EPDM and butadiene.

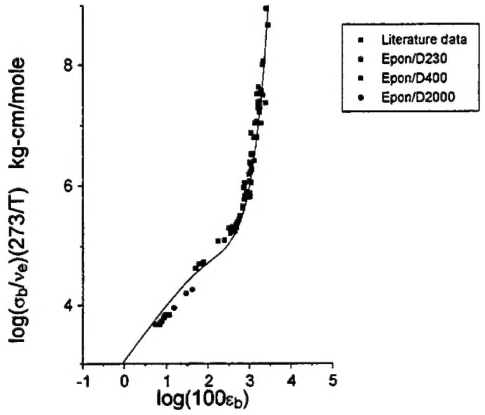

Figure 16 – Literature data and the Epon 828/Jeffamine network systems fitted on the expression in an analog of the MRS equation

The stress-strain behavior can be described by the analog of the Martin, Roth, and Stiehler equation,[19]

$$\sigma = E\left(\frac{\varepsilon}{\lambda^2}\right)^{A\left(\lambda-\frac{1}{\lambda}\right)} \tag{8}$$

where E is the equilibrium tensile modulus, λ is the extension ratio equal to $\varepsilon + 1$, and A is a constant. A relationship in the analog of the MRS equation,

$$\left(\frac{\sigma_b}{\nu_e}\frac{273}{T}\right) = E\left(\frac{\varepsilon_b}{{\lambda_b}^2}\right)^{A\left(\lambda_b-\frac{1}{\lambda_b}\right)} \tag{9}$$

where the left-hand side of the expression is the base of the y-axis used in the failure envelope, ε_b is the strain-to-break, λ_b is the extension ratio at break ($\lambda_b = \varepsilon_b + 1$), and A is a constant taken to be 0.43. This expression, replacing the stress and strain variables with the normalized failure stress and strain, turns out to fit the failure envelope markedly well (Fig. 16). A similar type of the interest in describing the shape of the failure envelope with the MRS equation was also expressed previously.[9, 19] More work is expected to investigate this correlation.

Conclusions

The crosslink density of the vinyl ester networks were varied via two methods, by changing the oligomer molecular weight of the main chain and by varying the amount of styrene used as a crosslinking agent. Shown from the dynamic mechanical spectra, the vinyl ester systems have rather stationary secondary relaxations. The glass transition temperatures and the breadth of the glass transitions of the four investigated networks undergo systematical variations. The glass transition temperature and the inverse average molecular weight between crosslinks exhibit a linear relationship that correlates to the Fox theory. The same relationship is found for the breadth of the glass transition and $1/M_c$. The two crosslink density variation methods revealed an interesting feature of these linear relationship, that is, no additional effects from the chemical composition were observed. The trends seem to be only related to the change of the average molecular weight between crosslinks. Furthermore, a systematical variation of the maximum damping was noticed as the molecular weights between crosslinks changed.

The studies on the glass formation based on the cooperativity model provided valuable insight on the different glass transitions of these crosslinked polymers due to the segmental constraints including the crosslink effects. A general trend was observed indicating an increase in cooperativity of the networks as the crosslink density increased. However, a declination of the degree of cooperativity of the networks was detected due to the increase in the styrene content. Also a striking correlation between the fracture toughness of the networks with the normalized domain size at T_g was found.

The concept of the master failure envelope proposed by Landel et al. was examined through the study of the epoxy resins. The failure data of the epoxy resins show that not only the data fit on the flow of the failure envelope constructed by the literature data, also they appeared to elaborate the failure envelope to a more highly crosslinked extent. The relationship of the normalized stress-to-break and strain-to-break can be described markedly well by an analog of the MRS equation. This might be an indication that the MRS equation is also suitable on the normalized ultimate stress-strain behavior.

In future work, more cooperativity analysis will be done on other networks to study the connection between the molecular interactive motions and their manifested mechanical properties. More evidence is needed to verify the established hypothesis in relating the fracture toughness with the normalized domain size. Furthermore, the distribution of the molecular weight between crosslinks and its influence on the mechanical response of a material are also of a research interest. Also, more crosslinked polymers will be tested to verify the influence of the tensile behavior brought by the changed crosslink density. The idea of a single failure curve used to describe multitude of crosslinked polymers independent of the testing conditions, will be further examined and applied for virtual engineering applications.

Acknowledgments

This work was sponsored by the National Science Foundation Science and Technology Center for High Performance Polymeric Adhesives and Composites, for the Summer Undergraduate Research Program. Materials contributions from the Dow Chemical, Shell, and Huntsman are acknowledged. Special thanks are expressed to Dr. G. L. Wilkes and Dr. D.

Dillard for providing their laboratories for testing. Also advice on the materials from Kurt Jordens is greatly appreciated.

References

(1) L. E. Nielsen, *Mechanical Properties of Polymers*, Van Nostrand Reinhold, New York, 1962
(2) R. F. Boyer, *Polymer Eng. Sci.*, Vol. 8, 161, 1968
(3) G. Adam and J. H. Gibbs, *J. Chem. Phys.*, Vol. 43, 139, 1965
(4) S. Matsuoka, *Relaxation Phenomena in Polymers*, Hanser, New York, 1992
(5) D. J. Plazek, K. L. Ngai, *Macromolecules*, Vol. 24, 1222, 1991
(6) M. Connolly and F. Karasz, *Macromolecules*, Vol. 28, 1872, 1995
(7) C. M. Roland and K. L. Ngai, *Macromolecules*, Vol. 24, 5315, 1991
(8) K. L. Ngai, and C. M. Roland, *Macromolecules*, Vol. 26, 2688, 1993
(9) L. E. Nielsen and R. F. Landel, *Mechanical Properties of Polymers and Composites*, 2nd Ed., Marcel Dekker, Inc., New York, 1994
(10) M. C. M. van der Sanden and H. E. H. Meijer, *Polymer*, Vol. 34(24), 5063, 1993
(11) H. Li, E. Burts, K. Bears, Q. Ji, J. J. Lesko, D. A. Dillard, and J. S. Riffle, *Network Structure and Properties of Dimenthacrylate-Styrene Matrix Materials*, submitted to Journal of Composites Materials
(12) H. Li, *Doctoral Dissertation*, Department of Chemistry, Virginia Polytechnic Institute and State University, 1997
(13) L. Heux, F. Laupretre, J. L. Halary and L. Monnerie, *Polymer*, Vol. 39, Number 6-7, 1998
(14) T. G. Fox and S. Loshaek, *Journal of Polymer Science*, Vol. 15, 371, 1955
(15) S. L. Rosen, *Fundamental Principles of Polymeric Materials for Practicing Engineers*, Barnes & Noble, New York, 1971
(16) J. D. Ferry, *Viscoelastic Properties of Polymers*, John Wiley & Sons, New York, 1961
(17) M. L. Williams, R. F. Landel and J. D. Ferry, *Journal of American Chemical Society*, Vol. 77, 3701, 1955
(18) C. G. Robertson and G. L. Wilkes, *Glassy Polymer*, eds., M. R. Tant and A. J. Hill, Washington DC: ACS Books, 1998
(19) T. L. Smith, *Journal of Polymer Science*, Part A, Vol. 1, 3597, 1963

1. L. E. Nielsen, Mechanical Properties of Polymers, Van Nostrand Reinhold, New York, 1962
2. R. F. Boyer, Polymer Eng. Sci., Vol. 8, 161, 1968
3. G. Adam and J. H. Gibbs, J. Chem. Phys., Vol. 43, 139, 1965
4. S. Matsuoka, Relaxation Phenomena in Polymers, Hanser, New York, 1992
5. D. J. Plazek, K. L. Ngai, Macromolecules, Vol. 24, 1222, 1991
6. M. Connolly and F. Karasz, Macromolecules, Vol. 28, 1872, 1995
7. C. M. Roland and K. L. Ngai, Macromolecules, Vol. 24, 5315, 1991
8. K. L. Ngai, and C. M. Roland, Macromolecules, Vol. 26, 2688, 1993
9. L. E. Nielsen and R. F. Landel, *Mechanical Properties of Polymers and Composites*, 2nd Ed., Marcel Dekker, Inc., New York, 1994
10. M. C. M. van der Sanden and H. E. H. Meijer, Polymer, Vol. 34(24), 5063, 1993
11. H. Li, E. Burts, K. Bears, Q. Ji, J. J. Lesko, D. A. Dillard, and J. S. Riffle, *Network Structure and Properties of Dimenthacrylate-Styrene Matrix Materials*, submitted to Journal of Composites Materials
12. H. Li, *Doctoral Dissertation*, Department of Chemistry, Virginia Polytechnic Institute and State University, 1997
13. L. Heux, F. Laupretre, J. L. Halary and L. Monnerie, *Polymer*, Vol. 39, Number 6-7, 1998
14. T. G. Fox and S. Loshaek, *Journal of Polymer Science*, Vol. 15, 371, 1955
15 S. L. Rosen, *Fundamental Principles of Polymeric Materials for Practicing Engineers*, Barnes & Noble, New York, 1971
16 J. D. Ferry, *Viscoelastic Properties of Polymers*, John Wiley & Sons, New York, 1961
17 M. L. Williams, R. F. Landel and J. D. Ferry, *Journal of American Chemical Society*, Vol. 77, 3701, 1955
18 C. G. Robertson and G. L. Wilkes, *Glassy Polymer*, eds., M. R. Tant and A. J. Hill, Washington DC: ACS Books, 1998
19 T. L. Smith, *Journal of Polymer Science*, Part A, Vol. 1, 3597, 1963